Doctoral Thesis

Thesis Title

Studies on Graphene Electrodes for Organic Light-emitting Diodes Application

Department of Electronic Engineering
Graduate School of Engineering,
TOHOKU UNIVERSITY

Jin-Wook Shin

(ID No. B6TD2501)

Doctoral Dissertation

submitted in partial fulfillment of the requirements for the degree of

DOCTOR of ENGINEERING

in the Department of Electronic Engineering,

Graduate School of Engineering

TOHOKU UNIVERSITY

Jin-Wook Shin

Thesis Committee: Professor Maki Suemitsu, Chair

Professor Shigeo Sato

Professor Toshiro Kaneko

Studies on Graphene Electrodes for Organic Light-emitting Diodes Application

Jin-Wook Shin

Abstract

Graphene has been intensively investigated as a material for components used in optoelectronic applications such as transparent electrodes, sensors, solar cells, and transistors, due to its outstanding transport and optical properties centered on its ultrahigh electron mobility and optical transparency. Its high mechanical compliance further opens applications for flexible devices. A number of research projects have focused on the development of graphene as a flexible transparent electrode material for OLED technologies to replace the brittle indium tin oxide (ITO) used in conventional electrodes.

Despite these efforts, various challenges still remain to be overcome in the use of graphene in flexible OLEDs. The major issues are the degradation in optical efficiencies, caused by reduced light extraction and light absorption within graphene, and the difficulty in achieving residue free graphene film pixel arrays with geometrical precision on large area. This study aims to solve these two problems. First, to overcome the efficiency issue, an internal random scattering layer has been introduced to extract the light. Also, the number of layers in the graphene electrode has been reduced to minimize the light absorption within the graphene layers. As a result, the maximum efficiency for the light extraction was obtained by using a single-layer graphene electrode together with a scattering layer.

Second, to overcome the patterning issues, a new method called the liquid bridge treatment has been developed to improve the adhesion of graphene. Using this method, a photolithographic patterning of graphene film, with dimensional precision and without surface contaminants, has been realized. A two-color graphene-OLED panel has been successfully demonstrated on a glass substrate and a flexible graphene-OLED panel on a polyimide film as well. The pixel size of the graphene film is $170 \times 250\ \mu m^2$ for both of the devices.

These results indicate that graphene can already be applicable to electrodes in commercial display products. In particular, flexible and foldable display applications are expected to be the main beneficiaries of our method.

CONTENTS

Chapter 1 Introduction 1

1.1 Organic light-emitting diodes 1

1.2 Technical issues of OLEDs for flexible displays 3

1.2.1 Flexible OLED applications 3

1.2.2 Transparent conductive electrode for flexible OLEDs 6

1.3 Graphene as an alternative material 9

1.3.1 Basic properties of graphene 9

1.3.2 Graphene electrode for OLED applications 11

1.3.3 Challenges on graphene electrode OLED 14

1.4 Outline 18

References 19

Chapter 2 Electrical and Optical Characterization of Graphene Electrode OLEDs 23

2.1 Introduction 23

2.2 Experimental methods 25

2.2.1 Graphene preparation 25

2.2.2 OLED fabrication process 26

2.2.3 Characterization of graphene film 29

2.2.4 Characterization of graphene electrode OLED 30

2.3 Results and discussion 32

2.3.1 Properties of graphene film 32

2.3.2 Characteristics of graphene electrode OLED 34

2.4 Conclusion 38

References 39

Chapter 3 Improvement of Light Extraction Efficiency of Graphene Electrode OLEDs 41

3.1 Introduction 41

3.2 Optical components in graphene electrode OLED 43

3.2.1 Influence of microcavity effect on graphene-OLED 43

3.2.2 Optical losses in OLEDs 45

3.2.3 Internal scattering layer 47

3.3 Experimental methods 49

3.4 Results and discussion 51

3.4.1 Structural properties of the scattering layer 51

3.4.2 Electrical and optical properties of the scattering layer 53

3.4.3 Simulation analysis of graphene-OLED with light extraction methods 55

3.4.4 Electrical and optical characteristics of graphene-OLED 58

3.4.5 Efficiency of graphene-OLED 61

3.4.6 Comparison of graphene Efficiency of graphene-OLED 63

3.5 Conclusion 66

References 67

Chapter 4 Formation of Accurate Graphene Patterns using Liquid Bridging Treatment 70

4.1 Introduction 70

4.2 Technical issues on the formation of graphene pattern 72
4.2.1 Weak adhesion properties of graphene 72
4.2.2 Concept of liquid bridge treatment 74
4.3 Experimental methods 77
4.3.1 Graphene preparation and patterning process 77
4.3.2 Liquid bridge treatment and characterization of graphene 77
4.3.3 OLED device structure 78
4.4 Results and discussion 80
4.4.1 Characterization of graphene with the liquid bridge treatment 80
4.4.2 Properties of graphene pattern 85
4.4.3 Characterization of OLEDs using patterned graphene electrode 87
4.5 Conclusion 90
References 92
Chapter 5 Integration of Graphene Electrode and Fabrication of OLED panel 93
5.1 Introduction 93
5.2 Experimental methods 95
5.3 Results and discussion 97
5.3.1 Characterization of graphene-OLED pixel 97
5.3.2 Graphene OLED display panel 99
5.3.3 Flexible graphene OLED display panel 100
5.4 Conclusion 102

References..... 103

Chapter 6 Conclusion..... 104

Publications and Conference Proceedings..... 107

Acknowledgements..... 115

List of Figures

Figure 1.1. OLEDs applications.

Figure 1.2. Technical trend of OLED technologies.

Figure 1.3. Schematic of flexible AMOLED unit pixel

Figure 1.4. Mechanical strain test of ITO and graphene and (b) bending radius test of various transparent electrodes on the flexible substrate.

Figure 1.5. Alternative TCEs for flexible OLED; (a) metal mesh, (b) silver nanowire, (c) conducting polymers, and (d) carbon based materials.

Figure 1.6. Honeycomb structure of graphene (a) and mechanical exfoliation for graphene using scotch tape method (b).

Figure 1.7. First demonstration of OLED with graphene; characteristics of current density-luminance-voltage (a) and efficiency (b)

Figure 1.8. Previous studies on graphene-OLED to modify graphene surface for the low R_{sh} and high WF using p-type dopant / interfacial layer; (a) HNO_3 / GraHIL, (b) OA / MoO_3 and (c) MoO_3

Figure 1.9. Efficiency issue of graphene OLED.

Figure 1.10. Processing issue of graphene film; damage of graphene during pattering processes.

Figure 2.1. (a) Schematic of graphene-OLED and (b) cross sectional image of graphene OLED. (Inset is actual emission of graphene device)

Figure 2.2. Schematic of graphene preparation processes.

Figure 2.3. Schematic of OLED fabrication processes (a) and device structures (b)

Figure 2.4. Measurement equipment of graphene films for (a) sheet resistance, (b) direction transmittance (c) surface roughness, and (d) graphene quality.

Figure 2.5. (a) Image of actual OLED unit cell, (b) measurement system and (c) output performances of OLED devices.

Figure 2.6. (a) The DT of four-layer graphene film and ITO (inset; surface morphology of graphene film) and (b) Raman analyses of four-layer graphene films.

Figure 2.7. (a) The luminance image, (b) *J-V*-luminance characteristics and (c) the angular-dependent luminance of the graphene-OLED and the ITO-OLED.

Figure 2.8. (a) CIE color coordinates and (b) the angular-dependent EL spectra of the graphene-OLED and the ITO-OLED.

Figure 3.1. (a) Schematic of OLED structure and optical components. (b) The simulated cavity enhancement factor of ITO and graphene.

Figure 3.2. The variation of radiance of OLEDs with ITO and graphene anode as a function of the organic thickness.

Figure 3.3. Simulated optical mode analysis in ITO-OLEDs (a) and graphene-OLED.

Figure 3.4. (a) Schematic of the OLED equipped with scattering layer, (b) the scattering layer. Electric field distributions in the OLED without the scattering layer (c) and with the scattering layer (d).

Figure 3.5. Process flows of the OLED with the scattering layer; (a) Deposition of Ag thin films, (b) Formation of Ag droplet by a thermally assisted dewetting process, (c) Dry etching substrate uncovered the Ag droplet, (d) Removal of Ag droplet for formation the nano-structure, (e) Planarization process on the nano-structure and (f) Graphene transfer on the scattering layer and OLED fabrication.

Figure 3.6. Schematic of graphene-OLED with the scattering layer (a), SEM image of the nanostructure (b) and (c), and AFM measurement of the nanostructure (d) without and with the planarization layer.

Figure 3.7. The sheet resistances (a) and the direct transmittances (b) of the graphene films on the glass and on the scattering layer with the variation of the graphene layer as one, two, and four.

Figure 3.8. The simulation results; (a) the effect of the microcavity and optical absorption of graphene electrodes on OLEDs and (b) The absorption effect of graphene electrodes on OLEDs with and without the scattering layer. (Inset ; the experiment results of the reflectance of the glass substrate and the scattering layer on the glass)

Figure 3.9. *J-V* characteristics of graphene-OLEDs; planar devices (a) and scattering devices (b). (Inset; EL spectra characteristics of graphene-OLEDs; planar devices (a) and scattering devices (b)) The number of the graphene layer was varied for one, two, and four and EL spectra of those OLEDs were measured at the normal direction.

Figure 3.10. The angular-dependent luminance of the graphene-OLEDs as planar devices (a) and scattering devices (b) with the variation of the graphene layer as one, two, and four.

Figure 3.11. The EQE (a) and LE (b) of graphene-OLEDs as planar devices and scattering devices. The number of graphene layers was varied as one, two, and four.

Figure 3.12. The Comparison of (a) EQE and LE, (b) The CIE color coordinates and (c), (d) EL spectra of SLG-OLEDs and IZO-OLEDs with and without the scattering layer. EL spectra of those OLEDs were measured at the normal direction.

Figure 4.1. (a) AM-OLED display panel and schematic of AM-OLED unit pixel.

Figure 4.2. Graphene damages from the pattering process (photo-lithography method); graphene smash (a), peeled off (b), and influence of graphene damage on the actual emission image of OLED (c).

Figure 4.3. Concept of liquid bridge treatment (similar to capillary bridge).

Figure 4.4. The concept of improvement in adhesion between graphene/substrate by liquid bridging; (a) air-pores between the graphene and the substrate, (b) the formation of water droplet inside the air-pores, and (c) the removal the water droplet.

Figure 4.5. Process flow of graphene patterning process.

Figure 4.6. Process flow of the liquid bridge treatment.

Figure 4.7. (a) Schematic of DCB specimens, the delamination tendency of graphene after DCB testing; (b) the pristine graphene, (c) the liquid bridge treatment, (d) the effective adhesion energy (histograms) and average surface roughness (symbol with dotted line) of all specimen, and the Raman analysis of pristine graphene (e) and the liquid bridge treatment (f) after DCB testing.

Figure 4.8. (a) Raman spectra and AFM images of graphene before (b) and after the liquid bridge treatment (c).

Figure 4.9. (a) SEM image of graphene pattern edge by the photolithographic patterning processes and (b) the Raman analyses before and after the pattering process.

Figure 4.10. (a) *J-V*-luminance and (b) LE of characteristics of graphene-OLED with the passivation wall and the pattering process. (c) EL spectra characteristics at normal direction. Actual emission image of graphene-OLED with (d) the non-patterned graphene film and (e) the patterned graphene film.

Figure 5.1. Schematics of typical AM-OLED pixel with TFT (a) and graphene-pixel electrode OLED with addressing metal line (b).

Figure 5.2. Process flow of graphene-pixel electrode OLED; backplane process (steps 1-4), graphene pattern process (steps 5-8), and OLED fabrication process (step 9).

Figure 5.3. (a) Actual image of a fabricated backplane with graphene film pixels. (b) A SEM image of graphene film pixel including the electrical pad, via hole and addressing metal line.

Figure 5.4. (a) The *J*-*V*-luminance and EL spectra characteristic of graphene-pixel electrode OLED, (b) Actual image of graphene pixel array and (c) emission image of OLED with graphene pixel array.

Figure 5.5. Two-color OLED with pixelated graphene films as transparent electrodes.

Figure 5.6. Process flow of flexible graphene-pixel electrode OLED.

Figure 5.7. Flexible OLED with pixelated graphene films as transparent electrodes

List of Table

Table 1.1. Schematic of flexible AMOLED unit pixel

Table 1.2. Comparison of the TCE materials for flexible display

Table 2.1. Comparison of properties of ITO and graphene.

Table 2.2. Measurement results of four-layer graphene film and ITO used in this chapter.

Table 2.3. Absolute value of the EQE and LE of the OLED with graphene and ITO.

Table 3.1. Summary of the average values of each mode for graphene-OLEDs and the ITO-OLEDs.

Table 4.1. Absolute value of adhesion energy and Ra of graphene before and after the liquid bridge treatment.

1

Introduction

1.1 Organic Light-Emitting Diodes

Organic light-emitting diodes (OLED) is a light source utilizing the phenomenon in which organic materials generate light in response to electrical signals. OLEDs provide near nature light spectra with wide color gamut, and they are of high transparency and flexibility [1-4]. Because of these properties, OLEDs have received attention as the next generation light source. OLED is composed of an organic compound layer as the active component, which is sandwiched by two electrical terminals of anode and cathode. First practical OLED device was demonstrated by C. W. Tang and S. V. S. Slyke at Eastman Kodak in 1987 [5]. Although this device exhibited only low efficiencies such as 1 % for the external quantum efficiency (EQE) and 1.5 lm/W for the luminous efficacy (LE), it demonstrated that organic material could actually be a viable alternative for optoelectronic applications. Today, OLEDs are being applied to commercialized displays and lighting products, replacing some of conventional light sources (Fig 1.1). There have been continuous efforts to improve the OLEDs performance up to that of commercialization level. The development of efficient phosphorescent emitting materials and thermally activated delayed fluorescence (TADF) materials has made it possible to achieve a nearly 100% internal quantum efficiency [6-13]. Furthermore, a stack design to consider the band alignment of materials can ensure high device performances by facilitating the charge transport [14,15]. Finally, with the development of a novel

light extraction method to enhance the low EQE (~20%), the LE of OLEDs has shown a dramatic improvement which exceeds 100 lm/W [16,17].

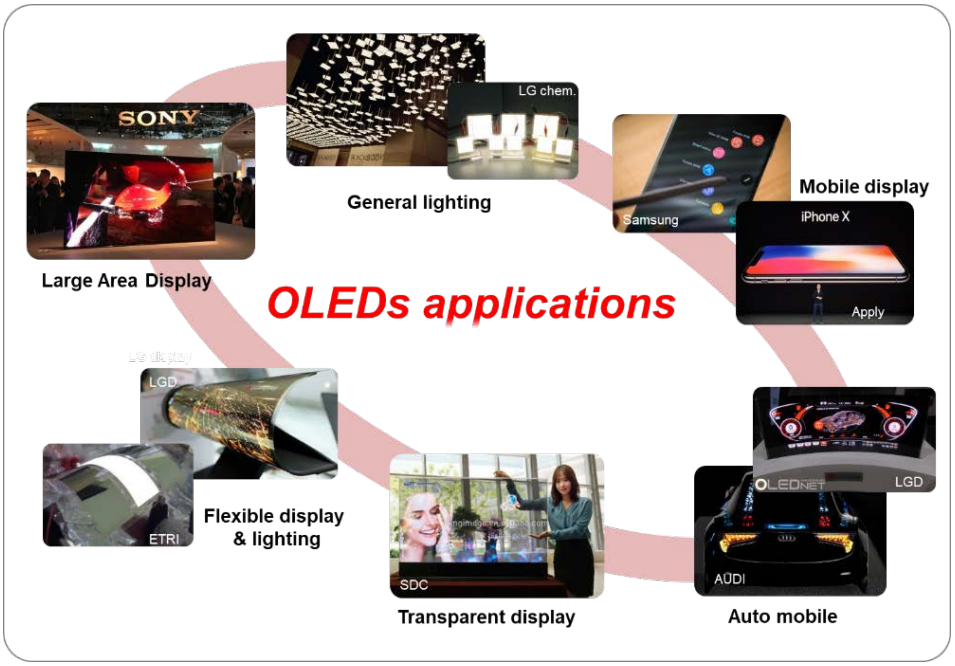

Figure 1.1. OLEDs applications.

1.2 Technical issues of OLEDs for flexible Displays

1.2.1 Flexible OLED applications

In response to recent demands for flexible displays and lighting devices, interests on OLED technology has shifted from rigid to flexible substrates (Fig 1.2). Flexible OLEDs have many advantages such as lighter, thinner and more durable as compared with glass-based OLEDs, and thus can be applied to various optoelectronics technologies. Because organic materials provide the transparent and flexible properties, it facilitates to apply the active components in flexible devices. Flexible OLED consists of various functional layers.

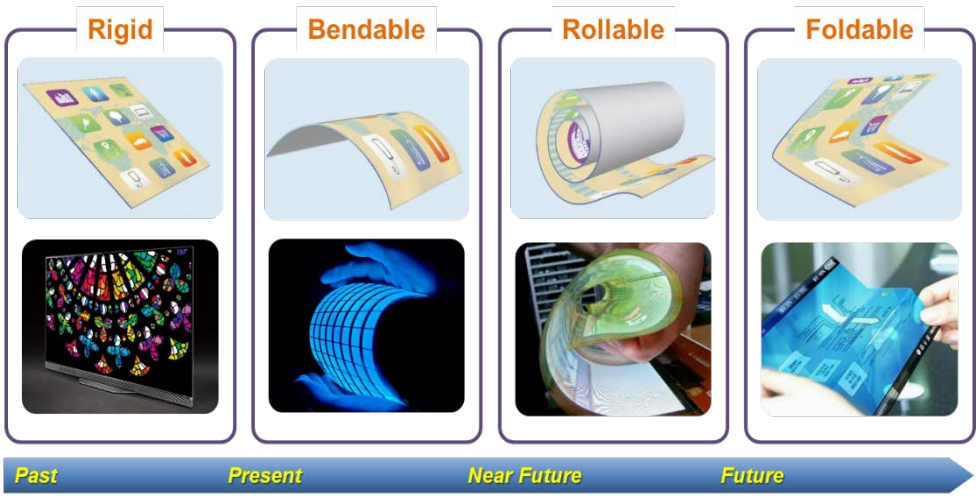

Figure 1.2. Technical trend of OLED technologies [18].

The basic structure of an Active matrix (AM)-OLED can be divided into two parts: a backplane TFT and an upper OLED (Fig 1.3). Its components and functionality are summarized in table 1.1. The backplane is composed of an array of thin film transistors (TFTs), contact metal lines within via holes and a passivation layer on the flexible substrate with a barrier layer. The TFT controls the current flow into the OLED. The passivation layer is necessary to protect the TFTs during subsequent

processes such as formation of anode as well as pixilation and deposition of organics. In addition, the passivation layer prevents the occurrence of electrical short circuits. The passivation layer was perforated to form electrical contact pads [19-21].

The OLED was fabricated on this backplane by stacking up multi-functional layers such as a transparent electrode as an anode, functional organic layers as a light emitter, and a highly reflective electrode as a cathode. The barrier layer and the encapsulation layer in Fig. 1.3 play important roles in flexible AM-OLED pixels. They protect the organic materials from being damaged by hydrogen and oxygen molecules in the ambient [22].

For realizing flexible devices, the relevant properties of all the components have to be stable under bending conditions. However, there are material issues in OLEDs. Bending causes a stress on each component. Stress can also be caused by difference in the thermal expansion coefficient of the material in the flexible device. These stresses cause damages to materials in the devices and deteriorate their performance [23,24]. Such deterioration can be serious in components using inorganic materials such as transparent conductive electrodes (TCEs). Oxide-based TCEs, such as indium tin oxide (ITO) and indium zinc oxide (IZO), have been commonly used for various electronic and optoelectronic devices including OLEDs. However, they cannot readily be used on flexible substrates because they are brittle. To realize flexible OLEDs, therefore, it is necessary to find an alternative electrode material bearing a sufficient mechanical compliance as well as excellent optical and electrical properties comparable to conventional TCE.

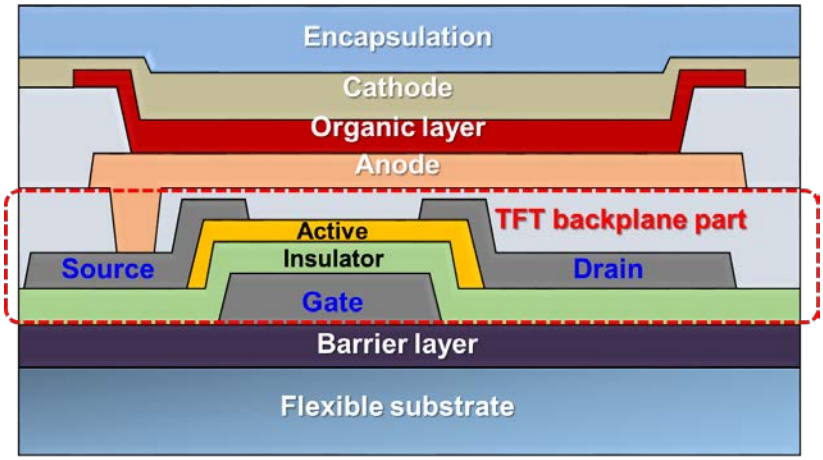

Figure 1.3. Schematic of flexible AMOLED unit pixel

Table 1.1. Schematic of flexible AMOLED unit pixel

Component	Functionality
Encapsulation	Protection of OLED damages from hydrogen and oxygen
Anode/Cathode	Electrode - Injection of current into organic layers
Organic layer	Light generation of Red/Green/Blue/White
TFT backplane	Control of the current flow into OLED pixels (on/off switch)
Barrier layer	Protection of OLED damages from hydrogen and oxygen
Substrate	Support of flexible OLED components

1.2.2 Transparent conductive electrode for flexible OLEDs

TCE is an essential component in OLEDs. ITO is the most widely used material for TCE in OLEDs due to its outstanding properties. Commercial ITO offers high optical transparency (~ 90% at a wavelength of 550 nm), low sheet resistance (R_{sh}) of 10-30 Ω/□, excellent surface smoothness, chemical stability, and good patternability. The major drawback of ITO, however, is its brittleness and is thus weak against external mechanical force. Typical ITO has a low failure strain of about 1.2 % and a low bending radius of 7-10 mm, with a low recover resistance due to crack generation under mechanical bendings (Fig 1.4) [25,26]. In addition, a high temperature process is required to produce high quality ITO, which may cause thermal damage to the flexible substrate having low thermal resistance [27]. These properties make ITO unsuitable for flexible electrodes.

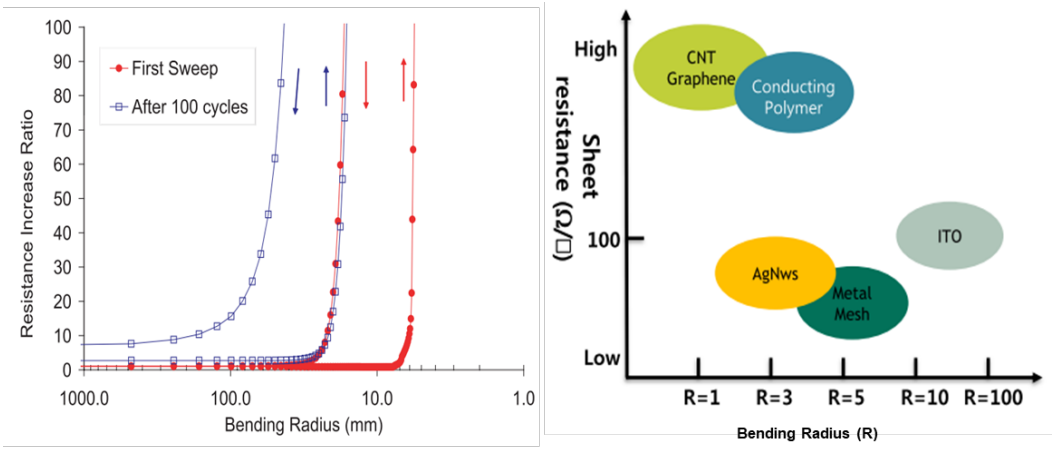

(a) (b)

Figure 1.4. (a) Mechanical strain test of ITO and graphene and (b) bending radius test of various transparent electrodes on the flexible substrate.

For flexible OLEDs, it is thus essential to find a new material for the flexible electrodes having excellent optical and electrical properties comparable to ITO. As for the flexibility, they should have a

bending radius less than 5 mm to realize rollable and foldable displays in future beyond the current bendable display (Fig 1.4(b) [28]. Various alternative materials have been proposed to replace ITO, such as Ag nanowires, metal meshes, conducting polymers, and carbon based material (Fig. 1.5) [29-33]. TCEs utilizing these materials showed excellent performances and exhibited better mechanical properties than ITO as well. In order to fabricate OLED, however, the TCE materials should be stable during the display manufacturing processes; low chemical and physical stability would cause damages to the TCE materials. Also, a high surface roughness on TCEs could cause high leakage current and deteriorate the device performance. From this viewpoint, graphene is being considered as one of the best candidates for the TCE to be used in flexible OLEDs. Graphene has a low surface roughness similar to that of ITO and has a higher compatibility with existing display manufacturing process due to its high process stability.

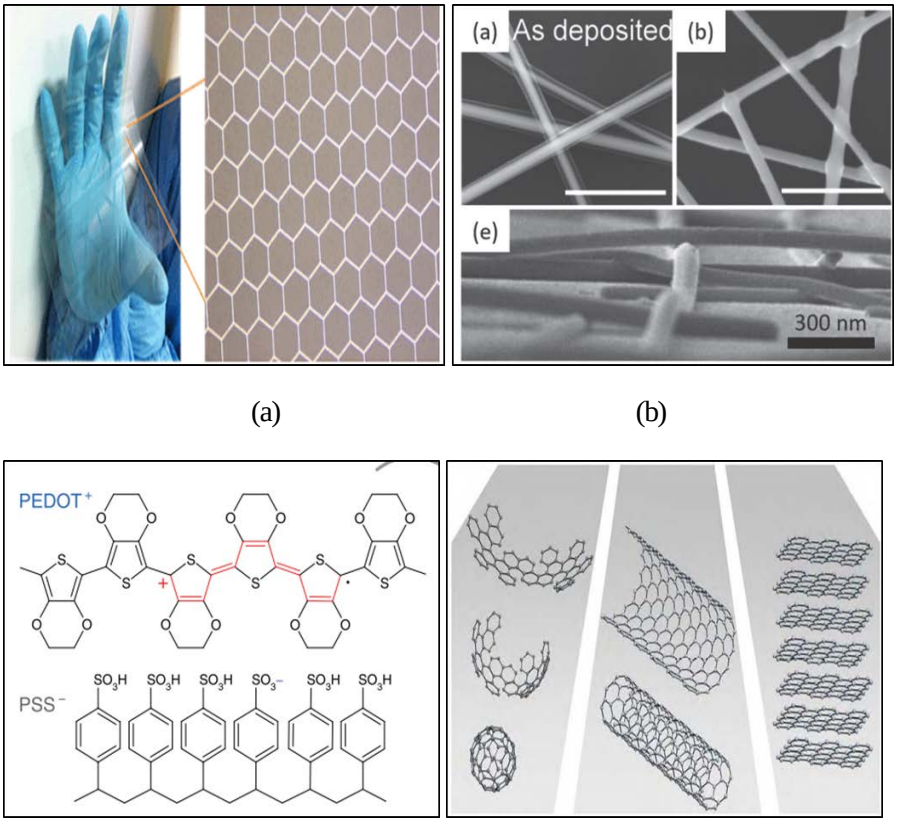

(a) (b)

(c) (d)

Figure 1.5. Alternative TCEs for flexible OLED; (a) metal mesh, (b) silver nanowire, (c) conducting polymers, and (d) carbon based materials.

Table 1.2. Comparison of the TCE materials for flexible display.

	ITO	Metal mesh	AgNW	Conductive polymer	Graphene
Status	Standard	commercialized	commercialized	commercialized	emerging
Sheet resistance * Transmittance ~90%	15 ~ 50 Ω/□	1~ 50 Ω/□	< 30 Ω/□	10~150 Ω/□	200~300 Ω/□ (Doping~ 65 Ω/□)
Flexibility	Bad	Good	Good	Good	Good
Chemical stability	Good	Normal	Normal	Bad	Good
Surface roughness	Good	Bad	Bad	Good	Good
Patternability	Good	Bad	Bad	Bad	Good

1.3 Graphene as an alternative material

1.3.1 Basic properties of graphene

Graphene belongs to a class of low dimensional carbon materials. In graphene, carbon atoms are mutually sp2-bonded to form a hexagonal 2D array. Graphene is one of the nanostructured carbon allotropes together with fullerene (C60: soccer ball), carbon nanotubes (CNT: cylinder) and multi-layered graphite. In graphene, three of the four outermost electrons are σ bonded to form a hexagonal 2D structure while the remaining one electron forms non-localized π bonds. This unique structure provides the well-known excellent electrical / optical properties (π bonds) and mechanical strength (σ bonds) to graphene [34]. Novoselv. et al. first demonstrated a visible graphene film on SiO_2 substrate obtained by mechanical exfoliation of graphite using a Scotch tape method [35]. Since it was first isolated in 2004, the past twelve years have witnessed a huge burst in fundamental and application research activities on graphene.

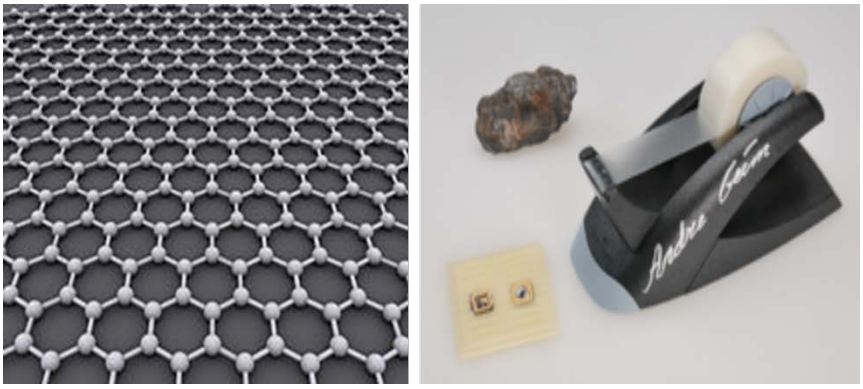

(a) (b)

Figure 1.6. Honeycomb structure of graphene (a) and mechanical exfoliation for graphene using scotch tape method (b).

Graphene, as a single entity, possesses various outstanding properties, including high electron mobility (> 10000 cm^2/Vs at room temperature), optical transmittance (~97.7% for sing layer), and thermal conductivity (~5000 W/mK). Defect-free monolayer graphene also has excellent mechanical properties with 42 N/m of mechanical strength and 20 % of failure strain [36]. The optical absorption of graphene is ~ 2.3% over the whole visible spectrum. With this, the optical transmittance of graphene is calculated to be T = 100% - 2.3% · N (N is the number of graphene layers), which is linearly proportional to the number of graphene layers. The initial graphene film, which was prepared using exfoliation method, showed an R_{sh} of 5k Ω/□ at a transmittance of 90%. This value is higher than the R_{sh} of the calculated single-layer graphene due to non-uniformity of graphene film and high interlayer resistance. The development of the chemical vapor deposition (CVD) method makes it possible to prepare a large-area graphene film with high uniformity and quality. Doping to graphene also decreases R_{sh} to a value similar to that of ITO level. Doping reduces R_{sh} by increasing the charge concentration. Graphene can be chemically doped at doping levels of $N_i = 10^{12}$ cm^{-2} with keeping the charge carrier mobility above $\mu = 10^5$ cm^2/Vs. Based on these values, R_{sh} of graphene can be calculated using the following equation (1.1) [37,38].

$$R_{sh} = \frac{1}{e\mu N_i N} = \frac{62.4}{N}\,\Omega/\square \qquad (1.1)$$

N is the number of graphene layers. Atomic or molecular doping can directly increase the charge carrier concentration of the graphene film. The doping process can sufficiently improve the electrical performance of the graphene up to ITO level. At the laboratory level, recent progress in graphene reduced the R_{sh} of single layer graphene from 275 Ω/□ to 125 Ω/□ after a p-type doping with HNO_3. Furthermore, four-layer doped graphene film showed R_{sh} as low as 30 Ω/□, which are comparable to those of ITO (10-20 Ω/□) [40].

1.3.2 Graphene electrode for OLED applications

Graphene based OLEDs have attracted attention due to their high flexibility and widely potential applications. Graphene is more advantageous for OLEDs than any other alternative electrodes. However, various challenges still remain to be overcome in graphene TCE. The first is the increase in the operating voltage of OLED due to the higher R_{sh} of graphene compared to the ITO. Second, graphene has relatively low work function (WF, 4.4~4.6 eV) than that of ITO (~4.8 eV). Simple replacement of ITO with graphene electrode increases the energy barrier for hole injection at the interface between the organic layer (> 5.4 eV) and the graphene. Such a large energy barrier hinders efficient hole injection from the electrode to the organic layer and can thus decrease the luminous (power) efficiency of graphene electrode OLEDs (graphene-OLEDs) [41,42]. In order to reduce the higher R_{sh} as well as the hole injection barrier, various surface modification methods have been proposed on graphene.

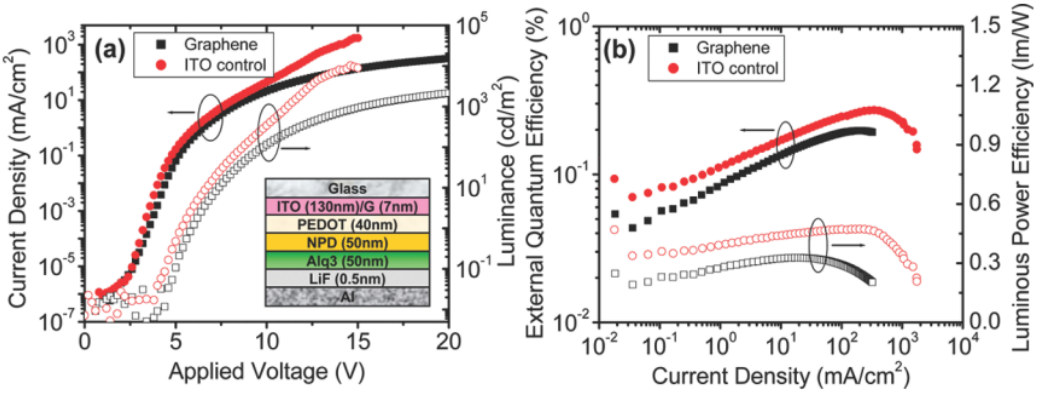

Figure 1.7. First demonstration of OLED with graphene; characteristics of current density-luminance-voltage (a) and efficiency (b)

The first graphene-OLED was demonstrated in 2010 [43]. Early studies demonstrated the feasibility of graphene as an electrode for OLED and focused on understanding its optical and

electrical properties. The graphene anode was prepared by spin-coating of an aqueous dispersion of functionalized graphene flake. This solution-processed graphene showed ~ 800 Ω/□ of R_{sh} of and 82% of transmittance (550 nm wavelength) at 7 nm in thickness. Such R_{sh} of graphene was higher than the theoretical estimation because the solution-processed graphene has numerous grain boundaries and defects. Although the graphene-OLED showed higher operating voltage and lower luminous efficacy than conventional ITO-OLEDs, it at least succeeded in demonstrating the possibility of graphene as a material for TCE in OLED. Later studies on OLEDs using solution-processed graphene have however shown that the device performance is not high enough: low electrical conductivity and low uniformity due to defects in the graphene film [44,45]. In order to realize graphene-OLEDs having comparable performance to ITO-OLEDs, the electrical conductivity and the surface properties of graphene should be improved preferentially. CVD graphene [46,47], in this respect, seems to have a much higher potential as compared to the solution-process method. OLEDs using the CVD graphene actually exhibited more stable and excellent electrical and optical properties. Meanwhile, the problems of the low WF and the high R_{sh} still remained as a challenge. A solution to this problem is to use a conducting polymer composite and to dope graphene with a p-dopant HNO_3. While the polymer composite introduces a WF gradient from graphene to the overlying organic layer (WF ~5.95 eV) the p-type dopant increases the electrical conductivity of graphene (R_{sh} ~ 54 Ω/□) [48]. These modifications on graphene brought about reduction of the operating voltage of the graphene-OLED to a similar level that of ITO-OLEDs. Another study [49,50] also utilized p-type dopants such as molybdenum trioxide (MoO_3), triethyloxonium hexachloroantimonate (OA), tungsten trioxide (WO_3) etc. As a result, an OLED using such surface-modified graphene gave rise to low operating voltages and high efficiencies (Fig 1.8)

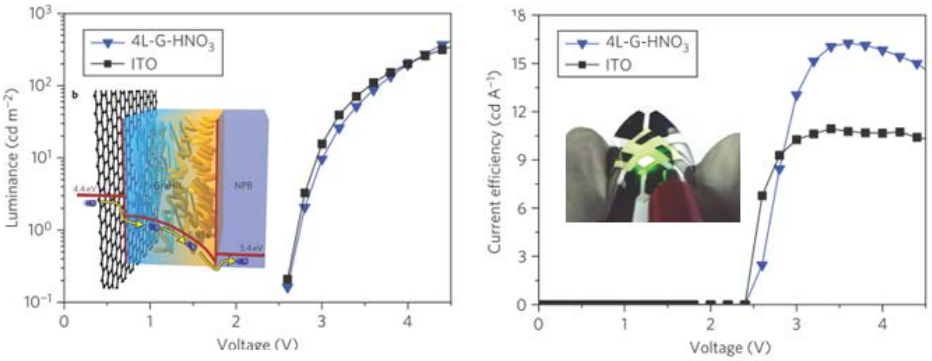

(a)

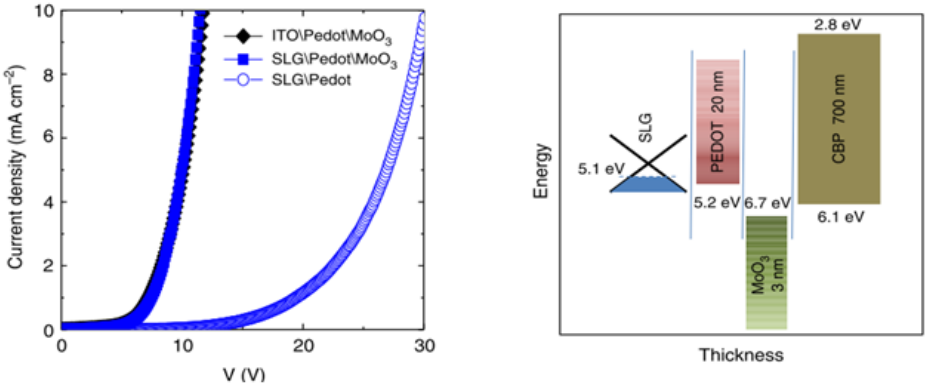

(b)

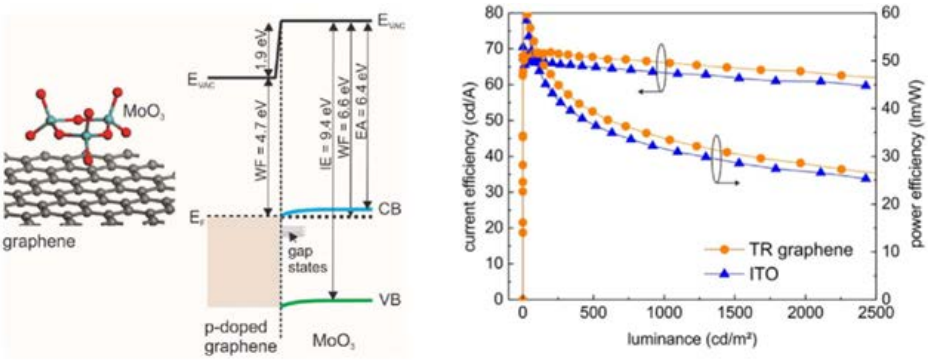

(c)

Figure 1.8. Previous studies on graphene-OLED to modify graphene surface for the low R_{sh} and high WF using p-type dopant / interfacial layer; (a) HNO_3 / GraHIL, (b) OA / MoO_3 and (c) MoO_3

1.3.3 Challenges on Graphene electrode OLED

As we have seen, graphene is a very attractive candidate as a material for TCE in OLEDs. Nevertheless, there have been no reports on commercial graphene-OLEDs. Several issues still impede the realization of graphene-OLEDs. The first one is the efficiency issue; The efficiency of the today's graphene-OLED is lower than that of classical OLEDs made with conventional TCEs such as ITO and IZO (Fig. 1.9). The major reason for this is the weaker microcavity effect in graphene-OLEDs. In conventional OLEDs the microcavity effect is substantial and has been utilized as an efficient means to improve the light extraction efficiency [51]. In graphene-OLEDs, however, this microcavity effect is weak because this effect originates from the reflectance of the anode and the graphene's reflectance is low [52,53]. In order for graphene to be used in flexible OLEDs, therefore, it is necessary to develop a technology that compensates the weak microcavity effect.

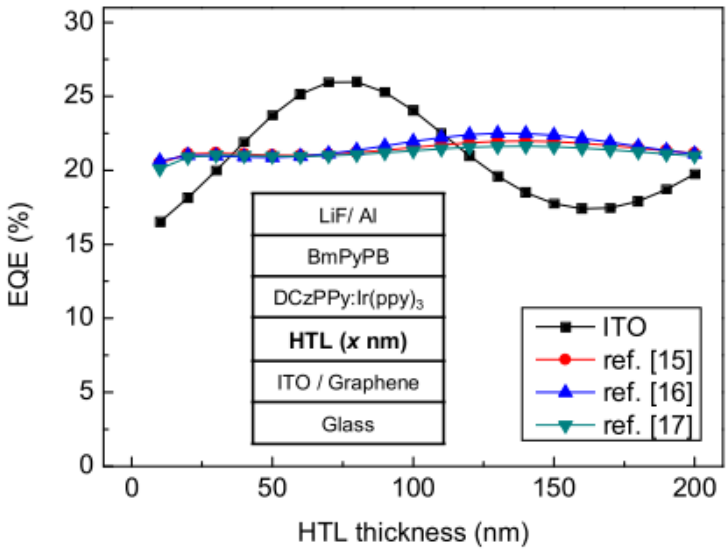

Figure 1.9. Efficiency issue of graphene OLED.

The second issue for the present graphene-OLED is the processing issue, which is confronted during the integration of graphene-OLED. To realize a graphene-OLED display, for instance,

graphene must be somehow patterned with a sufficient dimensional precision over a large area to define the anode or the pixel pattern without damages. Conventional methods used in the patterning of OLED, however, deteriorate graphene and thus do not meet the process requirement. This is due to the graphene's high reactivity with oxygen-bearing species as well as to its low adhesion to the substrate [54].

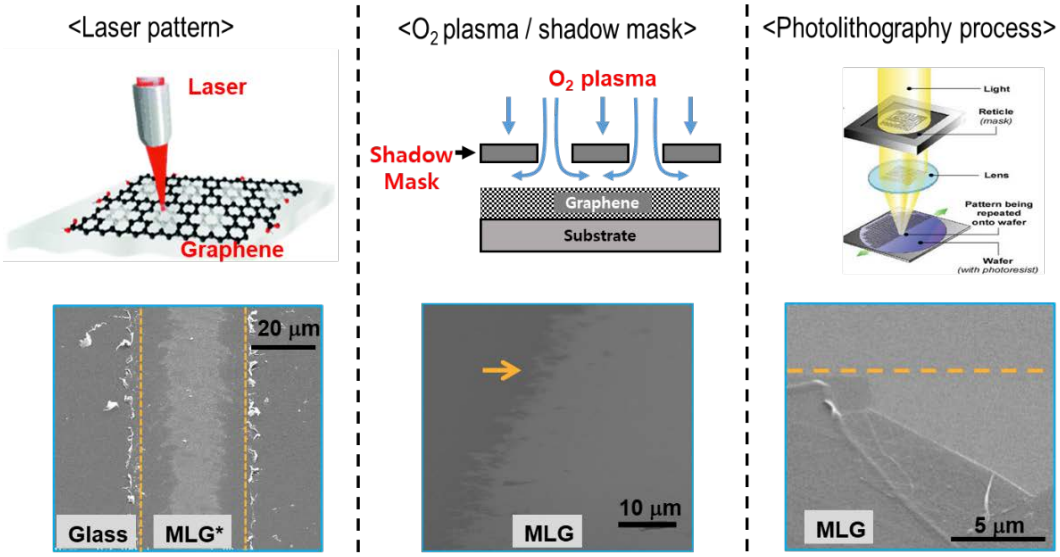

Figure 1.10. Processing issue of graphene film; damage of graphene during patterning processes.

In order for graphene to be used in commercial OLEDs, therefore, it is necessary to develop a technology to improve the optical efficiency of graphene-OLED and to form a fine pattern in the graphene sheet. For these two purposes, the following technologies have been developed in this study.

i) For the improvement of optical efficiency of graphene-OLED;

To improve the optical efficiency, we first introduced a scattering layer to enhance the internal light extraction. The scattering layer consists of a random nano-structure (RNS) array and a planarization layer. This structure out-couples the light trapped inside the device, which would

improve the light extraction efficiency. Second, we have minimized the number of graphene layers in order to minimize the light absorption of graphene.

ii) For a damage-free and precise patterning of graphene;

During the photolithography used in OLED processes, graphene can easily be damaged due to the graphene's weak adhesion to the supporting layer. To overcome this problem, we developed "liquid bridging treatment". This treatment greatly enhances the adhesion of graphene to the supporting layer and thus stabilizes graphene during photolithography. Formation of fine and accurate patterns has come to be possible by this method.

1.4 Outline

The outline of this thesis is as follows. Chapter 2 describes fabrication and characterization of classical graphene-OLED. Graphene was prepared by rapid thermal chemical vapor deposition (RT-CVD) process and transferred by the thermal release tape (TRT) method onto the target substrate. The graphene film and the graphene-OLED were evaluated with electrical and optical measurements. It is shown that graphene has comparable properties with that of ITO as a TCE. Although the graphene-OLED exhibited stable characteristics, its performance was still lower than conventional ITO-OLEDs, which is related to the weaker microcavity effect of the classical graphene-OLED, suggesting a need to improve the optical efficiency of the device.

Chapter 3 describes the technology to improve the optical efficiency of graphene-OLED. First, a scattering layer, consisting of nanopillar and planarization layer, was introduced into the graphene-OLED, which is to extract the confined light into the device. Second, the optical absorption of graphene was minimized by reducing the number of graphene layers. Graphene-OLED with these modifications improved the external quantum efficiency (EQE) and the luminous efficacy (LE) by more than 50 %, to a value that is comparable to that of conventional OLEDs. The optical properties showed much less dependency on the viewing angle.

Chapter 4 describes the liquid bridging treatment developed to improve the graphene patterning process. Consisting of liquid bridging and thermal treatment, this treatment enhances the effective adhesion energy by a factor of two and reduces the roughness of the transferred graphene. This technology serves to minimize the process damage to graphene as well. It is shown that combining the liquid bridge treatment with photolithography, provides an accurate graphene pattern without process damages.

Chapter 5 describes the integrated fabrication of the graphene pixel electrodes and a large area OLED panel. Graphene pixel pattern was formed by the newly developed patterning process (chapter

4). The graphene-pixel electrode OLED showed excellent properties with a low leakage current and a high on/off current ratio. Based on this result, a two-color OLED panel with pixelated graphene electrodes was fabricated and showed successful operation. A flexible graphene-pixel electrode OLED panel was also successfully fabricated, which will also be described.

Chapter 6 is the Conclusion.

Reference

[1] J. H. Burroughes, D. D. C. Bradley, A. R. Brwon, R. N. Marks, K. Mackay, R. H. Friend, P. L. Burns, and A. B. Holmes, Nature, **347**, 539 (1990).

[2] Kido, J., Kimura, M. & Nagai, K. Science **267**, 1332 (1995).

[3] R. H. Friend, R. W. Gymer, A. B. Holmes, J. H. Burroughes, R. N. Marks, C. Taliani, D. D. C. Bradley, D. A. Dos Santos, J. L. Br´edas, M. Lögdlund, and W. R. Salaneck, Nature **397**, 121 (1999).

[4] Williams, E. L., Haavisto, K., Li, J. and Jabbour, G. E. Adv. Mater. **19**, 197 (2007)

[5] C. W. Tang and S. A. VanSlyke, Appl. Phys. Lett., **53**, 913 (1987).

[6] Y. Sun, N.C. Giebink, H. Kanno, B. Ma, M.E. Thompson, and S. R. Forrest, Nature **440**, 908 (2006).

[7] A. Rizzo, N. Solin, L.J. Lindgren, M.R. Andersson, and O. Inganäs , Nano Lett. **10**, 2225, (2010)

[8] J. Lee, J.-I. Lee, J.-W. Lee, H.Y. Chu, ETRI J. **33**, 32 (2011)

[9] E. L. Williams, K. Haavisto, J. Li, and G. E. Jabbour, Adv. Mater. **19**, 197 (2007).

[10] M. Ikai, S. Tokito, Y. Sakamoto, T. Suzuki, and Y. Taga, Appl. Phys. Lett. **79**. 156 (2001).

[11] M. A. Baldo, D. F. O'Brien, Y. You, A. Shoustikov, S. Sibley, M. E. Thompson, and S. R. Forrest, Nature **395**, 151 (1998).

[12] A. Endo, M. Ogasawara, A. Takahashi, D. Yokoyama, Y. Kato, and C. Adachi, Adv. Mater. **21**, 4802 (2009).

[13] H. Tanaka, K. Shizu, H. Miyazaki, and C. Adachi, Chem. Commun. **48**, 11392 (2012).

[14] H. Sasabe and J. Kido, J. Mater. Chem. C. **1**, 1699 (2013).

[15] W.-Y. Wong and C.-L. Ho, J. Mater. Chem. **19**, 4457 (2009).

[16] C. Adachi, M. A. Baldo, M. E. Thompson, and S. R. Forrest, J. Appl. Phys. **90**, 5048 (2001).

[17] S. Reineke, F. Lindner, G. Schwartz, N. Seidler, K. Walzer, B. Lüssem, and K. Leo. Nature **459**, 234 (2009).

[18] Heraeus graphic flexible display, Heraeus, C-Touch (2016)

[19] M. Stewart, R. S. Howell, L. Pires and M. K. Hatalis, IEEE Trans. Electron Devices **48**, 845 (2001)

[20] S.-H. K. Park, C.-S. Hwang, M. Ryu, S. Yang, C. Byun, J. Shin, J.-I. Lee, K. Lee, M. S. Oh, and S. lm, Adv. Mater. **21**, 678 (2009).

[21] L. Zhou, A. Wanga, S.-C. Wu, S. Park, and T. N. Jackson, **88**, 083502 (2006).

[22] J.-S. Park, H. Chae, H. K. Chung, and S. I. Lee, Semicond. Sci. Technol. 26, 034001 (2011).

[23] I. Yagi, N. Hirai, Y. Miyamoto, M. Noda, A. Imaoka, N. Yoneya, K. Nomoto, J. Nomoto, J. Kasahara, A. Yumoto, and T. Urabe, Journal of the SID **16**, 15 (2008).

[24] S. Logothetidis, Mater. Sci. Eng. **B152**. 96 (2008).

[25] J. Lewis, materialstoday, **9**, 38 (2006).

[26] S. Bae, H. Kim, Y. Lee, X. Xu, J.-S. Park, Y. Zheng, J. Balakrishnan, T. Lei, H. R. Kim, Y. I. Song, Y.-J. Kim, K. S. Kim, B. Özyilmaz, J.-H. Ahn, B. H. Hong, and S. Iijima, Nat. Technol. **5**, 574 (2010)

[27] M. Boehme, C. Charton, Surf. Coat. Technol. **200**, 932 (2005)

[28] Flexible AMOLED report, UBI research (2016)

[29] T. Sannicolo, M. Lagrange, A. Cabos, C, Celle, J.-P. Simonato, and D. Bellet, Small, **12**, 6052 (2016).

[30] J. Rivnay, S. Inal, B. A. Collins, M. Sessolo, E. Stavrinidou, X. Strakosas, C. Tassone, D. M. Delongcharmp, and G. G. Malliaras, Nat. Comm. **19**, 1 (2016).

[31] D. Zhang, K. Ryu, X. Liu, E. Polikarpov, J. Ly, Mark. E. Tompson and C. Zhou, Nano Lett. **6**, 1880 (2006).

[32] J. Lewis, S. Grego, B. Chalamala, E. Vick and D. Temple, Appl. Phys. Lett. 18, 3450 (2004).

[33] K. Fehse, K. Walzer, K. Leo, W. Lövenich, and A. Elscher, Adv. Mater. **19**, 441 (2007)

[34] J.-C. Charlier, X. Blase, and S. Roche, Review of Modern Physics **79**, 677 (2007).

[35] K. S. Novoselov, A. K Geim, S. V. Morozov, D. Jiang, Y. Zhang, S. V. Dubonos, I. V. Grigorieva, and A. A. Firsov, Science **306**, 666, (2004).

[36] C. Lee, X. Wei, J. W. Kysar, and J. Hone, Science **321**, 385 (2008).

[37] S. Pang, Y. Hernandez, X. Feng, and K. Müllen, Adv, Mater. **23**, 2779 (2011).

[38] P. Blake, P. D. Brimicombe, R. R. Nair, T. J. Booth, D. Jiang, F. Schedin, L. A. Ponomarenko, S. V. Morozov, H. F. Gleeson, E. W. Hill, A. K. Geim, K. S. Novoselov, Nano Lett. **8**, 1704 (2008).

[39] T.-B. Song and N. Li, Electronics **3**, 190 (2014).

[40] S. Bae, H. Kim, X. Xu, J.-S. Park, Y. Zheng, J. Balakrishnan, T. Lei, H. R. Kim, Y. I. Song, Y.-J. Kim, K. S. Kim, B. Izyilmaz, J. H. Ahn, B. H. Hong, S. Iijima, Nat. Nanotechnol. **5**, 574, (2010).

[41] T.-H. Han, S.-J. Kwon, N. Li, H.-K. Seo, W. Xu, K.S. Kim, T.-W. Lee, Angew. Chem. Int. Ed. **55**, 6197 (2016).

[42] H. Cho, S.D. Kim, T.-H. Han, I. Song, J.-W. Byun, Y.-H. Kim, S. Kwon, S.-H. Bae, H. C. Choi, J.-H. Ahn, T.-W. Lee, 2D Mater. **2**, 014002 (2015).

[43] J. Wu, M. Agrawal, H. A. Becerril, Z. Bao, Z. Liu, Y. Chen and P. Peumans, ACS Nano **4**, 43 (2010).

[44] D.W. Lee, T.-K. Hong, D. Kang, J. Lee, M. Heo, J.Y. Kim, B.-S. Kim, H.S. Shin, J. Mater. Chem. **21**, 3438 (2011).

[45] X. Wu, S. Li, Y. Zhao, Y. Tang, J. Liu, X. Guo, D. Wu, G. He, ACS Appl. Mater. Interfaces **6**, 15753 (2014).

[46] K.S. Kim, Y. Zhao, H. Jang, S.Y. Lee, J.M. Kim, K.S. Kim, J.-H. Ahn, P. Kim, J.-Y. Choi, B.H. Hong, Nature **457**, 706 (2009).

[47] X. Li, W. Cai, L. Colombo, R.S. Ruoff, Nano Lett. **9**, 4268 (2009).

[48] T. H. Han, Y. Lee, M.-R. Choi, S.-H. Woo, S.-H. Bae, B. H. Hong, J.-H. Ahn and T.-W. Lee, Nat. Photonics **6**, 105 (2012).

[49] N. Li, S. Oida, G.S. Tulevski, S.-J. Han, J.B. Hannon, D.K. Sadana, T.-C. Chen, Nat. Commun. **4**, 2294 (2013).

[50] J. Meyer, P.R. Kidambi, B.C. Bayer, C. Weijtens, A. Kuhn, A. Centeno, A. Pesquera, A. Zurutuza, J. Robertson, S. Hofmann, Sci. Rep. **4**, 5380 (2014).

[51] J. Lee, N. Chopra, and F. So, Appl. Phys. Lett. **92**, 033303 (2008).

[52] H. Cho, J.-W. Shin, N. S. Cho, J. Moon, J.-H. Han, Y.-D. Kwon, S. Cho and J.-I. Lee, IEEE J. Sel. Top. Quantum Electron. **22**, 2000306 (2016).

[53] Hwang, H. K. Choi, J. Moon, T. Y. Kim, J.-W. Shin, C. W. Joo, J.-H. Han, D.-H. Cho, J. W. Huh, S.-Y. Choi, J.-I. Lee and H. Y. Chu, Appl. Phys. Letts. **100**, 133304 (2012).

[54] J. Moon, J.-W. Shin, H. Cho, J.-H. Han, N. S. Cho, T. J. Lim, S. K. Park, H. K. Choi, S.-Y. Choi, J.-H. Kim, M.-J. Maeng, J. Seo, Y. Park and J.-I. Lee, Diamond Relat. Mater. **57**, 68 (2015).

2

Electrical and Optical Characterization of Graphene Electrode OLEDs

2.1 Introduction

Graphene has attracted much research interest as a material for transparent conducting electrodes (TCE) due to its atomically thin thickness, extremely high electrical conductivity as well as its high mechanical compliance. In particular, due to the emergence of technical importance for flexible OLED, graphene has been considered as a strong candidate for the flexible electrode [1]. Recent progress in commercial graphene has demonstrated the possibility of producing p-doped large area graphene with ~ 65 Ω/□ of sheet resistance and ~ 90% of transmittance at 550 nm wavelength [2]. These values are comparable to those of ITO (10~20 Ω/□, ~90% at λ = 500 nm). Its properties are summarized in table 2.1. Also, graphene has excellent mechanical properties (failure strain > 20%) compared to that of ITO (~ 1.5%) [3], which is important as the anode material for flexible OLED applications. However, graphene's optical properties are substantially different from those of conventional transparent electrode (ITO) [4] and thus have different impacts on the OLED performance. This chapter describes the optical and electrical evaluation of classical graphene-OLEDs. For this purpose, conventional graphene-OLEDs were fabricated (Fig. 2.1(a)). The optical and electrical properties of the graphene-OLEDs were compared to those of OLED with conventional

electrodes. Based on the results, the remaining issues of the conventional graphene-OLED will be discussed.

Figure 2.1. Comparison of properties of ITO and graphene.

	ITO	Graphene (With doping)
Work function (eV)	4.8	4.6
Transmittance (%)	92 (@ 550 nm)	90.8 (@ 550 nm)
Thickness	100 nm	4 layer
Sheet resistance	21 Ω/Sq.	65 Ω/Sq.
Failure strain	1.15%	>20%
Surface roughness	1 nm	1 nm

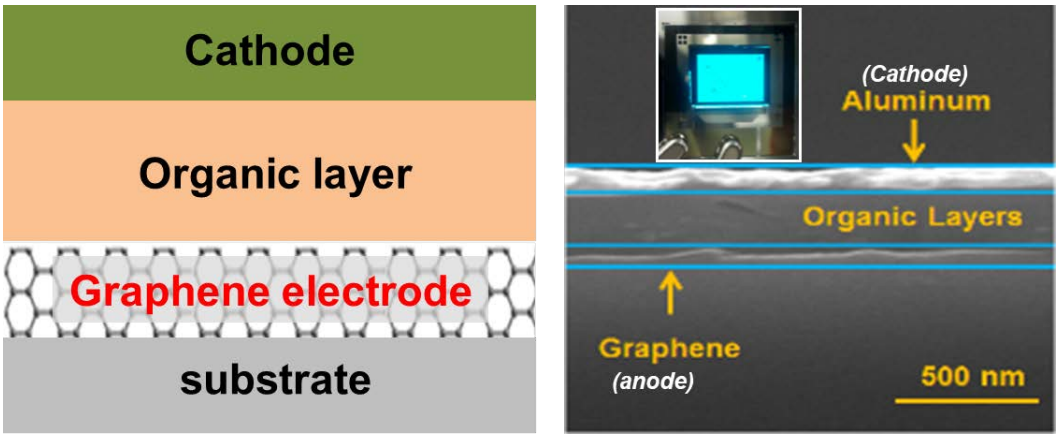

(a) (b)

Figure 2.1 (a) Schematic of graphene-OLED and (b) cross sectional image of graphene OLED.

(Inset is actual emission of graphene device)

2.2 Experimental methods

2.2.1 Graphene Preparation

In this chapter, four-layer-graphene films supplied from Hanwha Techwin R&D Center were used. Fig. 2.2 shows the graphene fabrication process. First, a single layer graphene was grown on the Cu film by a rapid thermal chemical vapor deposition (RT-CVD) process. The graphite susceptors were used for converting near-IR light into thermal radiation. CH_4 and N_2 gases were used for growth and cooling processes, respectively. Cu film was etched by using an etching solution containing H_2O, H_2SO_4 and benzimidazole. During the Cu etching process, benzimidazole p-dopes the graphene to have low sheet resistance. Four-layer-graphene films were prepared by repeatedly transferring the CVD-grown graphene by the thermal release tape (TRT) on the target substrate [5,6].

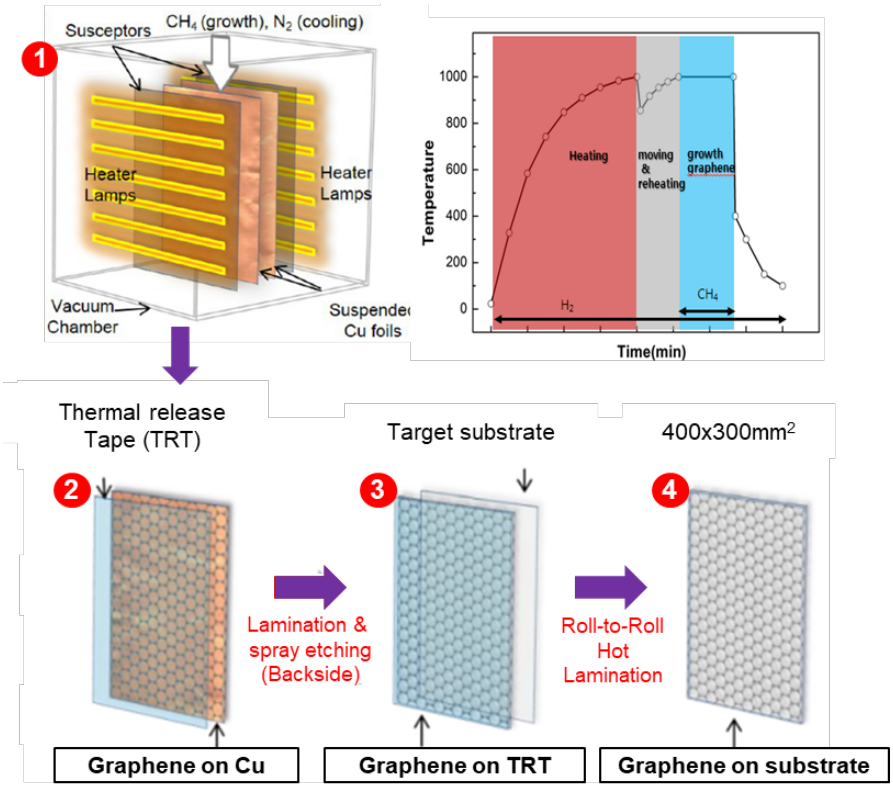

Figure 2.2. Schematic of graphene preparation processes.

2.2.2 OLED fabrication process

Figures 2.3(a) and (b) show the Schematic of the OLED fabrication process and device structures, respectively. OLEDs were fabricated using either ITO (100 nm) or four layers graphene as the TCE. In the case of graphene-OLED, the emitting area was defined by forming a non-conductive organic material banks on the graphene film. We used an alternating hole transport layer (HTL) 1,4,5,8,9,11-hexaazatriphenylene hexacarbonitrile [HAT-CN] (10 nm) and 1,1-bis[(di-4-tolylamino)phenyl]cyclohe-xane [TAPC] (40 nm) (t_{HTL}= 250 nm in total)/2,6-bis[30-(N-carbazole)phenyl]pyridine:Tris[2-phenylpyridinato-C2,N]Iridium(III) DCzPPy:-Ir(ppy)$_3$] (20 nm) as the emission layer (EML)/1,3-bis(3,5-dipyrid-3-yl-phenyl)benzene (BmPyPB) (60 nm) as the electron transport layer. The EML produced a green color with a main peak wavelength of λ = 517 nm. In order to stabilize the device, we used a hole-transport layer (HTL) with a thickness of 250 nm. Thick HTL can increase the operating voltage. To minimize the operating voltage, an alternating layer of NPB and HAT-CN was used as the HTL layer [7,8]. Such a stacking order improves the hole transport toward the emission layer. The active luminous area was 2×2 mm^2. All materials were electronics grade and were used without further purification. All organic layers were deposited in a high vacuum chamber below 6.67×10^{-5} Pa using a thermal evaporation method. LiF/Al was used as the cathode. To protect the organic layers from degradation by hydrogen and oxygen attacks, the fabricated OLEDs were encapsulated using a cavity-glass in a glove box.

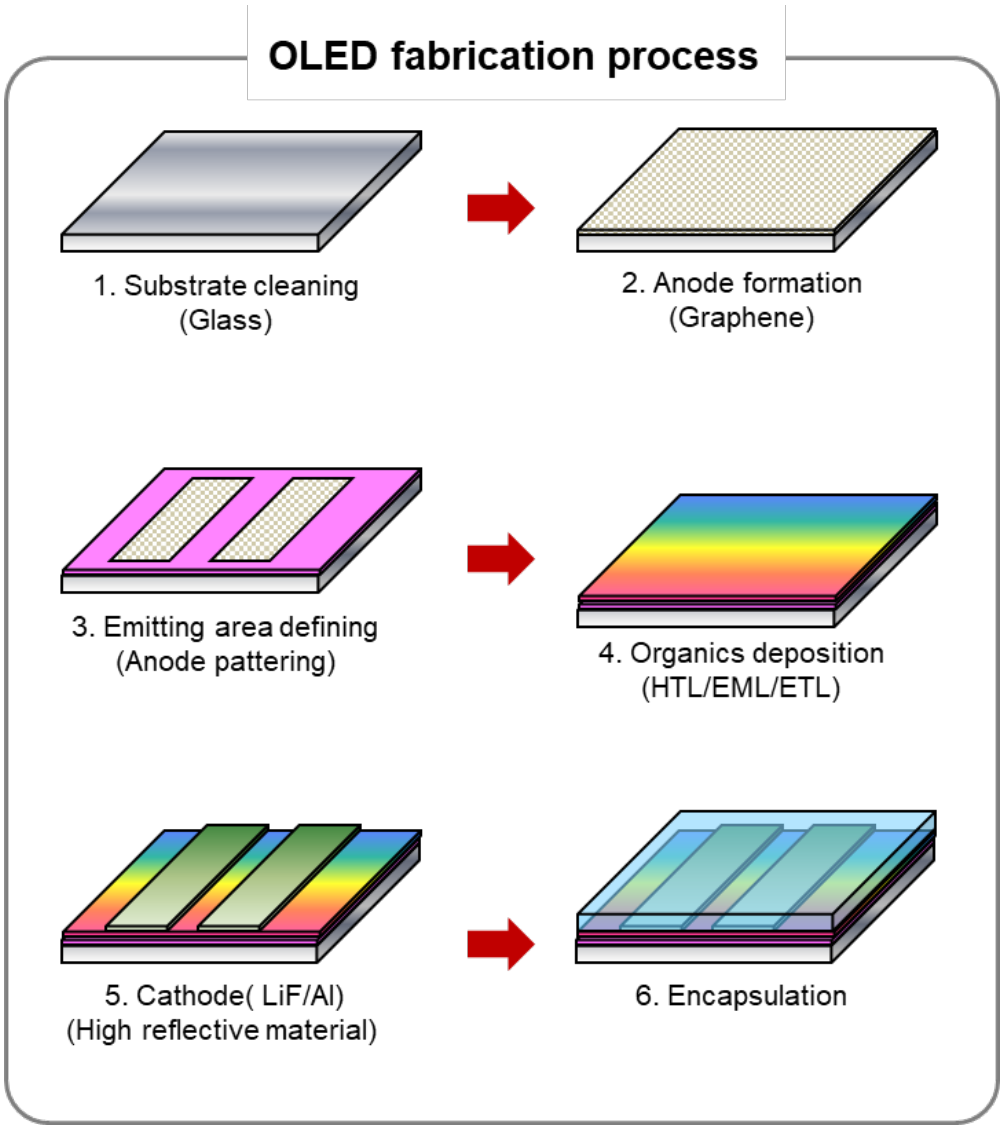
OLED fabrication process
1. Substrate cleaning
(Glass)
2. Anode formation
(Graphene)
3. Emitting area defining
(Anode pattering)
4. Organics deposition
(HTL/EML/ETL)
5. Cathode(LiF/Al)
(High reflective material)
6. Encapsulation

(a)

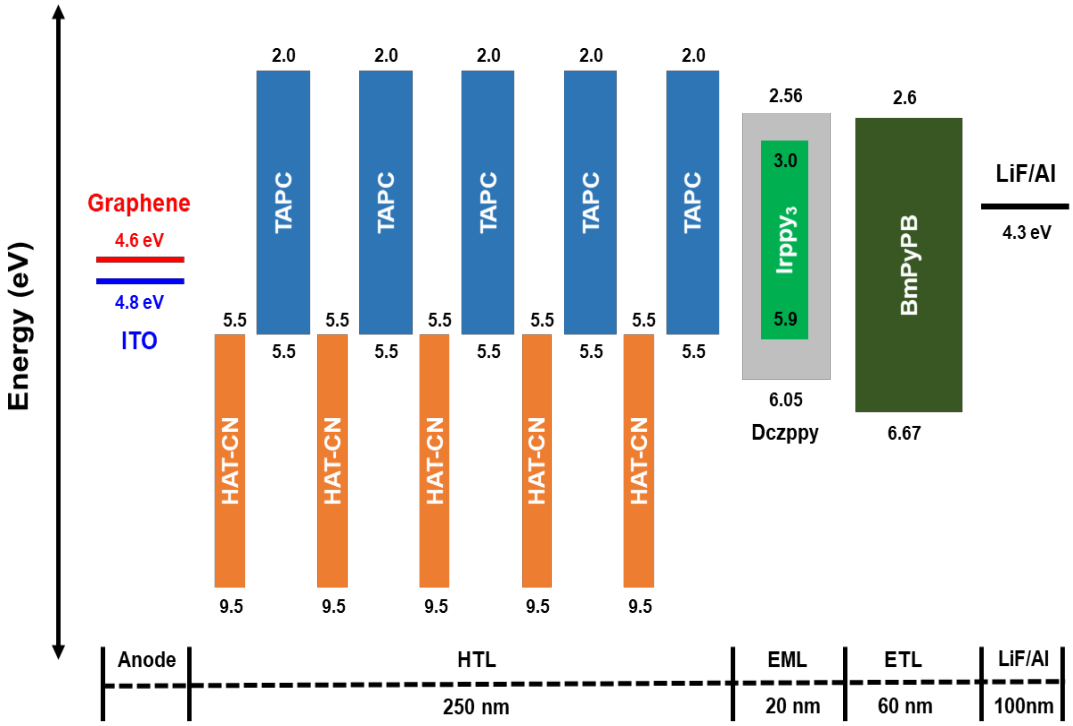

(b)

Figure 2.3. Schematic of OLED fabrication process (a) and device structures (b)

2.2.3 Characterization of graphene film

Graphene films were characterized by using the equipment shown in Fig. 2.4. Graphene sample was prepared on a glass substrate (Sample size; 20 mm × 20 mm). Sheet resistance of the graphene films was measured using a Hall measurement system (Model: HL 5500, Accent). To make a contact between probe and graphene with minimizing the contact damage, silver paste was pasted at four corners of the square specimen. The direct transmittance of the graphene films on the glass was measured using an UV visible spectrophotometer (Model: S-4100, SCINCO). Raman facility (Model: NTEGRA spectra, NT-MDT) was used to assess the quality of the graphene film surface. The surface morphology of graphene was observed using an atomic force microscope (Model: XE-100, PSIA).

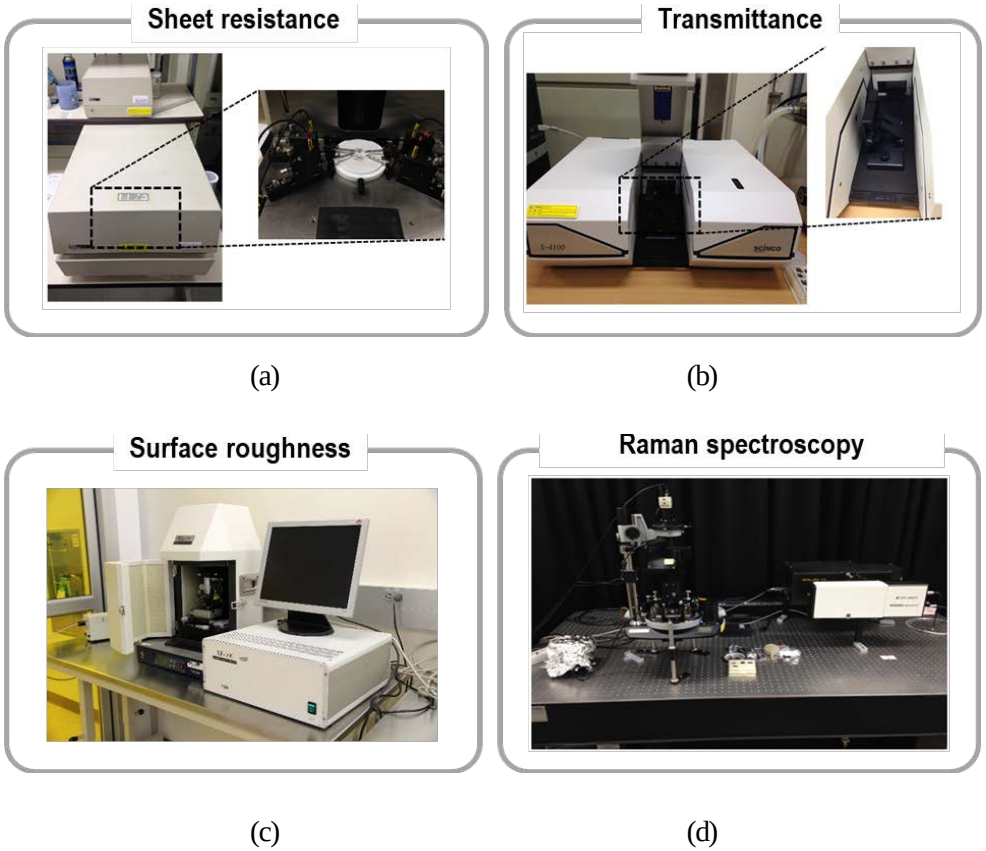

Figure 2.4. Measurement equipment of graphene films for (a) sheet resistance, (b) direction transmittance (c) surface roughness, and (d) graphene quality.

2.2.4 Characterization of graphene electrode OLED

Figure 2.5 shows the image of the actual OLED device, the concept of the measurement system and the output performance of the OLED in response to applied electrical signals. Fabricated OLED consists of four unit pixels on a 20 × 20 mm glass substrate. Each pixel has a luminous area of 2 mm × 2 mm. The current density–voltage (*J*–*V*) characteristics were measured using a current/voltage source unit (Keithley 238). The angular-dependent luminance and electroluminance (EL) spectra were measured using a goniometer-equipped spectroradiometer (Minolta CS-2000). The Efficiency of OLED was evaluated by EQE and LE using an integration half-sphere system (Otsuka electronics) at a constant current density level of 80 μA. The EQE is the ratio of the number of photons emitted by the OLED in all directions to the number of electrons injected. It can be defined as the total amount of photons came out from devices. The LE is the ratio of luminous power emitted to the total electrical power demanded to operate the OLED at a particular voltage. The LE was calculated using the photopic response of the human's eye and dependent on the visible wavelength of OLED spectrum. The EQE could be used to understand the fundamental physical mechanisms in response to light emission of OLEDs, whereas the LE is useful to interpret the power dissipated by a device within the OLEDs [9,10].

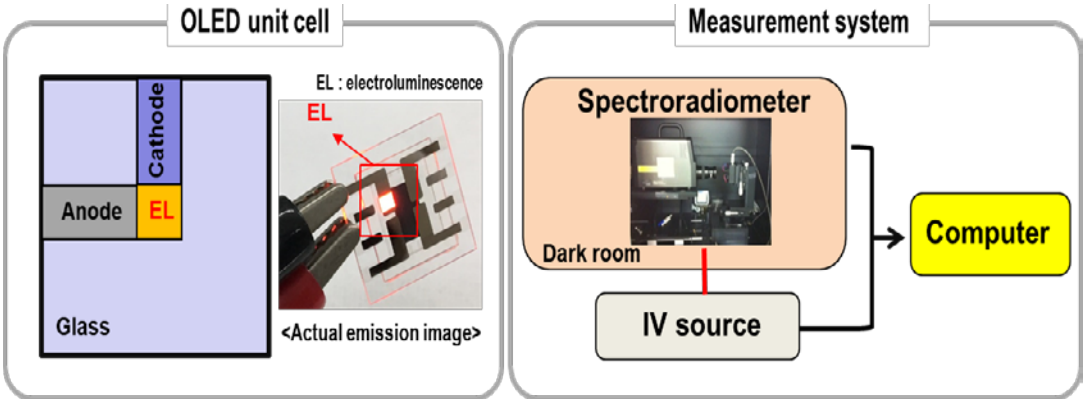

(a) (b)

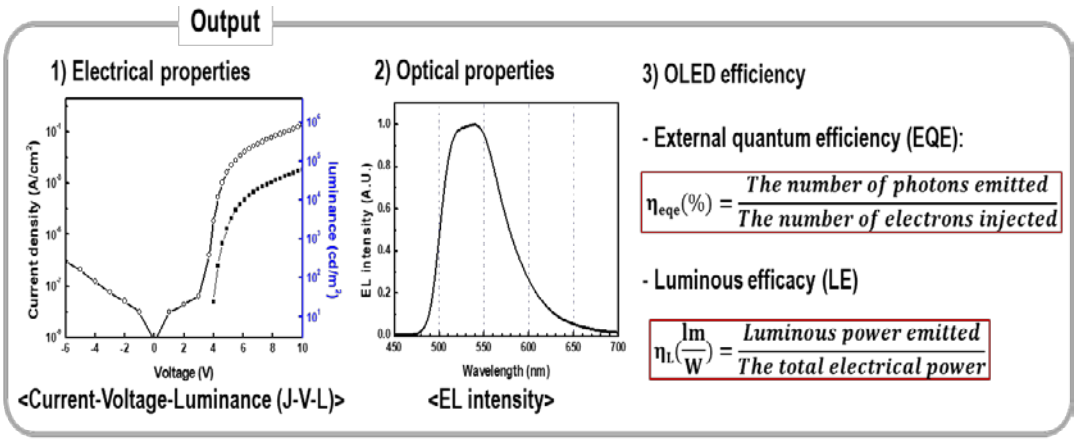

(c)

Figure 2.5. (a) Image of actual OLED unit cell, (b) measurement system and

(c) output performances of OLED devices.

2.3 Results and discussion

2.3.1 Properties of graphene film

In this chapter, we used graphene film with four layers which had similar optical and electrical properties to ITO. Figure 2.6 shows the direct transmittance (DT), the surface roughness (R_a) and the Raman spectra of the graphene films. Their properties are summarized in table 2.2. Our four-layer graphene film including the glass substrate has a DT of 82.2 % at 550 nm wavelength and a sheet resistance of 65 Ω/□. These values are comparable to those of ITO. The average R_a of graphene film was measured to be about 0.9 nm. Although this value is slightly higher than that for ITO (0.3 nm), it is still small enough to be applied for OLED. Raman spectroscopy is a useful tool in characterizing the graphene's quality [11,12]. Figure 2.6 (a) shows the Raman spectrum of the four-layer graphene film on the glass substrate, which exhibits peaks associated with graphene such as G-band at 1602 cm^{-1} and 2D band at ~ 2700 cm^{-1}. We also observed a small D-band at around 1350 cm^{-1}, which is defect-related. This D-band can be related to surface dislocations, corrugation, and interaction of graphene with the substrate [13]. In all the Raman spectra, the position and the intensity of each peak were almost identical regardless the measurement points in the sample, indicating that the graphene film was uniformly formed on the substrate.

Table 2.2. Measurement results of four-layer graphene film and ITO used in this chapter.

	Graphene	ITO
Thickness	4 layer	70 nm
Transmittance (%)	82.2 (@ 550 nm)	79.5 (@ 550 nm)
Sheet resistance	65 Ω/□	20 Ω/□
Average surface roughness (R_a)	0.9 nm	0.3 nm

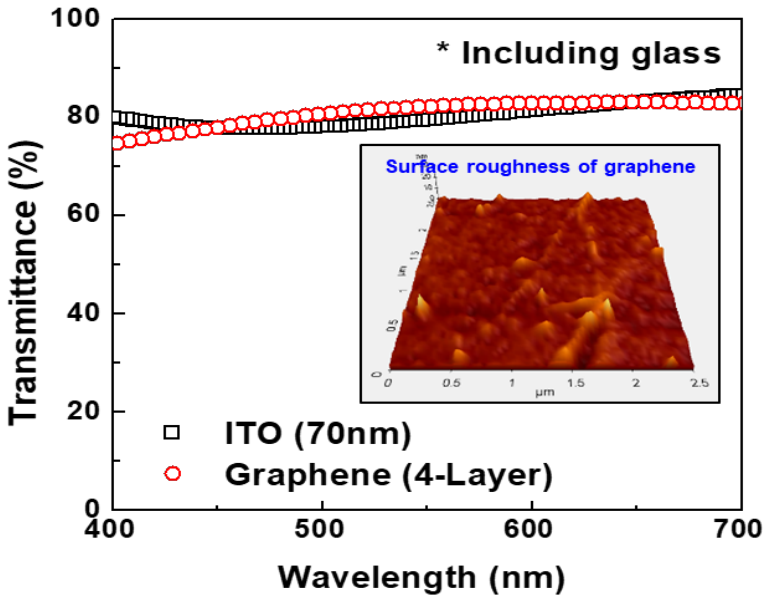

(a)

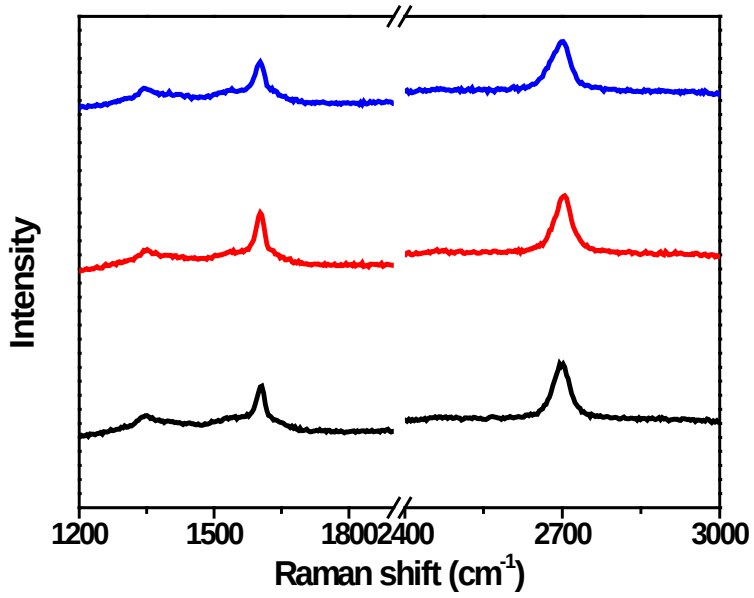

(b)

Figure 2.6. (a) The DT of four-layer graphene film and ITO (inset; surface morphology of graphene film) and (b) Raman analyses of four-layer graphene films.

2.3.2 Characteristics of graphene electrode OLED

Figure 2.7 (a) shows the luminance image of the OLED using graphene and ITO as the anode. In OLED, damages in the device components is reflected in the luminance image. The graphene-OLED shows a clear luminance image without any dark-spots, indicating that high-quality graphene films were formed on the glass substrate and no substantial damages were caused by the OLED fabrication processes. Figure 2.7 (b) presents the current density (*J*)-voltage (*V*)-luminance characteristics of graphene- and ITO-OLEDs. Although the graphene-OLED exhibits stable operating characteristics with a low leakage current level and a high on/off current ratio, the overall performance of the graphene-OLED is lower that of the ITO-OLED. At the same voltage of 5.2 V, the graphene-OLED and ITO-OLED show ~4 and ~13 mA/cm^2 in their *J* values, respectively, and their corresponding luminance values were ~2170 and ~6560 cd/m^2. The EQE and LE for both of the devices are summarized in Table 2.3. The graphene-OLED has lower efficiencies than those of ITO-OLED. Two factors can be considered that would limit the graphene-OLED performance. First is the electrical factor related to graphene such as the high sheet resistance, different surface quality, and the low WF [14]. Such factors may impede efficient hole injection from the electrode to the organic layer and would limit the electrical conductivity of the graphene in the OLED. The other is the optical factor, related to the lack of microcavity effect in the graphene-OLED. The microcavity effect is an optical interference phenomenon. Under a constructive interference condition, the out-coupling efficiencies of the OLED are maximized but with a distortion accompanied with a strong viewing angle dependence [15,16]. In conventional OLEDs, the microcavity effect has been an efficient means for improving the light extraction efficiency. In graphene-OLED, however, this microcavity effect is very weak because of the low reflectance of graphene. The influence of microcavity effect on OLEDs will be discussed in detail in chapter 3.

To characterize the optical properties of the graphene-OLED, the luminance and 1931 Commission internationale del'éclairage (CIE) color coordinates and EL spectra of the graphene-OLED were measured as a function of the viewing angle (Fig. 2.8). Unlike ITO-OLED, graphene-OLED showed lambertian-like luminance distributions and negligible viewing angle dependency in CIE coordinate and EL spectra. This is due to the diminished microcavity effect in the graphene-OLED.

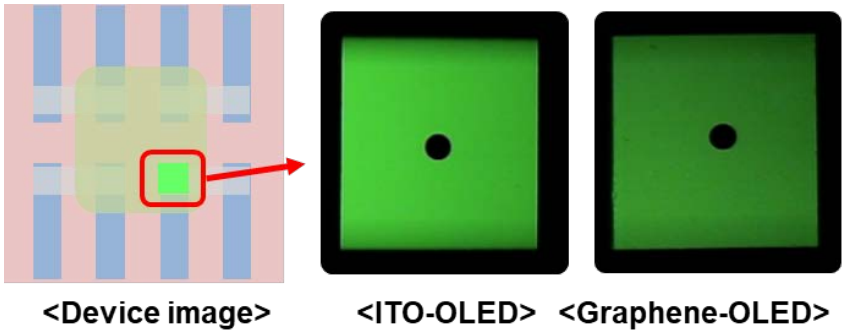

(a)

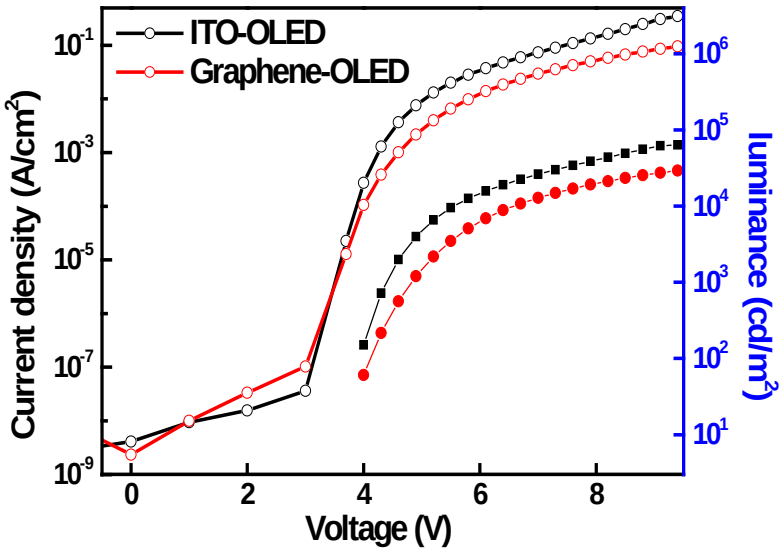

(b)

Figure 2.7. (a) The luminance image, (b) *J-V*-luminance characteristics and (c) the angular-dependent luminance of the graphene-OLED and the ITO-OLED.

Table 2.3. Absolute value of the EQE and LE of the OLED with graphene and ITO.

	Graphene-OLED	ITO-OLED
EQE (%)	18.04	22.5
LE (lm/W)	40.79	58.16

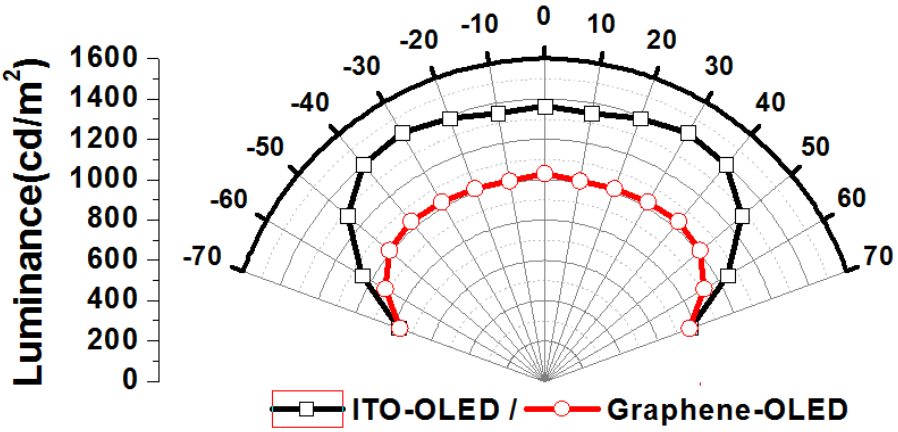

(a)

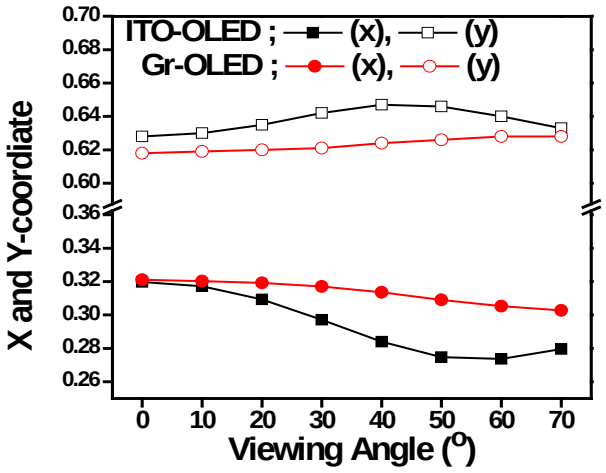

(b)

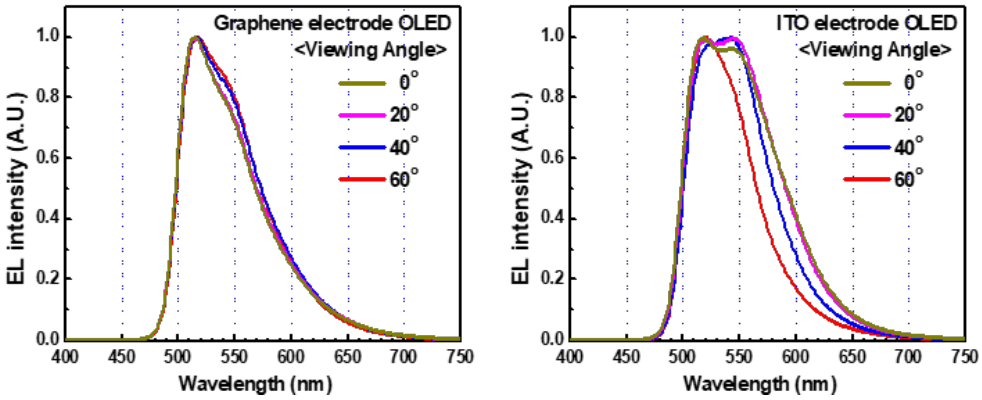

(c)

Figure 2.8. (a) CIE color coordinates and (b) the angular-dependent EL spectra of the graphene-OLED and the ITO-OLED.

2.4 Conclusion

In chapter 2, a classical graphene-OLED has been fabricated and evaluated. Graphene was CVD-grown on a Cu catalytic substrate and was transferred to the glass substrates. It has a DT of 82.2 % at 550 nm wavelength and sheet resistance R_{sh} of 65 Ω/□, respectively, which values are comparable to those of ITO. Although the graphene-OLED exhibits stable electrical and optical properties, its overall performance is lower that of the ITO-OLED. EQE and LE of graphene-OLED is approximately 80% and 70% of ITO-OLEDs, respectively. This lower performance is attributed to the lower electrical conductivity and the weaker microcavity effect in the graphene-OLED. In particular, the microcavity effect, which originates from the reflectance of the anode, is weaker in the graphene-OLED than that in ITO-OLED due to its lower reflectance. This lack of microcavity effect in graphene-OLEDs limits the out-coupling efficiency, but with improved optical stability over a wide angle range. Although graphene has several attractive properties as the anode for OLED, new technologies need to be developed to enhance the efficiency of graphene-OLED. In chapter 3, we will discuss the light extraction method to improve the optical efficiency of graphene-OLEDs.

Reference

[1] S. Pang, Y. Hernandez, X. Feng, and K. Müllen, Adv. Mater. **23**, 2779 (2011)

[2] J. Moon, J.-H. Han, J.-W. Shin, H. Cho, B.-H. Kwon, J.-I. Lee, S. Cho, and N. S. Cho, IMID'17 Technical Digest (2017)

[3] T.-H. Han, H. Kim, S.-J. Kwon, and T.-W. Lee, Mater. Sci. Eng. R Rep. **118**, 1, (2017)

[4] F. Bonaccorso, Z. Sun, T. Hasan and A. C. Ferrari, Nat. Photonics **4**, 611 (2010).

[5] J. Ryu, Y. Kim, D. Won, N. Kim, J. S. Park, E.-K. Lee, D. Cho, S.-P. Cho, J. S. Kim, G. H. Ryu, H.-A.-S. Shin, Z. Lee, B. H. Hong and S. Cho, ACS nano **8**, 950 (2014).

[6] S. J. Kim, J. Ryu, S. Son, J. M. Yoo, J. B. Park, D. Won, E.-K. Lee, S.-P. Cho, S. Bae, S. Cho and B. H. Hong, Chem. Mater. **26**, 2332 (2014).

[7] C. W. Joo, J. Moon, J. Hwang, J.-H. Han, J.-W. Shin, D.-H. Cho, J. W. Huh, H.Y. Chu, J.-I. Lee, Jpn. J. Appl. Phys. **51**, 09MH01 (2012).

[8] W. S. Jeon, J.S. Park, L. Li, D. C. Lim, Y. H. Son, M. C. Suh, J. H. Kwon, Org. Electron. **13**, 939 (2012).

[9] S. R. Forrest, D. D. C. Bradley, and M. E. Thompson, Adv. Mater. **15**, 1043 (2003).

[10] N. C. Greenhamm R. H. Friend, D. D. C. Bradley, Adv. Mater. **6**, 251 (1994).

[11] D. S. Lee, C. Riedl, B. Krauss, K. V. Klitzing, U. Starke, and J. H. Smet, Nano Lett. **8**, 4320 (2008).

[12] A. C. Ferrari, J. C. Meyer, V. Scardaci, C. Casiraghi, M. Lazzeri, F. Mauri, S. Piscanec, D. Jiang, K. S. Novoselov, S. Roth, and A. K. Geim, Phys. Rev. Lett. **97**, 187401 (2006).

[13] Z. H. Ni, W. Chen, X. F. Fan, J. L. Kuo, T. Yu, A. T. S. Wee, and Z. X. Shen, Phys. Rev. B **77**, 115416 (2010).

[14] H. Cho, S. D. Kim, T.-H. Han, I. Song, J.-W. Byun, Y.-H. Kim, S. Kwon, S.-H. Bae, H. C. Choi, J.-H. Ahn, T.-W. Lee, 2D Mater. **2**, 014002 (2015).

[15] V. Bulovic, V. B. Khalfin, G. Gu, P. E. Burrows, D. Z. Garbuzov, S. R. Forrest, Phys. Rev. B **58**, 3730 (1998).

[16] S.-H. Cho, Y.-W. Song, J.-G. Lee, Y.-C. Kim, J. H. Lee, J. Ha, J.-S. Oh, S. Y. Lee, S. Y. Lee, K. H. Hwang, D.-S. Zang, Y.-H. Lee, Opt. Express **16**, 12632 (2008).

3

Improvement of Light Extraction Efficiency of Graphene Electrode OLEDs

3.1 Introduction

Graphene has attracted attentions due to its benefitting properties as a transparent electrode to OLEDs. However, the efficiencies of the graphene-OLED have been lower than those of conventional OLEDs (e.g. ITO-OLED). A most likely reason for this lower efficiencies is the weaker microcavity effect confronted in graphene-OLED [1]. The microcavity effect has been used as an effective way to improve the light extraction efficiency of OLEDs. In graphene-OLED, this microcavity is weakened due to the low reflectance of graphene electrode. In order for graphene to be used in flexible OLEDs, therefore, it is necessary to develop a technology that compensates the weak microcavity effect. In this chapter, several efforts to improve the optical efficiency of graphene-OLED will be presented. The first one is the introduction of a light extraction layer. A typical OLED is composed of a stack of layers with different refractive indices, which sometimes optically confines the generated light within the device, lowering the out-coupling efficiency of the OLED. This optical loss occurs in the graphene-OLED as well and hinders the extraction of light from the device. The light extraction layer is an efficient method for overcoming this. It is a layer to alter the light paths to facilitate the escape of the emitted light from the device, which significantly reduces the internal reflection and thereby improves the light extraction efficiency [2]. The second strategy is to minimize

the optical absorption in the graphene electrode. Since graphene has an optical absorption of about 2.3% per layer, the absorption should increase in proportion to the number of graphene layers [3]. We investigated the impacts of varying the number of graphene layers on the optical properties of the graphene-OLEDs. Finally, optical simulations were conducted to optimize the OLED performance, and the optical and electrical properties of the optimized graphene-OLEDs were compared to those of OLEDs with conventional electrodes.

3.2 Optical components in graphene electrode OLEDs

3.2.1 Influence of microcavity effect on graphene-OLEDs

Microcavity effect, which is similar to the principle of Fabry-Pérot interferometer, is present when the light is spatially confined between two parallel mirrors [4,5]. In the case of OLED, the microcavity exists between the transparent anode and the reflective cathode. Microcavity is an optical interference phenomenon and can improve the out-coupling efficiency of OLED under a constructive condition [6,7]. Figure 3.1(a) schematically describes the structure of conventional OLED. In the OLED, the light generated in the emissive layer propagates not only in the glass direction (E_D) but also in the cathode direction (E_U). Some portion of the light toward to glass escapes out of the device, but some are reflected at the anode/glass interface (R_D) and on the metallic cathode (R_u). The microcavity effect is based on multi-beam interference between the emitted and the reflected lights and the light is eventually circulating in the OLED (E_{cir}) [8].

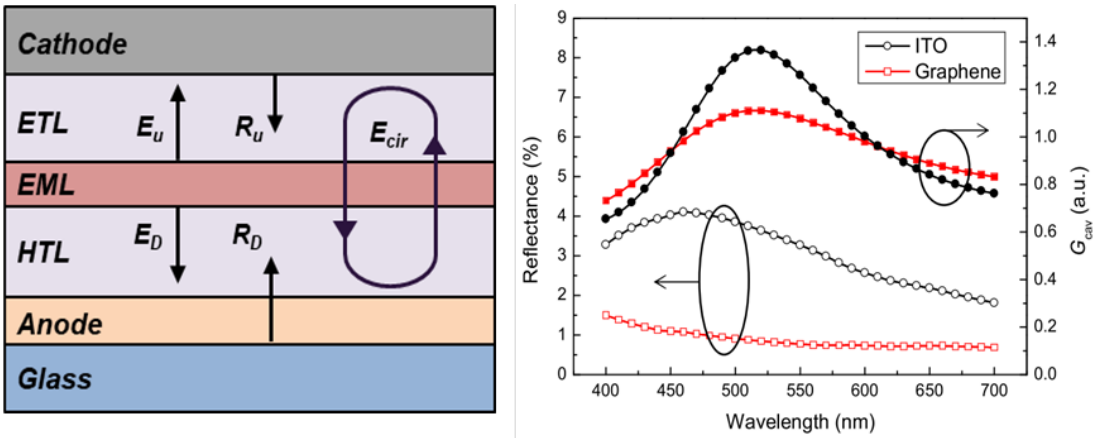

(a) (b)

Figure 3.1. (a) Schematic of OLED structure and optical components. (b) The simulated cavity enhancement factor of ITO and graphene [9].

The microcavity effect strongly depends on the optical length (the organic thickness) between the anode and the cathode. By adjusting the thicknesses of the organics, therefore, the interference can be constructive, destructive and something in between. In order to maximize the efficiency of OLEDs, the organics thickness has to be chosen at the constructive interference condition. Figure 3.2 shows the simulated efficiencies of ITO- and graphene-OLED as a function of the organic thickness. Here, the efficiency refers to the radiance. Radiances of both devices are observed to oscillate in a sinuous wave, which implies the presence of the microcavity effect. The ITO-OLED and graphene-OLED show a maximum radiance at the organic thickness of 140 nm and 210 nm, respectively, which is the constructive interference condition for each device. Compared with ITO-OLED, graphene-OLED shows a lower maximum radiance and a low dependency of the radiance on the organic thickness. The microcavity effect is dependent on the reflectance of the anode as well as the thickness of the organic layer. Because graphene's reflectance is much smaller than that of ITO, the microcavity effect should be weaker in graphene-OLEDs. To overcome this efficiency issue in graphene-OLED, we need to develop a technology that compensates the graphene's weak microcavity effect [9,10].

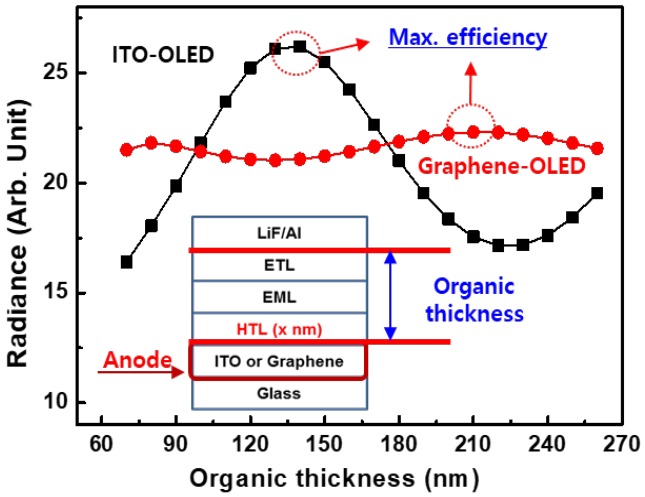

Figure 3.2. The radiance of OLEDs with ITO and graphene anode as a function of the organic thickness.

3.2.2 Optical losses in the OLEDs

The external quantum efficiency (EQE) of the OLED can be expressed as the product of internal quantum efficiency (IQE) and the light extraction efficiency [11]. As for the former, the development of efficient phosphorescent materials as the emissive layer has already achieved ~~the~~ almost 100% for IQE. Furthermore, the stack design of OLEDs considering the band alignment can also enhance the performance of the device by facilitating the charge transport. However, OLEDs still suffer from poor EQEs of ~20% or lower because of the low light extraction efficiency. A huge amount of the generated light is confined within the device as various loss modes [12,13]. The largest loss occurs in the refractive index difference of the constituent layers. Another important loss takes place at the metal/organic interface as the surface plasmon polariton (SPP) [14]. Most of the optical losses in OLEDs occur at the anode/glass interface as the waveguided mode and at the glass/air interface as the substrate mode. Figure 3.3 shows the simulated optical mode analysis in the ITO- and graphene-OLEDs as a function of the HTL thickness, and table 3.1 summarizes the average values of each mode. These optical losses exist in the graphene-OLED as well. Due to the presence of the microcavity effect, the optical modes in ITO-OLEDs depend on the HTL thickness. For graphene-OLED, however, the weaker microcavity effect has made graphene-OLED less dependent on the HTL thickness. From these results, we confirmed that a substantial amount of light was confined inside the graphene-OLED. Also, it could also be expected that by applying the light extraction method, the efficiency of graphene-OLEDs can be improved up to the level of ITO-OLEDs.

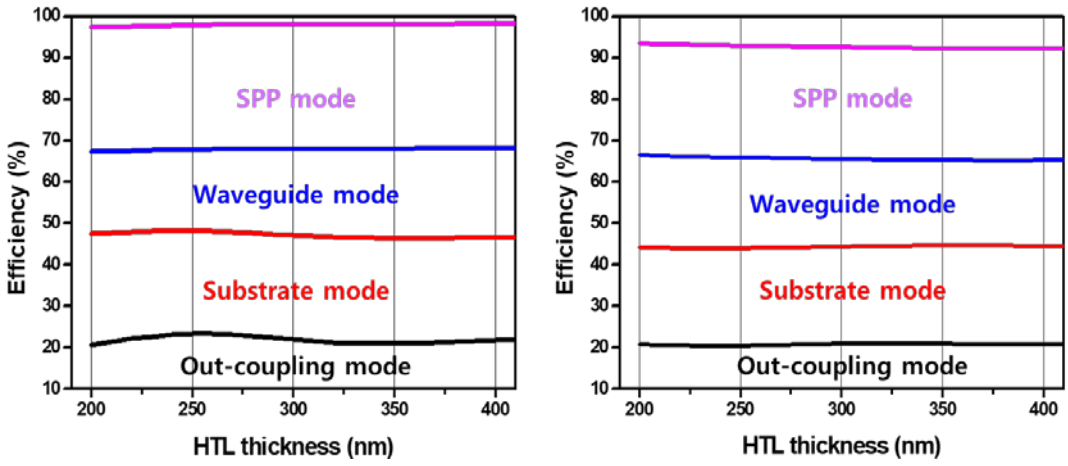

(a) (b)

Figure 3.3 Simulated optical mode analysis in ITO-OLEDs (a) and graphene-OLED.

Table 3.1. Summary of the average values of each mode for graphene-OLEDs and the ITO-OLEDs.

	Out-coupling mode	Substrate mode	Waveguide mode	SPP mode
ITO-OLED	21.95 %	25.17 %	20.82 %	30.2 %
Graphene- OLED	20.76 %	23.65 %	21.23%	27.2 %

3.2.3 Internal scattering layer

To extract the light confined in the OLED, several light extraction methods have been suggested and applied to OLEDs. The substrate mode can be extracted by attaching an external light extraction film such as micro-lens arrays, diffuser films and wrinkle films on the outside of the substrate [15,16]. However, these methods are difficult to apply to OLED display technologies which require a high resolution due to the high light diffusion properties. From this viewpoint, internal light extraction methods are advantageous for OLED display applications. In order to extract the optical loss due to the waveguided mode, the influence of the internal light extraction layer on the optical and electrical properties of OLEDs has to be considered. Most of the reported methods have technical problems which include distorted and shifted emission spectra, wavelength dependency on the extraction layer, and unstable electrical performance [17-19]. Recently, substrates with random textures have been proposed to solve these problems and improve the light extraction efficiency of the OLED [20,21]. These structures can alter the incident light path from the emitting layer to the glass substrate, resulting in a significant reduction of waveguided mode and total internal reflections. By using a random structure, the dependency and distortion of particular wavelengths can be avoided. In our approach, to improve the light extraction efficiency, we applied the scattering layer into graphene-OLED between the substrate and graphene as an anode. Figure 3.4(b) shows our scattering layer which consists of a random nanostructure and a planarization layer. The planarization layer plays an important role in preventing the electrical degradation of OLEDs due to the surface roughness such as the nanostructure. The effect of the scattering layer in the OLED can be observed in the simulation result shown in Fig 3.4(c) and (d). In the OLED without the scattering layer (Planar device), there are confined light in the OLED due to the waveguided mode. When the scattering layer was applied, a significant reduction in the confined light was observed due to the scattering effect. Our scattering layer is useful as a light extraction method to improve the performance of OLEDs [22].

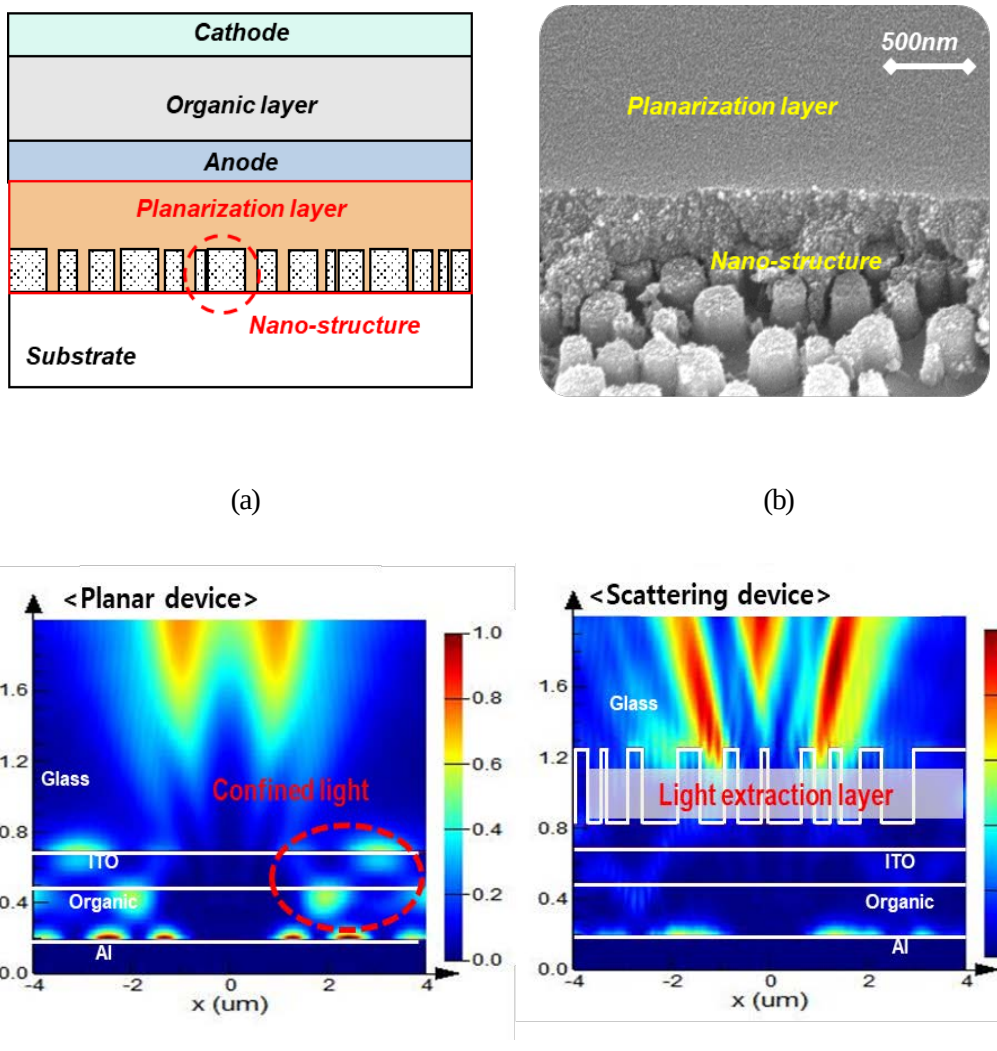

Figure 3.4 (a) Schematic of the OLED equipped with scattering layer, (b) the scattering layer. Electric field distributions in the OLED without the scattering layer (c) and with the scattering layer (d).

3.3 Experimental methods

Figure 3.5 presents the process flow of the scattering layer formation. First, a SiO_x layer of 500 nm thickness and an Ag film of 30 nm thickness were sequentially deposited on the glass substrate. The SiO_x and Ag layers were deposited by plasma-enhanced chemical vapor deposition and thermal evaporation methods, respectively. Second, the sample was heated to 250 ^oC in order to rupture the Ag film; this process resulted in formation of irregularly distributed Ag particles. Nano-sized Ag droplets were formed by thermally assisted dewetting process. To form the scattering layer, the exposed portion of the SiO_x layer was etched using an induction-coupled plasma etching method. A mixture of CF_4 and Ar gas was used as the etching gas. And then, the Ag mask was removed using HNO_3 etchant. The scattering layer consists of irregular nano-sized pillar with a random distribution. The planarization layer had a higher refractive index (n = 1.81 at a wavelength of 550 nm) than the nanostructure (n = 1.48). This refractive index difference was sufficient to produce the scattering effect for the light extraction. To planarize the scattering structure, a 1.5-μm-thick layer of SiN_x was deposited on the scattering structure and the film was then polished using cerium as a slurry until it reached a total thickness of 1 μm including the scattering structure, to remove the residual surface roughness. The graphene was finally transferred onto the target substrate using a thermal release tape method. The active luminous area was 2 mm × 2 mm. In the case of graphene-OLED, the emitting area was defined by forming a non-conductive organic material banks on the graphene film. Each device contained a stack structure of graphene (one, two, and four layers)/an alternating HTL structure of HAT-CN (10 nm) and TAPC (40 nm) (t_{HTL} = 250 nm in total)/ DCzPPy:$Ir(ppy)_3$ (20 nm) as the emission layer (EML)/ BmPyPB (60 nm) as the electron transport layer. The EML produced a green color with a main peak wavelength of λ = 517 nm (Fig. 2.3 (b)). The optical simulations were conducted using SETFOS (Fluxim), which is an OLED-specialized simulator. To obtain realistic

results, we extracted the optical constants (n: k) of the organic materials, which were measured using an ellipsometer (M-2000D, J.A. Woolam Co.).

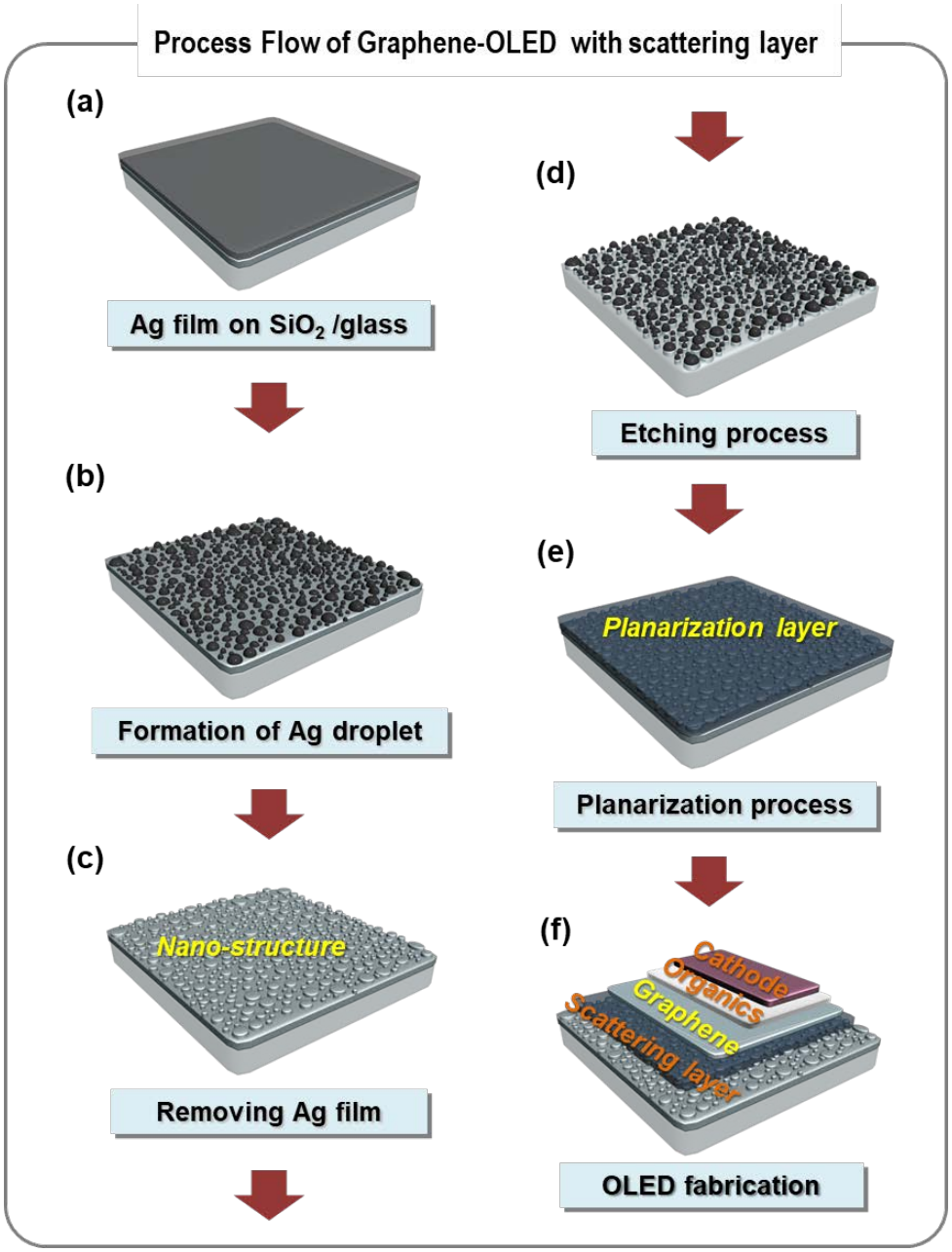

Figure 3.5. Process flows of the OLED with the scattering layer; (a) Deposition of Ag thin films, (b) Formation of Ag droplet by a thermally assisted dewetting process, (c) Dry etching substrate uncovered the Ag droplet, (d) Removal of Ag droplet for formation the nano-structure, (e) Planarization process on the nano-structure and (f) Graphene transfer on the scattering layer and OLED fabrication.

3.4 Results and discussion

3.4.1 Structural properties of the scattering layer

The nanostructure was composed of nano-pillars with their height of ~500 nm and diameters of 300–500 nm, with a proper random distribution as shown in Figs. 3.6(b) and (c). Such a structure can effectively diffuse the incident light from the organic light-emitting layer and reduce the optical confinement [23]. In addition, unlike periodic structures with fixed feature sizes, it enables wavelength-independent optical scattering of all visible lights [24,25]. Surface planarization is essential when using a nanostructure in an OLED because a rough surface can easily degrade the operational stability of the OLED. The planarization layer should reduce the surface roughness without causing micro-faults and transfer the light generated in the light-emitting layer to the nanostructure without substantial absorption. The planarization layer material and its fabrication process should not degrade the graphene properties. In a previous study, we used an organic/TiO_2 sol-based hybrid material for the planarization layer [26]. However, this material was inadequate as a supporting layer for graphene because of its friable surface with a roughness (R_a) of approximately 2.1 nm, which is greater than the thickness of monolayer graphene. In this study, silicon nitride (SiN_x) was chosen as the planarization layer material to satisfy the aforementioned requirements. This planarization process significantly decreased the surface roughness, from 500 nm to 0.4 nm, as shown in Figs. 3.6(d) and (e).

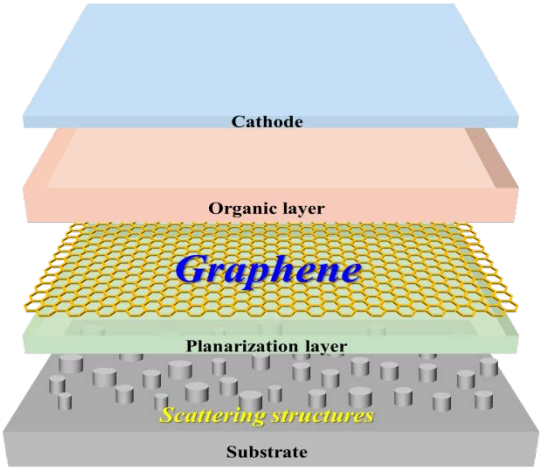

(a)

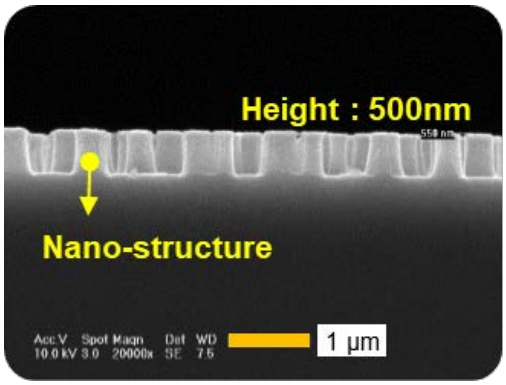

(b)

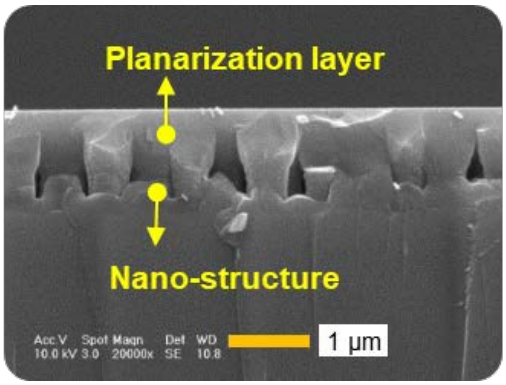

(c)

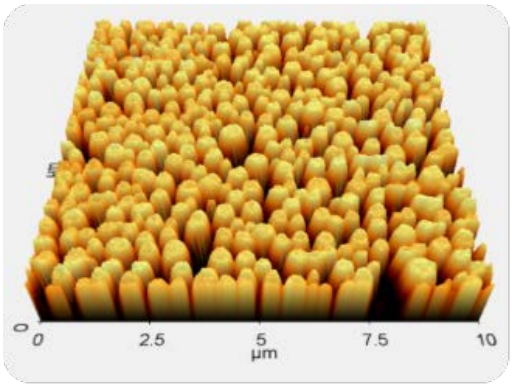

(d)

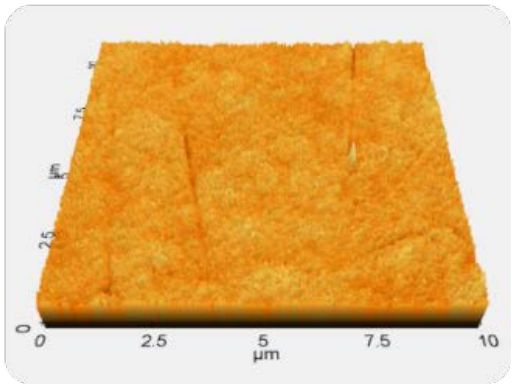

(e)

Figure 3.6. Schematic of graphene-OLED with the scattering layer (a), SEM image of the nanostructure (b) and (c), and AFM measurement of the nanostructure (d) without and with the planarization layer.

3.4.2 Electrical and optical properties of the scattering layer

The sheet resistance (R_{sh}) (Fig. 3.7(a)) and the direct transmittance (DT) (Fig. 3.7(b)) of the graphene films on the glass and on the scattering layer were measured. As the number of graphene layers increases, both the sheet resistance and DT decrease. The R_{sh} of monolayer and four-layer graphene film are approximately 270 Ω/□ and 70 Ω/□, respectively. The graphene films on the scattering layer exhibit sheet resistances slightly lower than those of the films on glass. This is attributed to the SiN_x in contact with the graphene. Previous studies also suggest that the graphene's R_{sh} decrease if the dielectric constant of the layer supporting the graphene increases [27], but no significant impact is evident in the present results. The DT decreased with the number of graphene layers for both "graphene only" and "graphene on scattering layer" samples (Fig. 3.7(b)). The DT of the graphene/glass structure was higher than that of the graphene/scattering layer/glass structure. Since the glass substrate used in the experiment has a DT value that is higher than 95% whole the visible range, the transmittance is primarily affected by the layers on the glass. For the graphene on the glass samples, DT was always larger than 70% while it never exceeded 50% in the "graphene on scattering layer" samples. The scattering layer with a nano-structure diffuses the incident light in forward directions. This result demonstrates the scattering layer's capacity of widely diffusing the incident light. This light diffusion, expressed as a diffuse transmittance, amounts 31% in our scattering layer, which was higher than that of the glass substrate (less than 1%).

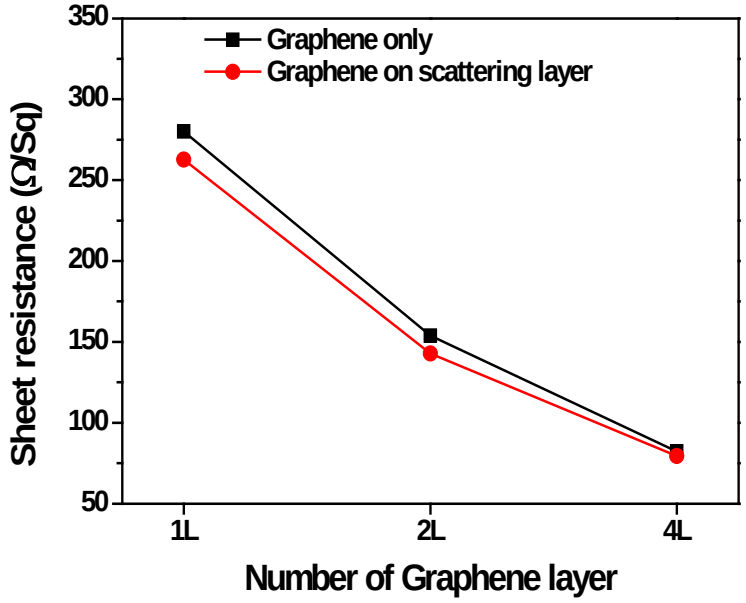

(a)

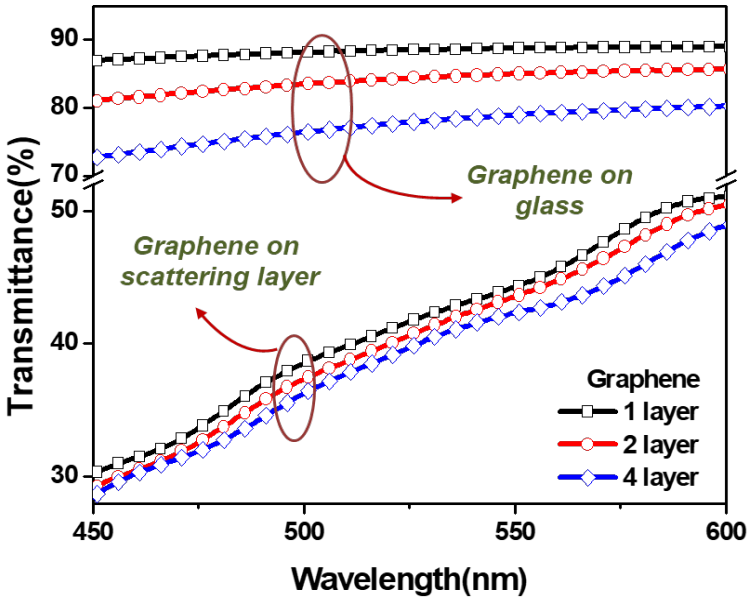

(b)

Figure 3.7. The sheet resistances (a) and the direct transmittances (b) of the graphene films on the glass and on the scattering layer with the variation of the graphene layer as one, two, and four.

3.4.3 Simulation analysis of graphene-OLED with light extraction methods

Figure 3.8 presents the simulation results. The simulation was made assuming the multiple interference, with the layer thickness and the optical constants being chosen as the main parameters. The thickness of the graphene layer was varied for one, two, and four atomic layers while the thickness of the monolayer graphene was fixed at 0.34 nm. To consider the microcavity effect, which changes as a function of the OLED thickness, the hole transport layer (HTL) thickness (t_{HTL}) was varied from 250 nm to 400 nm. The HTL plays an important role in facilitating the hole charge transport in OLED structures [28,29]. For comparison, we also conducted a simulation on the OLED with an oxide anode (indium zinc oxide: IZO). The radiance of the graphene-OLEDs increases as the number of graphene layers decreases for a fixed t_{HTL} value. Its dependence on t_{HTL}, however, is not so sensitive as that of the IZO-OLED. Although the graphene-OLEDs exhibit higher radiances than that of the IZO-OLED for t_{HTL} ~ 350 nm, the order is inverted for t_{HTL} values greater than 360 nm. The radiance of the IZO-OLED significantly oscillates in a sinusoidal fashion due to its strong microcavity effect, and its highest value at t_{HTL} = 380 nm is greater than any values of graphene-OLEDs. Because graphene has a lower reflectance than IZO, the microcavity effect is weak in graphene-OLEDs and their efficiency is rather insensitive to the HTL thickness [9].

The increase of the radiance with the decrease of the number of graphene layers is ascribed to the reduced optical absorption in the graphene electrode. The extinction coefficient (k) of monolayer graphene was reportedly larger than 1 [31,31], which obviously attenuates the light passing through the graphene. To explore the maximum attainable radiance, we conducted a simulation on a monolayer graphene-OLED with a virtual k of zero (open squares in Fig. 3.8(a)). Even in this case, however, the radiance could not exceed the maximum value of the IZO-OLED at t_{HTL}~ 380 nm. This result clearly indicates that it is not possible for a graphene-OLED, without additional light extraction methods, to exceed the efficiency of OLEDs with conventional oxide electrodes. To explore

alternative possibilities, we examined introduction of a scattering layer between graphene and the substrate using the simulation (Fig. 3.8(b)). The structure was designed to have a scattering layer with a total thickness of 1 μm with a root-mean-square roughness of 500 nm and a planarization layer. The actual refractive index (n) of silicon oxide (SiO_x; n = 1.48 at a wavelength of 550 nm) was used for the nanostructure layer and that of SiN_x (n = 1.81) was used for the planarization layer. The number of graphene layers was varied from one to 10 while the t_{HTL} value was held constant at 250 nm. We hereafter refer to the OLEDs with and without the nanostructure layer as a scattering device and a planar device, respectively. As the number of graphene layers decreases, the radiances of both the planar and the scattering devices increase. The impact of introducing the scattering layer is evident. At a graphene film thickness of 1.5 nm, the scattering device shows a radiance which is higher than that of the planar device by 35.77%. This enhancement becomes even stronger for thinner graphene layers.

The radiance of the scattering device appears to be more sensitively varying with the graphene thickness as compared with the planar device. To understand this trend, we measured the reflectance of the glass substrate itself and compared it with that of the scattering layer on the glass (Fig. 3.8(b) inset). The reflectance of the scattering layer fluctuates rapidly, which is compared to the monotonic behavior of the glass. This difference implies a presence of complicated optics in the scattering device than in the planar device. In the planar device, the generated light travels toward the transparent electrode and the reflective cathode surface. The light components interfere and create internal optics analogous to those of a Fabry–Pérot interferometer. The reflectance measurement on the scattering layer suggests that some of the generated light is back-reflected from the scattering layer surface in random directions. Because the back reflection occurs repeatedly, the absorption effect is expected to play a dominant role in scattering devices, which accounts for the rapidly decreasing radiance as a function of the graphene number in this device.

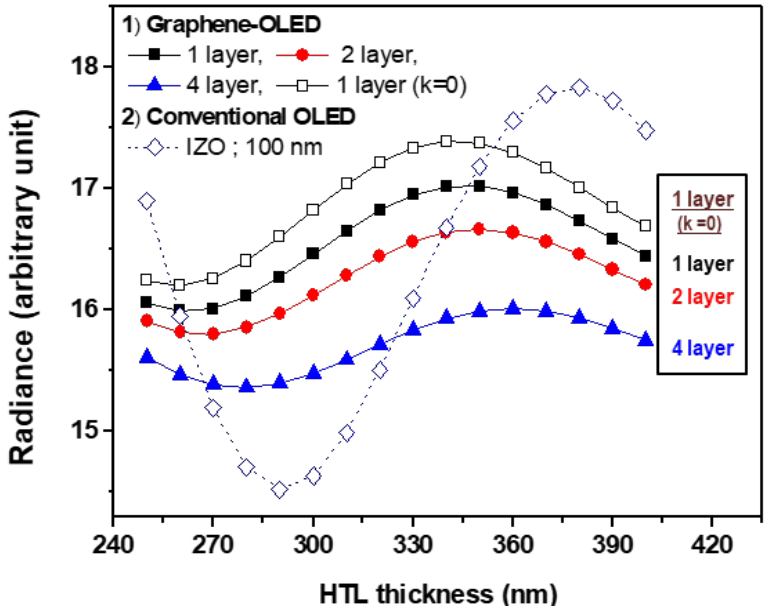

(a)

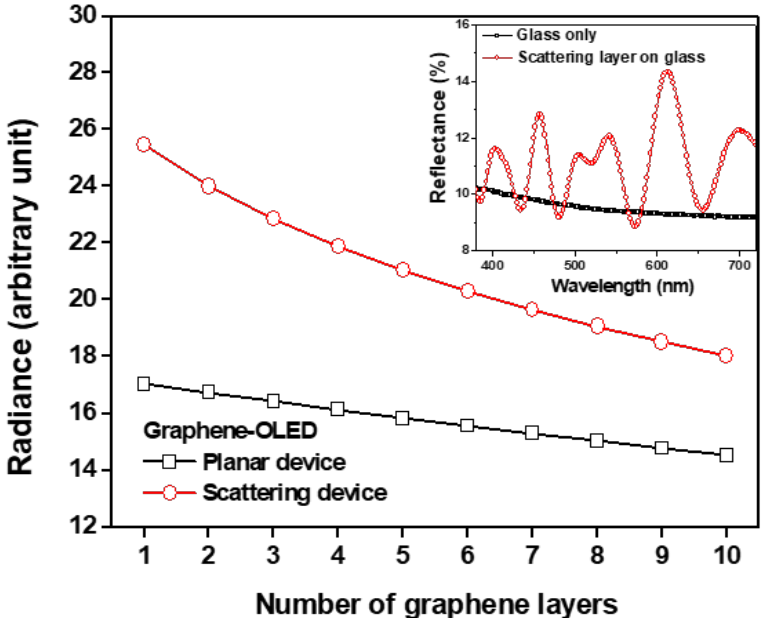

(b)

Figure 3.8. The simulation results; (a) the effect of the microcavity and optical absorption of graphene electrodes on OLEDs and (b) The absorption effect of graphene electrodes on OLEDs with and without the scattering layer. (Inset ; the experiment results of the reflectance of the glass substrate and the scattering layer on the glass)

3.4.4 Electrical and optical characteristics of graphene-OLEDs

Figure. 3.9 presents the current density (*J*)-voltage (*V)* characteristics and the electroluminance (EL) spectra in directions normal to the graphene-OLEDs with and without the scattering layer. Devices with one, two, and four graphene layers were used. All of them exhibit similar *J–V* characteristics with low leakage current levels and on/off current ratios higher than 10^8, as shown in Figs. 3.9 (a) and (b), respectively. This high electrical stability is ascribed to the low R_a (~ 0.4 nm) of the SiN_x planarization layer. The graphene used in this experiment had a sheet resistance of about 270, 148, and 80 Ω/□ for one, two, and four layers, respectively. Such a substantial difference in the sheet resistance could have affected the driving voltage of large OLEDs, but no significant difference was observable for the present 2×2 mm^2 devices. The EL main peak remained at a same position for all the OLED devices, as shown in Fig. 3.9(a) and (b) inset. The shape of the EL spectrum however slightly changed by introducing the scattering layer. The planar graphene-OLEDs showed a small shoulder at around 560 nm, which is related to the microcavity effect. Without the scattering layer, the reflectance of one, two, and four graphene layers on a glass substrate were obtained as 0.42%, 0.85%, and 2.38% at 550 nm, respectively, which accounts for the presence of this shoulder as well as its graphene-thickness dependence through the microcavity effect. Introducing a scattering layer beneath the graphene might have hindered this effect via random scattering.

The angular-dependent luminance of the devices was measured as a function of the number of graphene layers (Figs. 3.10(a) and (b)). For both devices, the one with fewer graphene layer numbers exhibits a higher luminance in all directions. As was expected, the luminance is greater for the scattering devices and increases with decreasing number of graphene layers. For devices with fewer layers of graphene in particular, the impact of the light absorption by graphene is more significantly reduced in the scattering devices than in the planar devices. Furthermore, the scattering structure diffuses the incident light to a wider range of angles.

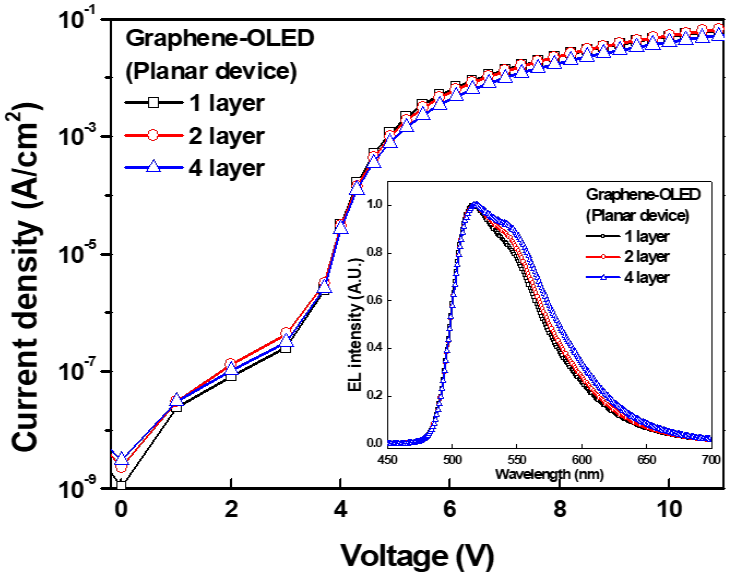

(a)

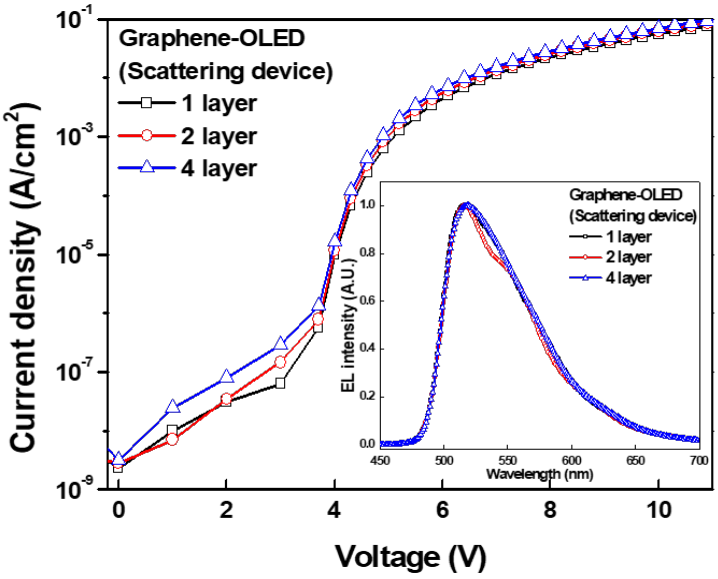

(b)

Figure 3.9. *J-V* characteristics of graphene-OLEDs; planar devices (a) and scattering devices (b). (Inset; EL spectra characteristics of graphene-OLEDs; planar devices (a) and scattering devices (b)) The number of the graphene layer was varied for one, two, and four and EL spectra of those OLEDs were measured at the normal direction.

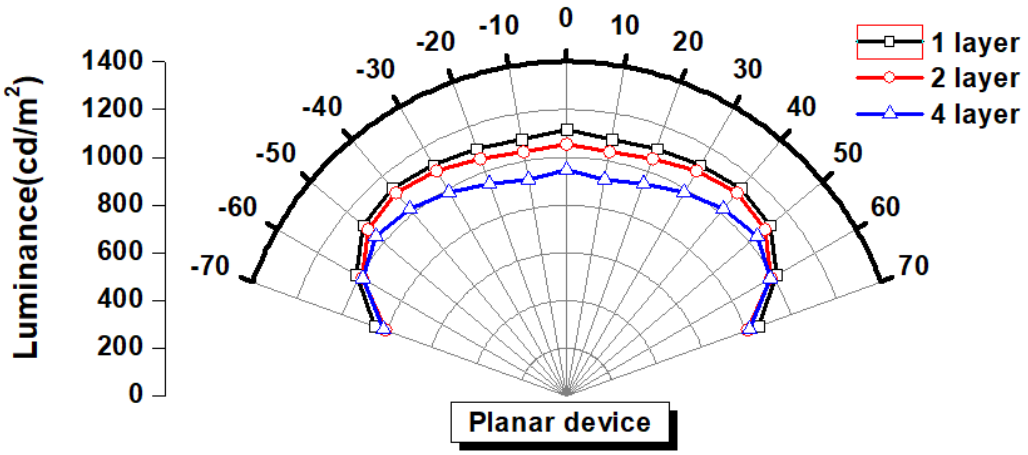

(a)

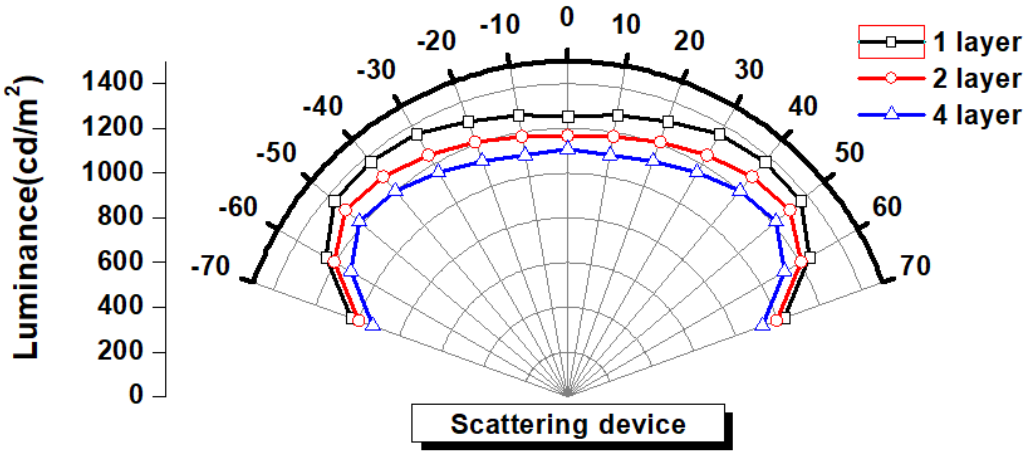

(b)

Figure 3.10. The angular-dependent luminance of the graphene-OLEDs as planar devices (a) and scattering devices (b) with the variation of the graphene layer as one, two, and four.

3.4.5 Efficiency of Graphene-OLEDs

Figure 3.11 plot the EQE (Fig. 3.11(a)) and the LE (Fig. 3.11(b)) of the graphene-OLEDs with and without the scattering layer, as a function of the number of graphene layers. They also show the enhancement ratio. At the same number of graphene layers, the scattering devices exhibit much higher efficiencies than the planar devices. This improvement can be understood by considering the scattering effect, which effectively compensates the optical losses that occur during the internal reflections. In general, the absorption of a transparent electrode lowers the efficiency of the OLED device. Decreasing the number of graphene layers from four to one thus improves the EQE and LE. The amount of the improvement however differs between the two devices; while EQE and LE increase only by 8.22% and 7.96% in the planar devices those for the scattering device amounts as large as 16.14% and 13.24%, respectively. This result is consistent with the simulation result depicted in Fig. 3.8(b). The backscattering and the reflection caused by the scattering layer may create complicated optical paths inside the OLEDs [32], thereby increasing the absorption rate of the graphene. Since this absorption increases with the number of graphene layers, the impact of the number of graphene layers on the efficiencies should be more pronounced in the scattering devices than in the planar devices, which accounts for the present result. Specifically, decreasing the number of graphene layers from four to one in the scattering device increases the EQE and LE enhancement from 39.6% to 52.78% and from 40.95 % to 49.52 %, respectively.

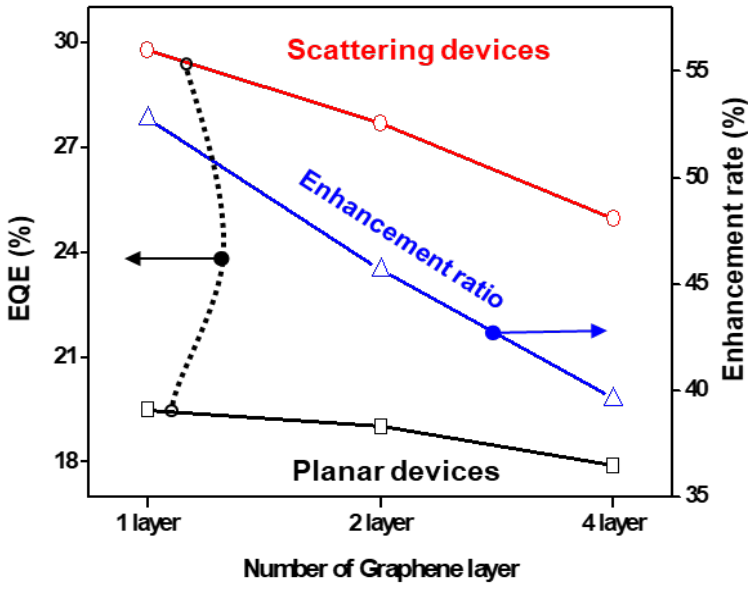

(a)

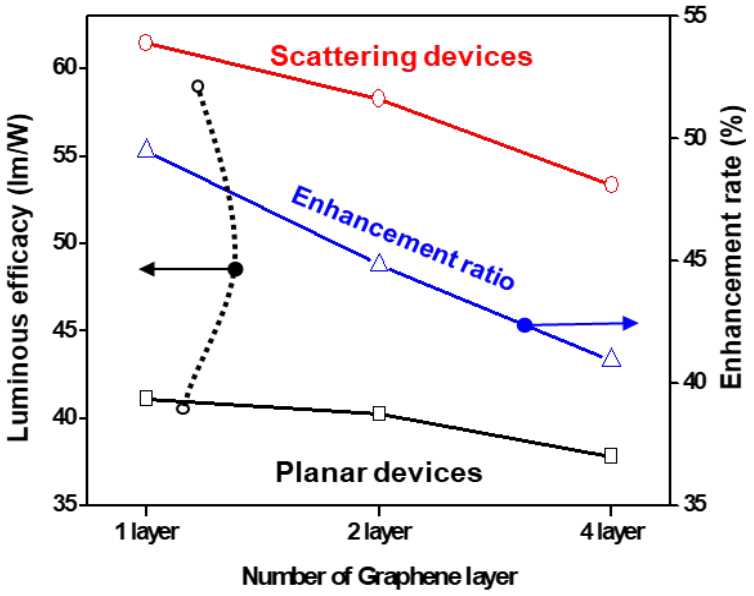

(b)

Figure 3.11. The EQE (a) and LE (b) of graphene-OLEDs as planar devices and scattering devices.

The number of graphene layers was varied as one, two, and four

3.4.6 Comparison of the graphene-OLED and the ITO-OLED with light extraction

Based on the above results, we compared the property of the single-layer graphene (SLG)-OLED with that of IZO-OLEDs (as a typical OLED). Except for the transparent electrodes, the IZO-OLED (thickness: 100 nm) had the same organic stack as that of the SLG-OLEDs. Fig. 3.12(a) summarizes the EQE and the LE of the devices. The planar SLG- and IZO-OLEDs show similar EQE and LE values when t_{HTL} = 250 nm is shared by both of the devices. Introduction of a scattering layer minimizes the microcavity effect, which on the other hand alters the optical traveling path and thereby contributes to the elimination of internal reflection loss [23]. Thus the use of the scattering layer increased the EQE and the LE values by almost the same amount for both types of the devices. The scattering layer made the OLEDs less dependent on the cavity length, and, hence, the organic thickness [26].These experimental results demonstrate the possibility of achieving graphene-OLEDs with efficiencies similar to those of conventional OLEDs with oxide anodes. The CIE color coordinates of the SLG and IZO devices were extracted from the EL spectra (Fig. 3.12(b)). Compared to the IZO-OLEDs, the CIE coordinates of the SLG-OLEDs remained almost constant, less than ±0.001 and ±0.002 for x and y coordinates, respectively, over a wide range of viewing angles, which corresponds to a negligible color shift. This is presumably due to the very low reflectance of the graphene surface. The proposed device is also very useful for stabilizing the angular EL spectra (Fig. 3.12(c) and (d)). Although the scattering layer cannot totally eliminate the microcavity because its SiN_x surface acts as a weak mirror, the distortion of the EL spectrum of the graphene-OLEDs caused by the residual microcavity effect is negligible compared to that exhibited by IZO-OLEDs.

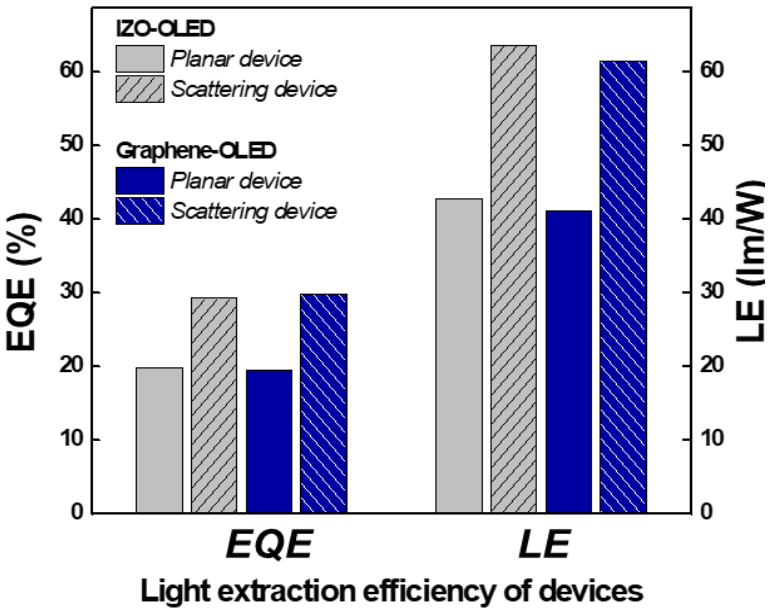
IZO-OLED
Planar device
Scattering device
Graphene-OLED
Planar device
Scattering device
EQE (%)
LE (lm/W)
0
10
20
30
40
50
60
EQE
LE
Light extraction efficiency of devices

(a)

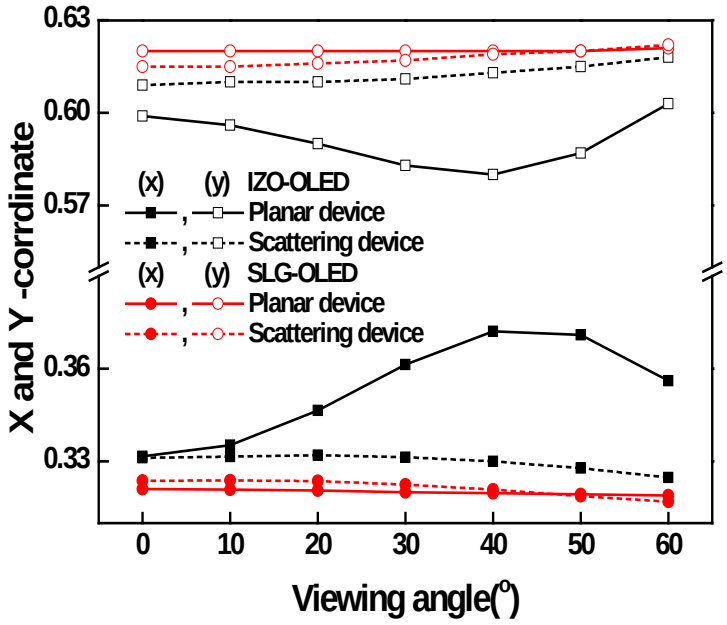
0.63
0.60
0.57
0.36
0.33
X and Y -corrdinate
(x) (y) IZO-OLED
Planar device
Scattering device
(x) (y) SLG-OLED
Planar device
Scattering device
0
10
20
30
40
50
60
Viewing angle(°)

(b)

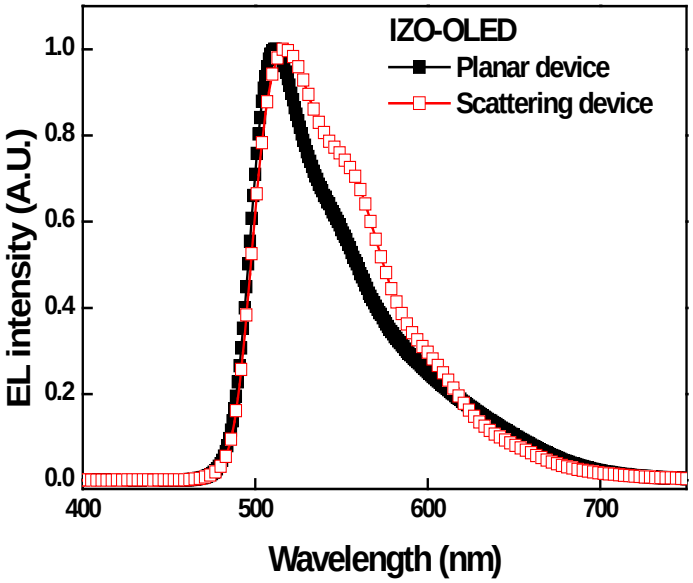

(c)

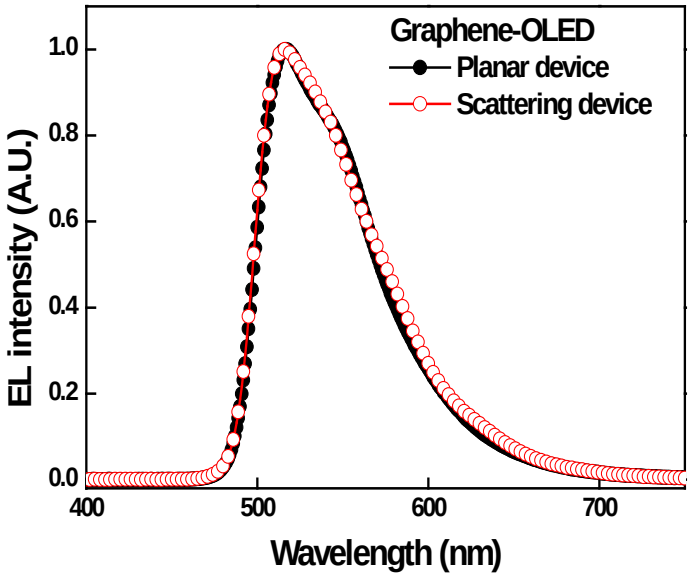

(d)

Figure 3.12. The Comparison of (a) EQE and LE, (b) The CIE color coordinates and (c), (d) EL spectra of SLG-OLEDs and IZO-OLEDs with and without the scattering layer. EL spectra of those OLEDs were measured at the normal direction.

3.5 Conclusion

To improve the efficiencies of graphene-OLEDs, we evaluated the optical absorption of graphene and explored the use of the scattering layer containing an array of aperiodic SiO_x nano-pillars and a SiN_x planarization layer. A comparison between simulations and device characterizations have shown that the optical absorption and the substantial reduction of the microcavity effect limit the efficiencies of the OLED with graphene anodes. Introduction of a scattering layer between the substrate and the graphene anode was found to enhance EQE and LE by more than 50%. As a result, we succeeded in the fabrication of graphene-OLEDs having efficiencies comparable to those of conventional OLEDs with oxide anodes. Furthermore, the angular EL spectrum variations were stabilized, which is difficult to achieve using conventional OLEDs with microcavity designs. Therefore, we believe that these results provide important insights for the betterment of the graphene-OLED performance.

Reference

[1] Hwang, H. K. Choi, J. Moon, T. Y. Kim, J.-W. Shin, C. W. Joo, J.-H. Han, D.-H. Cho, J. W. Huh, S.-Y. Choi, J.-I. Lee and H. Y. Chu, Appl. Phys. Letts. **100**, 133304 (2012).

[2] K. Saxena, V. K. Jain and D. S. Mehta, Opt. Mater. **32**, 221 (2009).

[3] F. Bonaccorso, Z. Sun, T. Hasan and A. C. Ferrari, Nat. Photonics **4**, 611 (2010).

[4] C. Fabry and A. Pérot, Ann de Chim. Et de Phys. **16**, 115 (1899)

[5] N. Ismail, C. C. Kores, D. Geskus, and M. Pollnau, Opt. Express **24**, 16366 (2016).

[6] C. Xiang, W. Koo, F. So, H. Sasabe and J. Kido, Light Sci. Appl. **2**, e74 (2013).

[7] H. K. Kim, S.-H. Cho, J. R. Oh, Y.-H. Lee, J.-H. Lee, J.-G. Lee, S.-K. Kim, Y.-I. Park, J.-W. Park, and Y. R. Do, Org. Electron. **11**, 137 (2010).

[8] J. W. Huh, J.-W. Shin, D.-H. Cho, J. Moon, C. W. Joo, S. K. Park, J. Hwang, N. S. Cho, J. Lee, J.-H. Han, H. Y. Chu, and J.-I. Lee, Nanoscale **6**, 10727 (2014)

[9] H. Cho, J.-W. Shin, N. S. Cho, J. Moon, J.-H. Han, Y.-D. Kwon, S. Cho and J.-I. Lee, IEEE J. Sel. Top. Quantum Electron. **22**, 2000306 (2016).

[10] M.-K. Wei, C.-W. Lin, C.-C. Yang, Y.-W. Kiang, J.-H. Lee, and H.-Yan, Lin, Int. J. Mol. Sci. **11**, 1527 (2010).

[11] N. K. Patel, S. Cinà, J.H. Burroughes, IEEE J. Sel. Top. Quantum Electron. 8, **346** (2002).

[12] S. Nowy, C. Krummacher, J. Frischeisen, N. A. Reinke and W. Brü tting, J. Appl. Phys. **104**, 123109 (2008).

[13] G. Gu, D.Z. Garbuzov, P.E. Burrows, S. Venkatesh, S.R. Forrest, Opt.Lett. **22**, 396 (1997).

[14] R. Meerheim, M. Furno, S. Hofmann, B. Lüssem and K. Leo, Appl. Phys. Lett. **97**, 253305 (2010).

[15] W. H. Koo, W. Youn, P. Zhu, X. H. Li, N. Tansu and F. So, Adv. Funct. Mater. **22**, 3454 (2012).

[16] H. Cho, E. Kim, J. Moon, C. W. Joo, E. Kim, S. K. Park, J. Lee, B.-G. Yu, J.-I. Lee, S. Yoo and N. S. Cho, Org. Electron. **46**, 139 (2017).

[17] Y.-J. Lee, S.-H. Kim, J. Huh, G.-H. Kim, Y.-H. Lee, S.-H. Cho, Y.-C. Kim, Y.R. Do, Appl. Phys. Lett. **82**, 3779 (2003).

[18] Y.-H. Cheng, J.-L. Wu, C.-H. Cheng, K.-C. Syao, M.-C.M. Lee, Appl. Phys. Lett. **90**, 091102 (2007).

[19] Y. Sun, S.R. Forrest, Nat. Photonics **2**, 483(2008).

[20] C. Lee and J. J. Joo, Small **9**, 3858 (2013).

[21] D. H. Cho, J. W. Shin, J. Moon, S. K. Park, C. W. Joo, N. S. Cho, J. W. Huh, J. H. Han, J. Lee, H. Y. Chu and J. I. Lee, ETRI J. **36**, 847 (2014).

[22] K. Lee, J.-W. Shin, J.-H. Park, J. Lee, C. W. Joo, J.-I. Lee, D.-H. Cho, J. T. Lim, M.-C. Oh, B.-K. Ju and J. Moon, ACS Appl. Mater. Interfaces **8**, 17409 (2016).

[23] J.-W. Shin, D.-H. Cho, J. Moon, C. W. Joo, S. K. Park, J. Lee, J.-H. Han, N. S. Cho, J. Hwang, J. W. Huh, H. Y. Chu and J.-I. Lee, Org. Electron. **15**, 196 (2014).

[24] K. Ishihara, M. Fujita, I. Matsubara, T. Asano and S. Noda, Appl. Phys. Letts. **90**, 111114 (2007).

[25] M. Fujita, K. Ishihara, T. Ueno, T. Asano, S. Noda, H. Ohata, T. Tsuji, H. Nakada and N. Shimoji, Jpn. J. Appl. Phys. **44**, 3669 (2005).

[26] J.-W. Shin, D.-H. Cho, J. Moon, C. W. Joo, J. Lee, J. W. Huh, S. K. Park, J.-H. Han, N. S. Cho, J. Hwang, H. Y. Chu and J.-I. Lee, Opt. Lett. **39**, 3527 (2014).

[27] S. M. Song and B. J. Cho, Nanotechnol. **21**, 335706 (2010).

[28] N. K. Patel, S. Cinà and J. H. Burroughes, IEEE J. Select. Topics Quantum Electron. **8**, 346 (2002).

[29] C. W. Joo, J. Moon, J. Hwang, J.-H. Han, J.-W. Shin, D.-H. Cho, J. W. Huh, H. Y. Chu and J.-I. Lee, Jpn. J. Appl. Phys. **51**, 09HM01 (2012).

[30] Z. H. Ni, H. M. Wang, J. Kasim, H. M. Fan, T. Yu, Y. P. Feng and Z. X. Shen, Nano Lett. **7**, 2758 (2007).

[31] P. Blake, E. W. Hill, A. H. Castro Neto, K. S. Novoselov, D. Jiang, R. Yang, T. J. Booth and A. K. Geim, Appl. Phys. Lett. **91**, 063124 (2007).

[32] J.-W. Kim, J.-H. Jang, M.-C. Oh, J.-W. Shin, D.-H. Cho, J. Moon and J. I. Lee, Opt. Express **22**, 498 (2014).

4

Formation of Accurate Graphene Patterns using Liquid Bridging Treatment

4.1 Introduction

Currently, OLEDs are widely used in display technology because they provide higher quality images, lower power consumption, simpler design, and better durability than conventional display technologies such as Liquid crystal display (LCD). Also, the important thing is that OLED can be applied to the next-generation displays due to its excellent properties such as ultra-thin thickness, flexibility, and transparency. In order for graphene to be used in OLEDs, the whole fabrication process must be compatible with that of commercial AM-OLED display products that are made up of millions of unit pixels (Fig 4.1). Since the number of pixels in the display panel determines the resolution of the image graphene has to be precisely positioned into the AM-OLED unit pixels to achieve commercial level products. However, there are hurdles in graphene-OLED that impede the realization of such production, which include the compatibility and stability of the fabrication process with existing display process [1-3]. In this chapter, we discussed the processing issues relevant to the integration of graphene transparent electrodes and OLED panels. The processing issues in graphene AM-OLEDs can be succinctly summarized as follows. Graphene films must be patterned in correct dimensions with a defect free manner over a large area of the device. Although various graphene

patterning methods have been proposed [1, 4-6], the majority of the methods cause deterioration of the graphene surface and incorrect pattern dimensions. In this chapter, a new method is proposed for the formation of accurate graphene patterning using the photolithography. Photolithography is currently the most widely used patterning method in the display industry and forms the accurate patterns that meet the commercialization requirements. However, graphene can easily be damaged during the patterning process due to the weak adhesion of graphene to its supporting layer. In order to make accurate graphene patterns without any damages, a new method was developed to improve the adhesion between the graphene film and the support. The liquid bridge treatment, when combined with photolithography, allows us to pattern the graphene films with dimensional accuracy without deterioration of the surface properties.

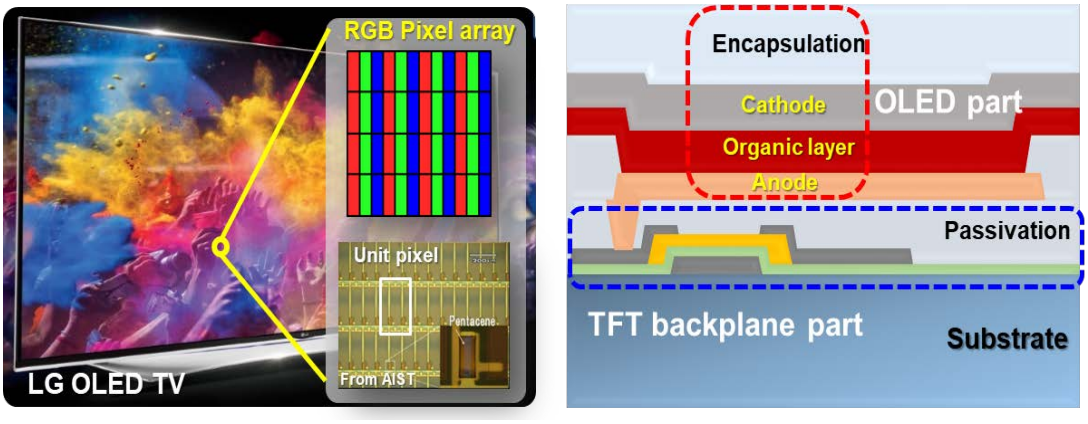

(a) (b)

Figure 4.1. (a) AM-OLED display panel and schematic of AM-OLED unit pixel

4.2 Technical issues on the formation of graphene pattern

4.2.1 Weak adhesion properties of graphene

Due to poor adhesion of graphene to its supporting layer, it was difficult to make accurate patternings over the large area without degradation. This weak adhesion may cause damages to graphene during the patterning process, which deteriorate the device performance. Figure 4.2 shows the images of actual graphene pattern using the photolithography process. These images were obtained from the graphene having weak adhesion to the substrate. After the photolithographic patterning process, the graphene films were observed to be crumbled and/or peeled off (Fig. 4.2(a) and (b)). As a result, the emission image of fabricated OLED failed to reach the acceptable standard (Fig. 4.2(c)). The emission uniformity is low and many defective regions are readily observable. Based on the observation of Fig. 4.2, we draw a conclusion that direct application of photolithographic patterning processes to graphene films is not suitable. Unlike thin-films formed by vacuum deposition methods, graphene films are physically transferred from a catalytic surface, on which graphene is grown, to a substrate of interest. Thus, due to the nature of the transfer process, graphene film will not necessarily lie globally flat on the surface. This unsuitability of the direct application of photolithography seems to have originated from the weak adhesion between the graphene films and the substrate, which is Van der Waals force [7-11]. Van-der Waals forces are instantaneous dipoles interactions and far weaker than permanent chemical bonds such as covalent or ionic bonds. In photolithographic patterning processes, samples are directly exposed to various liquid solutions frequently. Thus, the chances of liquid permeation through the substrate/graphene interface are high [12]. Furthermore, presence of undesirable conditions, such as structural defects in the graphene, surface roughness, and residues from underlying layers, can diminish the adhesion of graphene to the supporting layer [13-15].

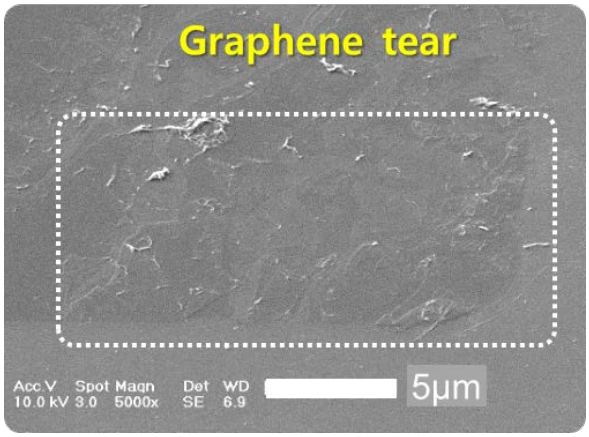

(a)

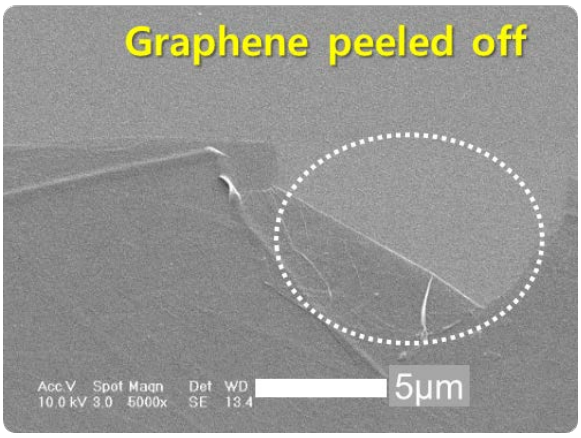

(b)

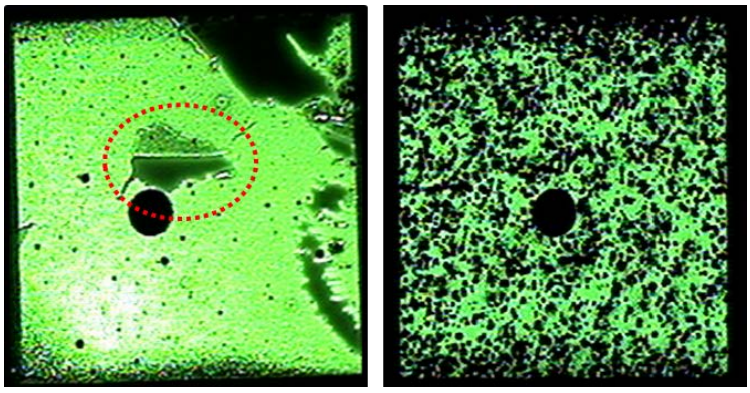

(c)

Figure 4.2. Graphene damages from the patterning process (photolithography method); graphene smash (a), peeled off (b), and influence of graphene damage on the actual emission image of OLED (c)

4.2.2 Concept of liquid bridge treatment

In order to stabilize the photolithography patterning process, graphene's adhesion must be improved. In an effort to improve the adhesion and flatten the graphene film, we utilized the concept of "liquid bridging". Liquid bridging provides a connection between two solid surfaces via liquid molecules and forms an attractive force between interfaces (Fig 4.3). This bridge, whose stability is dependent on the separation distance between the interfaces, is stable below the critical separation distance. In addition, the attractive force becomes stronger as the distance decreases [16-18].

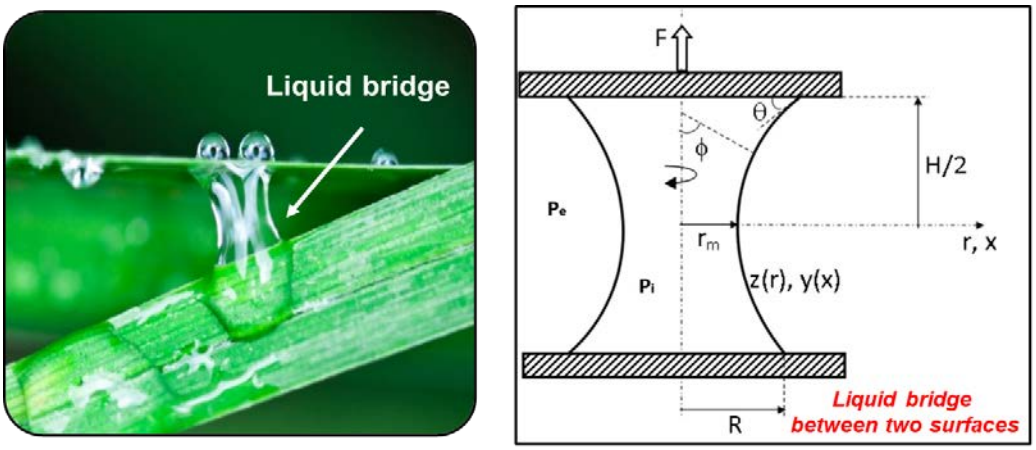

Figure 4.3. Concept of liquid bridge treatment (similar to capillary bridge) [19].

As the imperfection due to graphene defects and surface/residue on the support may generate pores at the interface between the graphene and the substrate. (Fig. 4.4(a)), the graphene adhesion based on Van-der Waals forces can be weakened by reducing the conformal contact area. In addition, these pores can act as the defect seeds that may facilitate solution permeation during liquid solution processes. To improve the poor adhesion of graphene, we reduced the density of these pores by utilizing the liquid bridging. By allowing water to permeate into the air pores that exist between graphene and the substrate, the formation of liquid bridge can be induced (Fig. 4.4(b)). The water

inside the pores is in physical contact with every part of the internal surface of the graphene film. Owing to the mechanical compliance of graphene, upon removal of the water, the graphene film can be stretched to eliminate the air pores and achieve close physical contact between the substrate and the graphene film with stronger adhesion (Fig. 4.4(b) and (c)).

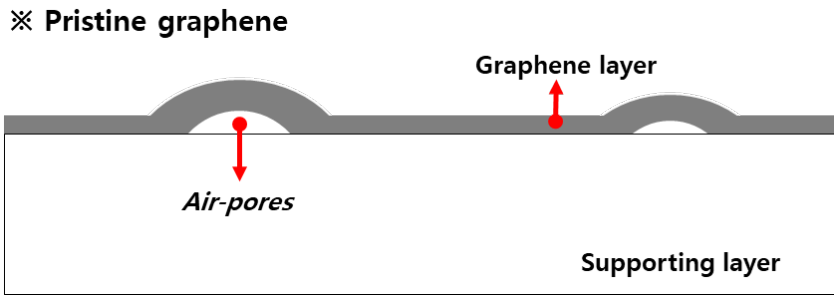

(a)

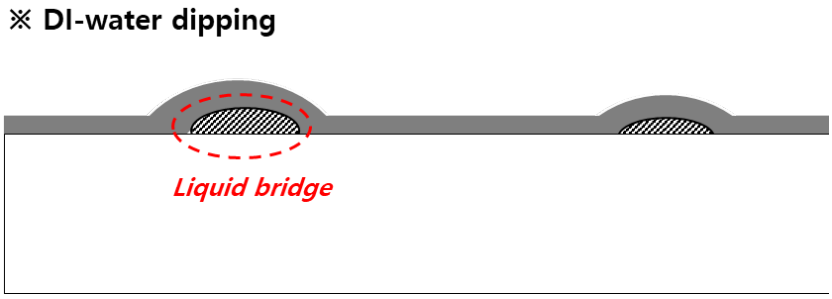

(b)

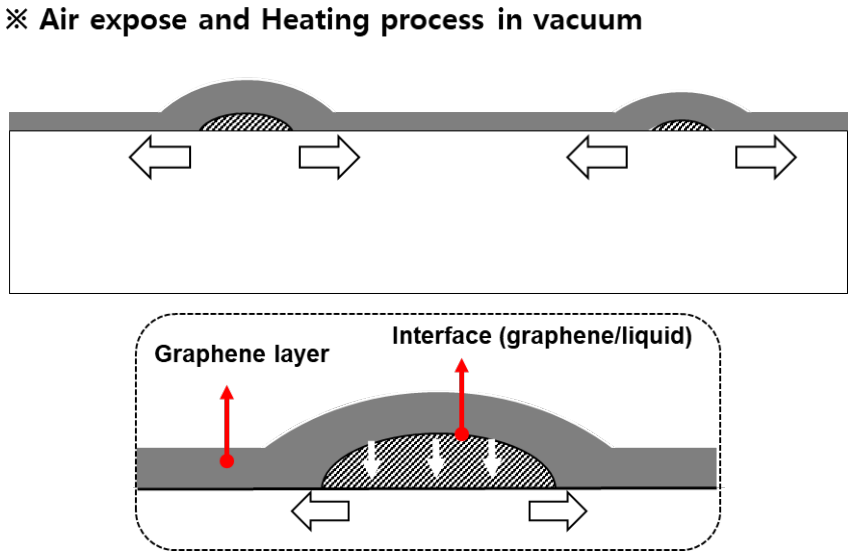

(c)

Figure 4.4. The concept of improvement in adhesion between graphene/substrate by liquid bridging; (a) air-pores between the graphene and the substrate, (b) the formation of water droplet inside the air-pores, and (c) the removal the water droplet.

4.3 Experimental methods

4.3.1 Graphene preparation and patterning process

In this chapter, four layer graphene films were used. Graphene film was grown on a Cu film by a RT-CVD process. Cu film was etched by using an etching solution containing H_2O, H_2SO_4 and benzimidazole. During the Cu etching process, benzimidazole p-dopes the graphene to have low sheet resistance. Four layer-graphene films were transferred by the thermal release tape (TRT) on the passivation layer (SiO_x)/glass substrate layer by layer. The sheet resistance of the graphene films was ~65 Ω/□.

Figure 4.5 shows the process flow of graphene patterning process. Photolithography process was used for the graphene film patterning. Positive type photoresist (PR) was coated on graphene surface by using the spin coater (Karl Suss Micro Tec 80T) and soft baking was carried out at 90 ^oC for 120 secs on a hot plate. To define an anode area, a photomask was aligned on the PR/graphene and it was then exposed to ultraviolet (UV) light by using the contact aligner system (Karl Suss MA6 mask aligner) followed by the development process. The exposed portion of graphene was etched by O2 plasma at 40 Watt with 30 sccm of O_2. After etching process, the PR residue on the graphene was removed by the PR remover.

4.3.2 Liquid bridge treatment and characterization of graphene

The process flow of the liquid treatment is presented in Figure 4.6. We have immersed the sample into deionized (DI)-water for 2 min. Immersion time longer than 2 min resulted in peel off of the graphene film. In this case, water is thought to have formed a continuous layer between the substrate and acted as a detachment layer. Thus, we limited the immersion time to 2 minutes. To

remove the DI-water, thermal treatment was performed at 200 ^{o}C for 2 hours in a conventional vacuum oven.

The adhesion energy of graphene was measured by a double cantilever beam (DCB) fracture mechanics testing with a micromechanical test system (Delaminator Adhesion Test System; DTS Company, Menlo Park, CA). Specimen were prepared by cutting a 6 mm × 28 mm rectangular beam from a four layer graphene/SiO_x/glass and bonding it to a glass counterpart by using epoxy (Epo-Tek 353ND consisting of bisphenol F and imidazole; Epoxy Technology). The epoxy was cured for 2 hours at 125 ^{o}C in electric oven. Raman facility (Model: NTEGRA spectra, NT-MDT) was used to assess the quality of the graphene film surface. The surface morphology of graphene was observed using an atomic force microscope (Model: PSIA XE-100) and a scanning electron microscope (FEI Sirion), respectively.

4.3.3 OLED device structure

We used an alternating hole transport layer (HTL) of HAT-CN (10 nm) and TAPC (40 nm). The number of HAT-CN/TAPC pairs correspond to the 350 nm of HTL thickness. The devices were composed of a stack structure of four-layer graphene/the alternating structure of HTL (350 nm)/ EML/ BmPyPB (60 nm) (ETL). Lithium fluoride (LiF)/aluminum (Al) was evaporated on ETL for a high reflective metal cathode. In the case of graphene-OLED for patterning test, the organic material of DCzPPy:$Ir(ppy)_3$ (20 nm) was used for EML with the main peak at λ = 515 nm.

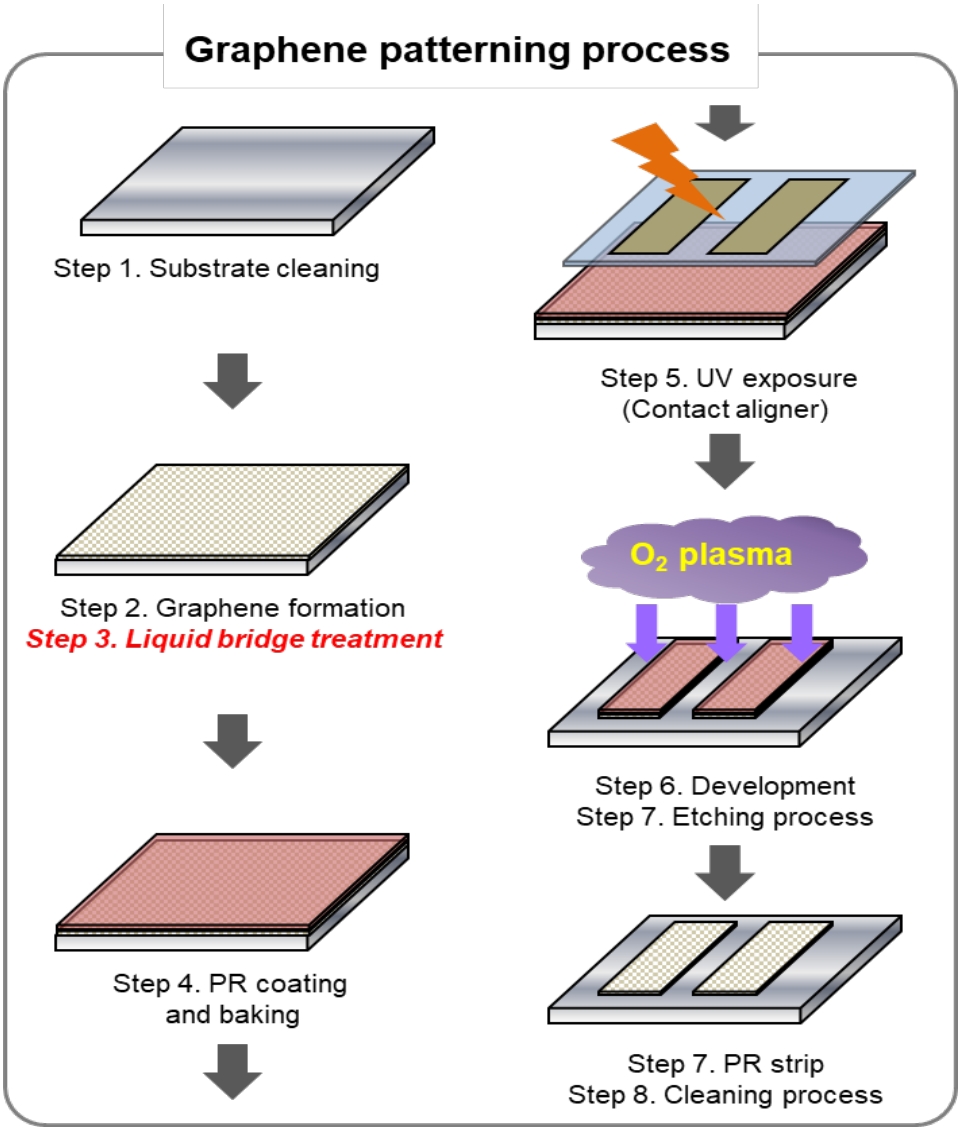

Figure 4.5. Process flow of graphene patterning process

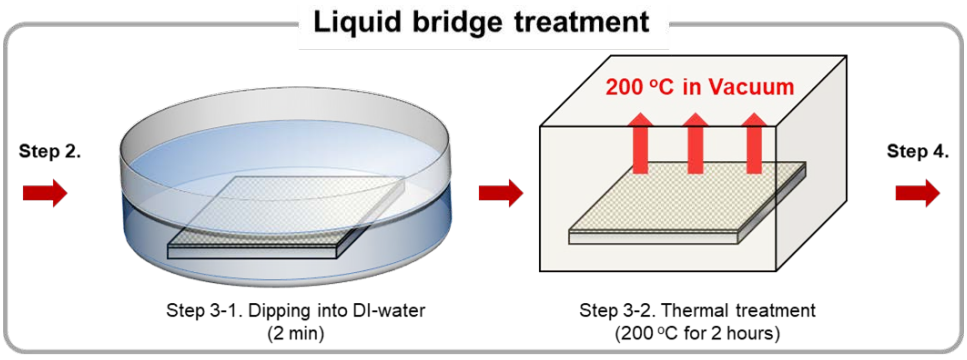

Figure 4.6. Process flow of the liquid bridge treatment.

4.4 Results and discussion

4.4.1 Characterization of graphene with the liquid bridge treatment

In order to quantitatively analyze the effect of the liquid bridging method, we used the DCB fracture mechanics to test the adhesion energy and AFM to examine the surface morphology (Fig. 4.7). DCB testing is a widely used method for measuring the effective adhesion energy of two dimensional materials [20,21]. The specimen was prepared on the same surface condition with OLED panel structure. To accurately evaluate our surface treatment we prepared two samples. i) a pristine graphene film without any treatment and, ii) a graphene film with the water and thermal treatment in the vacuum as the liquid bridge method. We have immersed the sample into deionized (DI)-water for 2 min. To remove the DI-water, thermal treatment was performed at 200 ^{o}C for 2 hours in a conventional vacuum oven.

Figure 4.7(a) shows the cross-sections of the DCB testing specimens. The graphene film is sandwiched between a SiO_x layer and an epoxy layer. The upper and the lower glass substrates act as physical supports for the structure in between. We choose SiO_x because it is used in OLEDs as a passivation layer material. A vertical bi-directional load was continuously applied to all specimens until the graphene was detached from the SiO_x surface. When the applied force exceeds the effective adhesion energy of the weakest bond in the specimen, cracking or detachment is initiated. In this process, the crack length was measured and the effective adhesion energy was extracted [22].

After DCB testing, Raman analyses were performed on the interface where graphene cracking occurred. Figure 4.7(b) and (c) show the tendency of graphene to peel off under each condition after DCB testing. Figure 4.7(d) shows the effective adhesion energy and the surface roughness of the graphene samples. The average surface roughness (R_a) and adhesion energy are summarized in table 4.1. The R_a of pristine graphene was measured to be about 2.33 nm, which is about 4 times higher

than the R_a of 0.52 nm for SiO_x. The pristine graphene include many air pores, the surface roughness is thought to be high. The R_a values of graphene films of the graphene with the liquid bridge treatment is low as 0.65 nm. This result signifies the effectiveness of our approach to reduce the surface protrusion. The effective adhesion energy value of the graphene with pristine condition and the liquid bridge treatment was extracted as 0.9 ± 0.14 Jm^{-2} and 1.71 ± 0.21 Jm^{-2}, respectively.

Table 4.1. Absolute value of adhesion energy and R_a of graphene before and after the liquid bridge treatment

Graphene	Untreated	Treated
Adhesion$^+$(J/m^2)	0.9 ± 0.14	1.71 ± 0.21
R_a (nm)	2.33	0.52

Due to differences in the tendency of graphene peeling off, it is difficult to directly compare these absolute values. However, it can be interpreted that the effective adhesion energy of the graphene film that underwent the liquid bridge treatment is improved by about a factor of two relative to that of a pristine graphene film. The graphene with the liquid bridge treatment shows the highest effective adhesion energy with lowest surface roughness. Without any treatment, the graphene film was observed to detach completely from the glass surface. Raman scans yielded no graphene signals on the glass surface, whereas a clear graphene peak was observed on the counterpart surface (Fig. 4.7(e)). In contrast, the Raman scans of the graphene films that underwent the treatment showed clear graphene peaks on both sides. This means that the multilayered graphene film was cleaved. In other words, our method improves the adhesion of the graphene to the SiO_x which is stronger than of the graphene interlayer binding. More importantly, by combining the liquid bridging and the water removal, it is possible to not only reduce the surface roughness of the graphene film but also to

improve adhesion. Conversely, we can draw a conclusion that the weak adhesion of untreated graphene film is due to the defects at the graphene film/substrate interface. For this reasons, untreated pristine graphene is easily damaged and delaminated by external factors. This improvement in the effective adhesion energy can be explained by Van-der Waals force, as graphene and SiO_x have chemically stable surfaces.

From this theoretical framework, the energy required for separating the two surfaces as the effective adhesion energy (Γ) is expressed as the following [23,24].

$$\Gamma = \int_r^{\infty} F dr = \frac{A}{12\pi} r^{-2} \qquad (4.1)$$

Here F is the Van-der Waals force. A and r is Hamaker constant and the distance between the surfaces [25]. The value of Γ is proportional to the inverse square of the distance between the two surfaces. In our method, the overall distance between the graphene film and the substrate was effectively reduced by eliminating pores. In summary, the improvement in adhesion can be interpreted as an increase in Van-der Waals force which is due to the very close contact between the graphene film and supporting layer. In addition, Raman analysis of each condition was carried out as shown in figure 4.8(a). No significant changes in the intensity and in the shift of graphene peaks were observed, which means that our approach is applicable to enhance the graphene film adhesion to the support without deteriorating the graphene film quality. The AFM images in figure 4.8(b) and (c) show the flattened surface morphology of graphene film which has undergone the treatment.

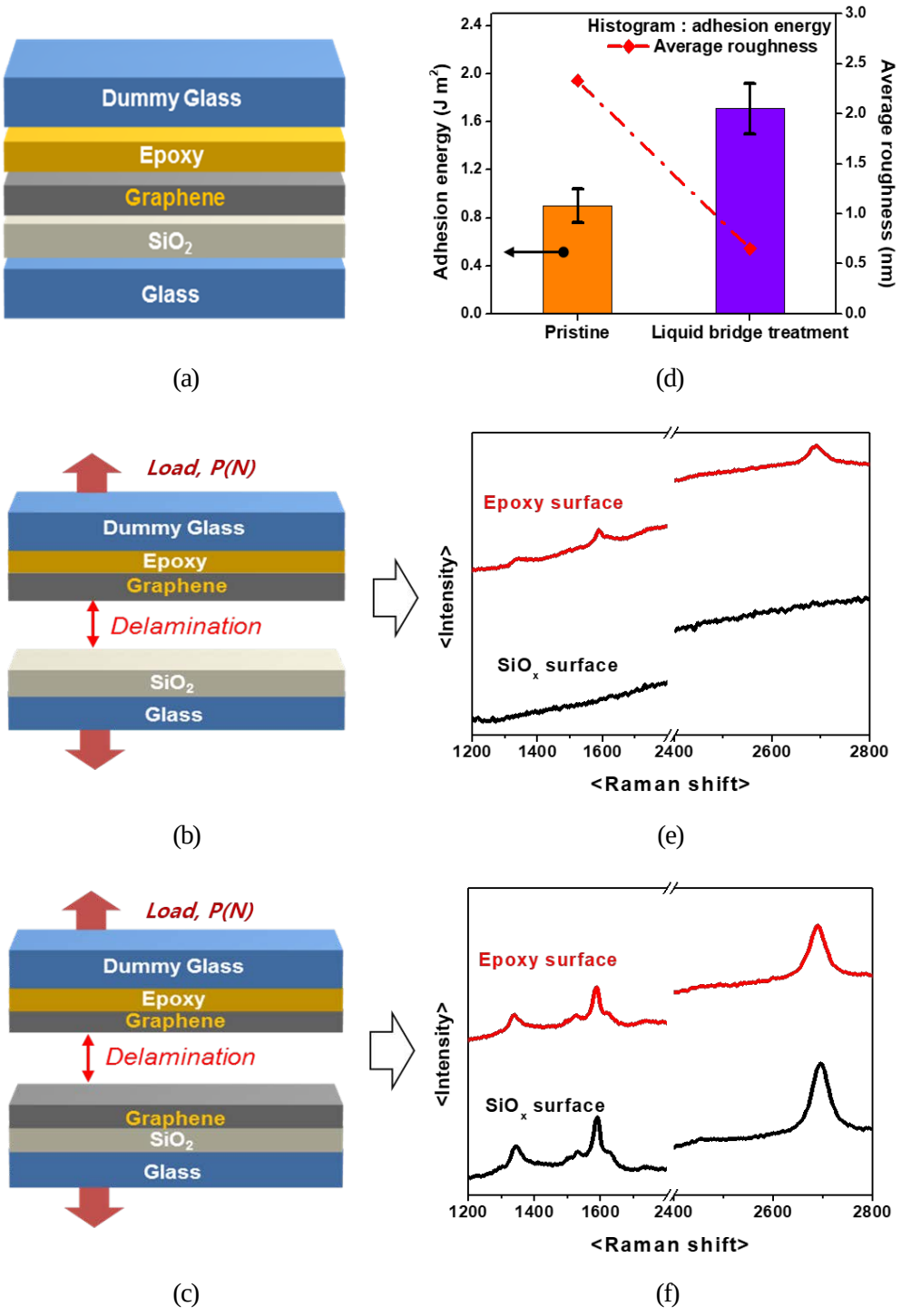

Figure 4.7. (a) Schematic of DCB specimens, the delamination tendency of graphene after DCB testing; (b) the pristine graphene, (c) the liquid bridge treatment, (d) the effective adhesion energy (histograms) and average surface roughness (symbol with dotted line) of all specimen, and the Raman analysis of pristine graphene (e) and the liquid bridge treatment (f) after DCB testing.

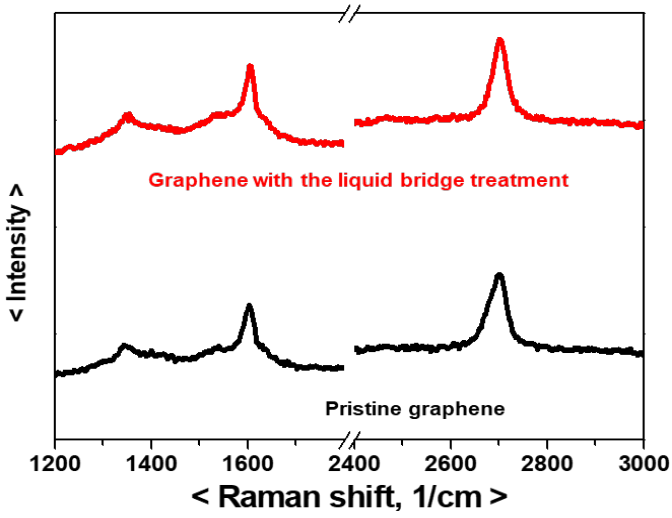

(a)

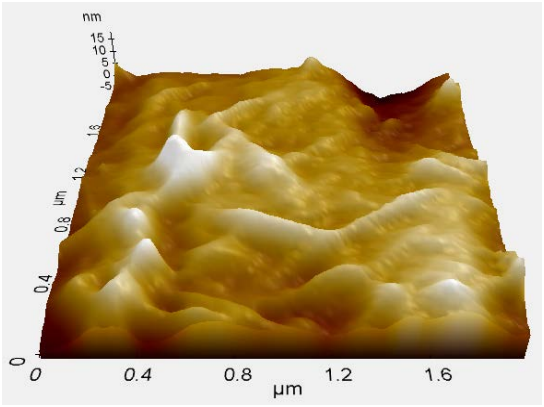

(b)

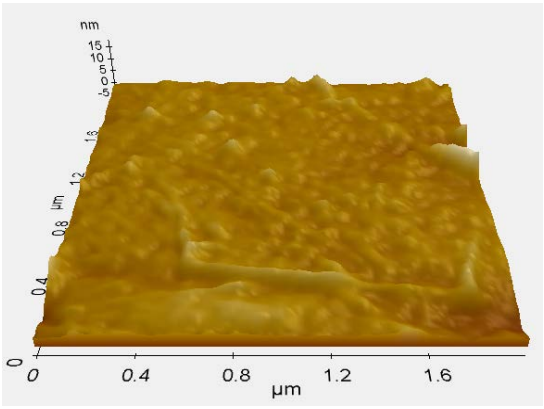

(c)

Figure 4.8. (a) Raman spectra and AFM images of graphene before (b) and after the liquid bridge treatment (c).

4.4.2 Properties of graphene pattern

Figure 4.9 shows the typical Raman spectra obtained after the graphene film patterning. By comparing the SEM images of Figs. 4.9(a) and (b), one can readily notice the surface smoothness and the dimensional accuracy of the patterned graphene film. It should especially be noted that the pattern edge is clearly straight (Fig. 4.9(a)). Raman analyses show that the graphene film surface is well preserved after the patterning process (Fig. 4.9(b)). After the patterning process the small shoulder close to the G (graphite) peak (1591 cm^{-1}) disappears. Because this shoulder is reportedly associated with organic residues, its disappearance strongly implies the absence of organic residues, such as photoresist (PR) or other containments, on the surface, which is expected to contribute to inhibiting aberrational behavior in OLEDs [26,27].

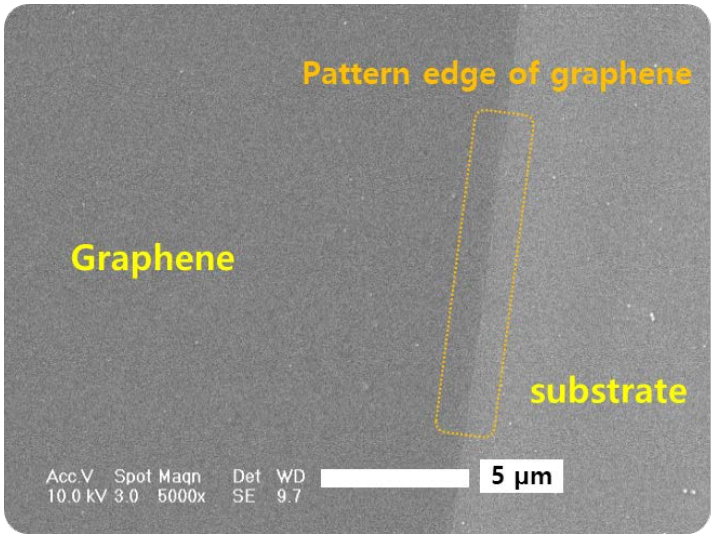

(a)

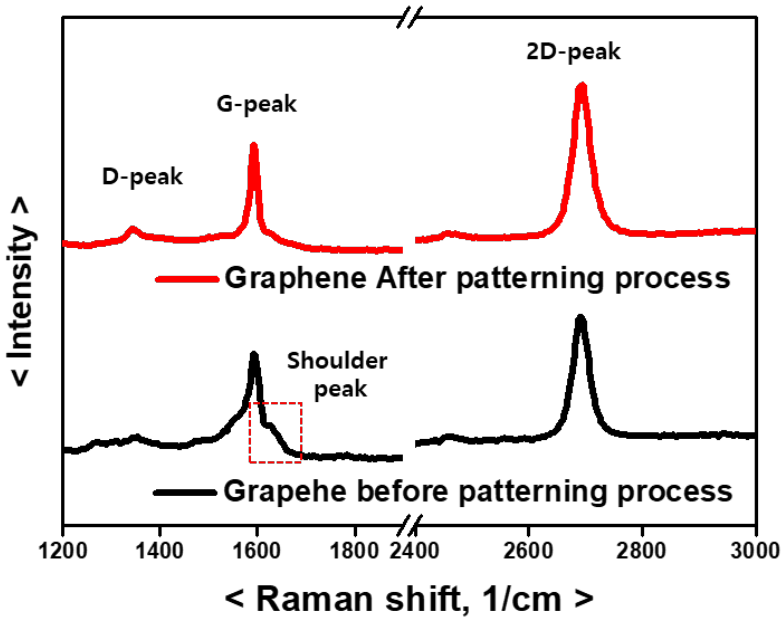

(b)

Figure 4.9. (a) SEM image of graphene pattern edge by the photolithographic patterning processes and (b) the Raman analyses before and after the patterning process.

4.4.3 Characteristics of OLEDs using patterned graphene electrode

In order to evaluate our patterning process on the OLED device level, we fabricated phosphorescent green bottom emission OLEDs using patterned and non-patterned graphene electrodes. The organic stack structure of OLED is listed in the experimental section. In the case of non-patterned graphene-OLED, the emitting area was defined by forming a non-conductive organic material banks on the graphene film. Figures 4.10(a), (b) and (c) show the current density (*J*)-voltage (*V*)-luminance, luminance efficacy (LE), and electroluminance (EL) spectra characteristics of OLEDs with non-patterned or patterned graphene. The graphene-OLEDs have a green emission with its main peak at $\lambda = 515$nm. The optical and electrical properties of both devices are almost identical. In the *J*-*V*-luminance curves (Fig 4.10(a)), the characteristics of OLEDs with patterned and non-patterned graphene electrode almost superimpose in the on-state region (V> 4V). Significant luminance (> 5×10^3 cd/m^2) is observed at an almost identical current density level. These measurement results strongly indicate that the liquid bridging is not inducing significant change in the values of sheet resistance and the work function of the graphene film. The luminance efficacy of these devices also have the same characteristics (Fig 4.10(b)). The EL spectra show no distinguishable feature (Fig 4.10(c)). The actual emission image of the OLED with patterned graphene electrode shows no black spot or overly charged white region. We attribute the results of Fig. 4.10 to our surface treatment that yields strong adhesion of graphene film to its support and enables accurate and defect free patterning of graphene films into pixelated electrodes. The successful implementation of photolithographic patterning opens the door to utilizing established display compatible patterning processes, which is of high technical importance for realizing commercial level graphene electrode OLED products.

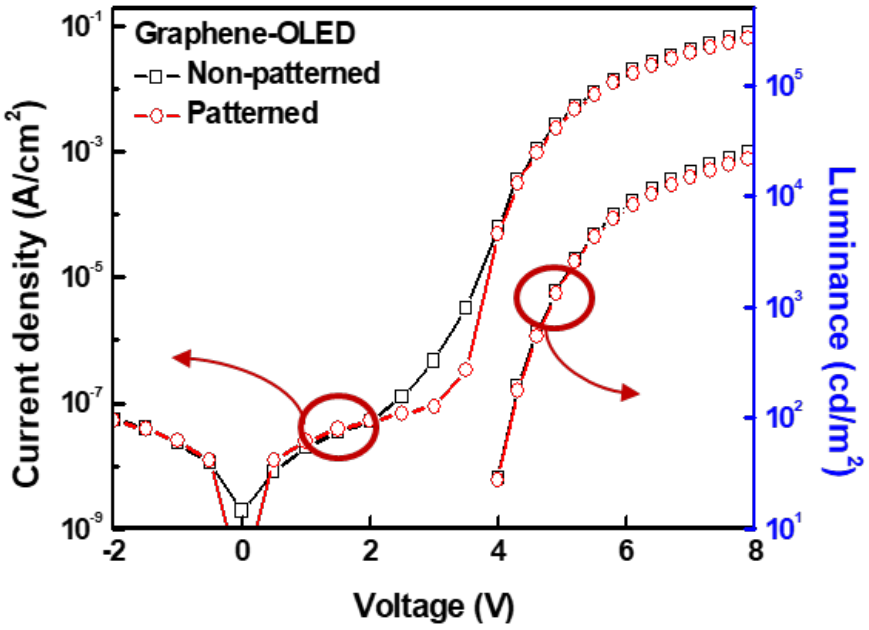
Graphene-OLED
Non-patterned
Patterned
Current density (A/cm²)
Luminance (cd/m²)
Voltage (V)
10⁻¹
10⁻³
10⁻⁵
10⁻⁷
10⁻⁹
10⁵
10⁴
10³
10²
10¹
-2
0
2
4
6
8

(a)

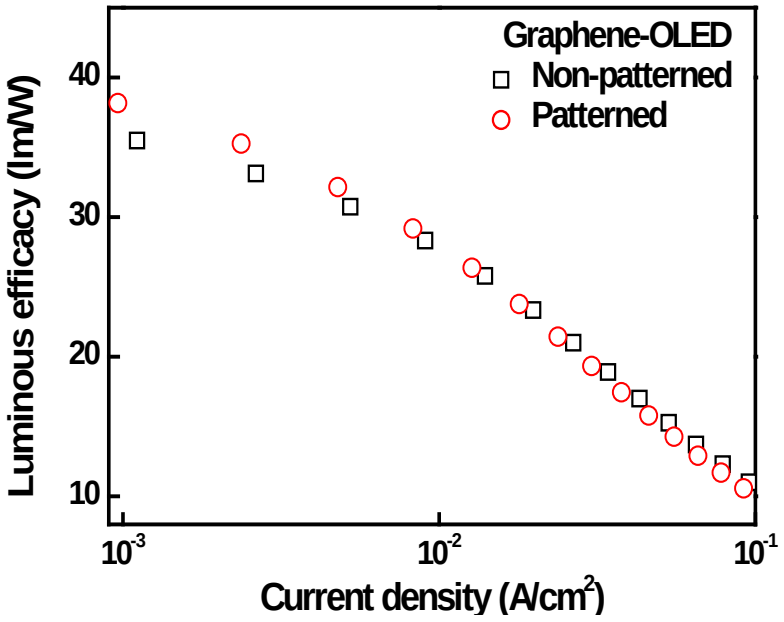
Graphene-OLED
Non-patterned
Patterned
Luminous efficacy (lm/W)
Current density (A/cm²)
40
30
20
10
10⁻³
10⁻²
10⁻¹

(b)

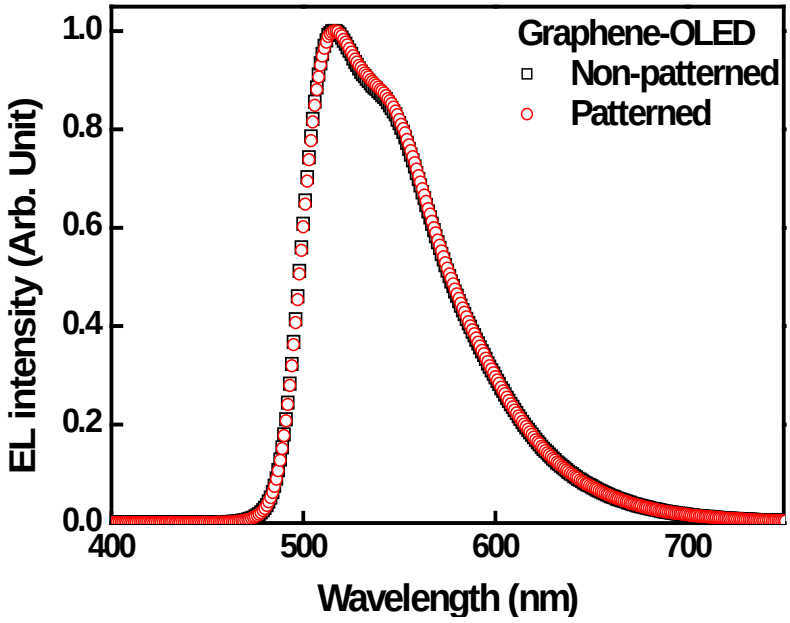

(c)

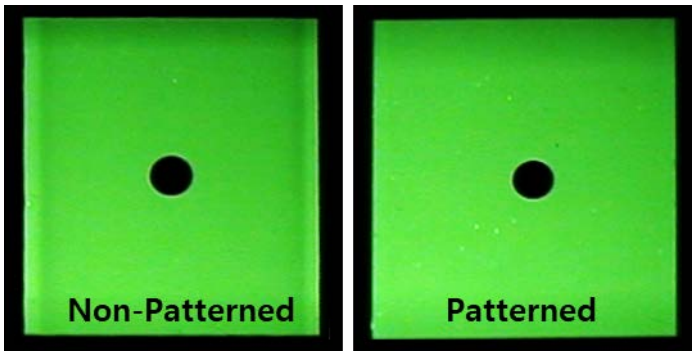

(d) (e)

Figure 4.10. (a) *J-V*-luminance and (b) LE of characteristics of graphene-OLED with the passivation wall and the patterning process. (c) EL spectra characteristics at normal direction. Actual emission image of graphene-OLED with (d) the non-patterned graphene film and (e) the patterned graphene film.

4.5 Conclusion

The weak adhesion of graphene impedes the formation of graphene pattern by causing graphene damages during photolithographic patterning process. In order to position the graphene electrodes as the critical component in the OLED display, accurate graphene patterns have to be achieved. To overcome the weak adhesion of graphene and to enable the patterning process, we developed the liquid bridge treatment to improve the effective adhesion energy of graphene film. Our patterning method provided a correct dimensions of graphene pattern and preserve its quality without surface contamination. Also, the OLED using pattered graphene electrode exhibited a stable electrical and optical performance. we believe that our result is an important precursor toward graphene AM-OLED display.

Reference

[1] J. Moon, J.-W. Shin, H. Cho, J.-H. Han, N. S. Cho, T. J. Lim, S. K. Park, H. K. Choi, S.-Y. Choi, J.-H. Kim, M.-J. Maeng, J. Seo, Y. Park and J.-I. Lee, Diamond Relat. Mater. **57**, 68 (2015).

[2] J.-Y. Hong and J. Jang, J. Mater. Chem. **22**, 8197 (2012).

[3] Y. Zhou and K. P. Loh, Adv. Mater. **22**, 3615 (2010).

[4] J.-H. Yoo, J. B. Park, S. Ahn, C. Grigoropoulos, Small **24**, 4269 (2013)

[5] E. Climent-Pascual, M. García-Vélez, Á. L. Álvarez, C. Coya, C. Munuera, X. Díez-betriu, M. García-Hernández and A. D. Andrés, Carbon **90**, 101 (2015).

[6] D. C. Bell, M. C. Lemme, L. A. Stern, J. R. Williams, and C. M. Marcus, Nanotechnology **20**, 455301 (2009).

[7] Y. Chen, X.-L. Gong, and J.-G. Gai, Adv. Sci. **3** 1500343 (2016).

[8] Z. Lu and M. L. Dunn, J. Appl. Phys. **107**, 044301 (2010).

[9] M. S. Song, B. J. Cho, Nanotechnology **21**, 335706 (2010).

[10] Y. He, W. F. Chen, W. B. Yu, G. Ouyang, and G. W. Yang, Sci. Rep. **3**, 2260 (2013).

[11] S. Kumar, D. Parks, and K. Karmrin, ACS Nano **10**, 6552, (2016).

[12] W. Jung, J. Park, T. Yoon, T.-S. Kim, S. Kim, and C.-S. Han, Small **10**, 1704, (2014).

[13] W. Gao and R. Huang, J. Phys. D: Appl. Phys. **44**, 452001 (2011).

[14] Z. H. Aitken an R. Huang, J. Appl. Phys. **107**, 123531 (2010).

[15] D. H. Cho, L. Wang, J.-S. Kim, G.-H. Lee, E. S. Kim, S. Lee, S. Y. Lee, J. Hone, and C. Lee, Nanoscale **5**, 3063 (2013).

[16] G. Lian, C. Thornton, and M. J. Adams, J. Colloid Interface Sci. **161**, 138 (1993).

[17] N. Maeda, J. N. Israelachvili, M. M. Kohonen, Proc. Natl Acad. Sci. USA **4**, 803 (2013).

[18] J. K. Hwang, S. Cho, J. M. Dang, E. B. Kwak, K. Song, J. Moon, and M. M. Sung, Nat. Nanotechnol. **5**, 742 (2010).

[19] ‘Capillary bridges’ in Wikipedia

[20] R. J. Hohlfelder, D. A. Maidenberg, R. H. Dauskardt, Y. Wei, and W. Hutchinson, J. Mater. Res. **16**, 243 (2001)

[21] W. C. Shin, T. Yoon, J. H. Mun, T. Y. Kim, S.-Y. Choi, T.-S. Kim, and B. J. Cho, Appl. Phys. Lett. **103**, 243504 (2013).

[22] T. Yoon, W. C. Shin, T. Y. Kim, J. H. Mun, T. S. Kim, and B. J. Cho, Nano Lett. **12**, 1448 (2012).

[23] D. Tabor, F. R. S. Winterton, and R. H. Winterton, Proc. R. Soc. A **312**, 435 (1969).

[24] L. R. White, R. R. Dagastine, P. M. Jones and Y.-T. Hsia, J. Appl. Phys. **97** 104503 (2005).

[25] H. C. Hamaker, Physica **4**, 1058 (1937).

[26] J. Hong, M. K. Park, E. J. Lee, D. Lee, D. S. Hwang, and S. Ryu, Sci. Rep. **3**, 2700 (2013)

[27] C. Gong, H. C. Florescat, D. Hinojos, S. McDonnell, X. Qin, Y. Hao, S. Jandhyala, G. Mordi, J. Kim, L. Colombo, R. S. Ruo, M. J. Kim, K.. Cho, R. M. Wallace, and Y. J. Chabal, J. Phys. Chem. **117**, 23000 (2013).

5

Integration of Graphene Electrode and Fabrication of OLED panel

5.1 Introduction

Figure 5.1(a) shows the typical structure of the AM-OLED pixel that is composed of TFT backplane part and OLED part [1-3]. The replacement of graphene anode may provide the benefit of structure and fabrication process to the AM-OLED. The along edge of the patterned anode is covered using a dielectric material layer, which refers to a bank process [4,5], to prevent the electrical field concentration. This issue can lead to the electrical crosstalk with adjacent pixels and degrade the pixel performances. Also, additional processes for the bank layer has to be complex in the fabrication processes of AM-OLED. In the case of graphene electrode, the bank layer can be omitted, because its thin-thickness (about 0.23 nm per layer) property prevents the electrical concentration at pattern edge. In this chapter, we applied our graphene patterning process to fabricate graphene pixilated OLED panel. In an effort to effectively investigate the technical issues associated with pixelated graphene electrodes, we adopted a simplified bottom emission type OLED structure as shown in fig 5.1(b). Instead of the TFT part, addressing metal lines were installed to control the on/off states of OLED pixels. On the surface of the passivation layer, graphene film was patterned into pixelated electrodes. Finally, we successfully demonstrated a fully operational two-color graphene pixilated OLED panel. In addition, flexible graphene pixelated OLED was fabricated and came to the demonstration.

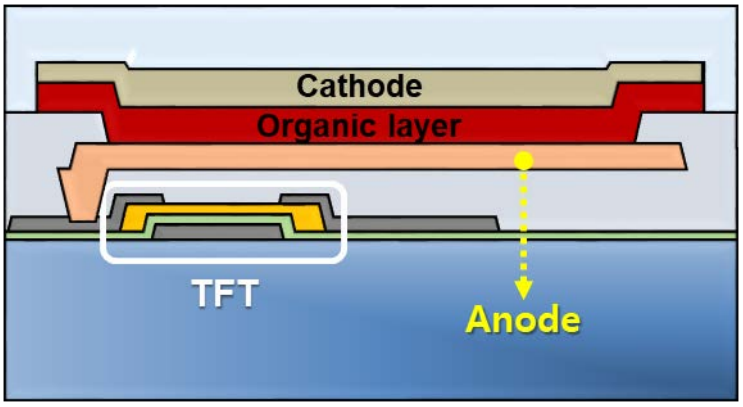

(a)

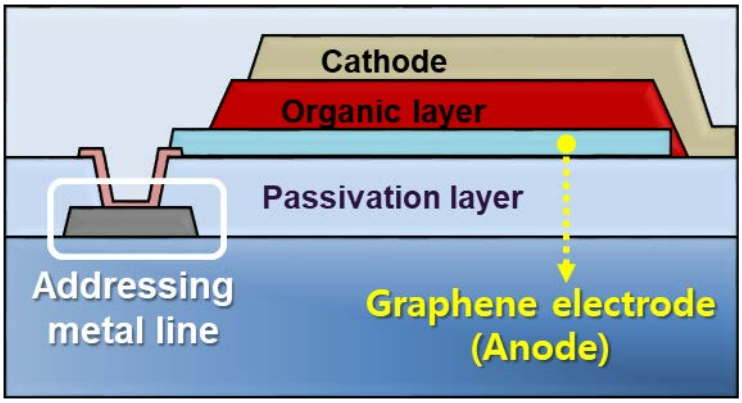

(b)

Figure 5.1. Schematics of typical AM-OLED pixel with TFT (a) and graphene-pixel electrode OLED with addressing metal line (b).

5.2 Experimental methods

The process flow is described in Fig. 5.2. For the formation of addressing metal line, molybdenum was evaporated on glass substrate and patterned by a photolithography process (step. 1). The SiO_x passivation layer was formed on the addressing metal line (step 2). In order to contact with addressing metal line and graphene pixel, the via hole and the ITO contact pad was formed into the passivation layer (step 3). The graphene film was transferred on the passivation layer with the contact pad (step 4 and 5). The graphene film was then patterned by our new patterning process with combination of the liquid bridge treatment and photolithography process (step 6 and 7) and then etched using O_2 plasma (step 8). Finally, OLED was fabricated on graphene (step. 9). In this work, four-layered graphene film was obtained by sequentially stacking monolayer graphene. Monolayer graphene was grown on Cu foils using a chemical vapor deposition (CVD) method. The sheet resistance (R_a) and direction transmittance (DT) of the graphene films on glass was ~65 Ω/□ and 82.2 % (at 550 nm wavelength), respectively. The devices were composed of a stack structure of four-layer graphene/the alternating structure of HTL (350 nm)/ EML/ BmPyPB (60 nm) (ETL). Lithium fluoride (LiF)/aluminum (Al) was evaporated on ETL for a high reflective metal cathode. To protect the organics from atmospheric degradation, the fabricated OLEDs were glass encapsulated in a glove box. An alternating HTL of HAT-CN (10 nm) and TAPC (40 nm) was used. In the case of pixelated graphene-OLED, the organic material of DCzPPy:$Ir(ppy)_3$ (20 nm) was used for EML with the main peak at $\lambda = 515$ nm. The EML of graphene-pixel electrode OLED panel offers the two color with red ($\lambda = 620$ nm) and yellow-green ($\lambda = 560$ nm).

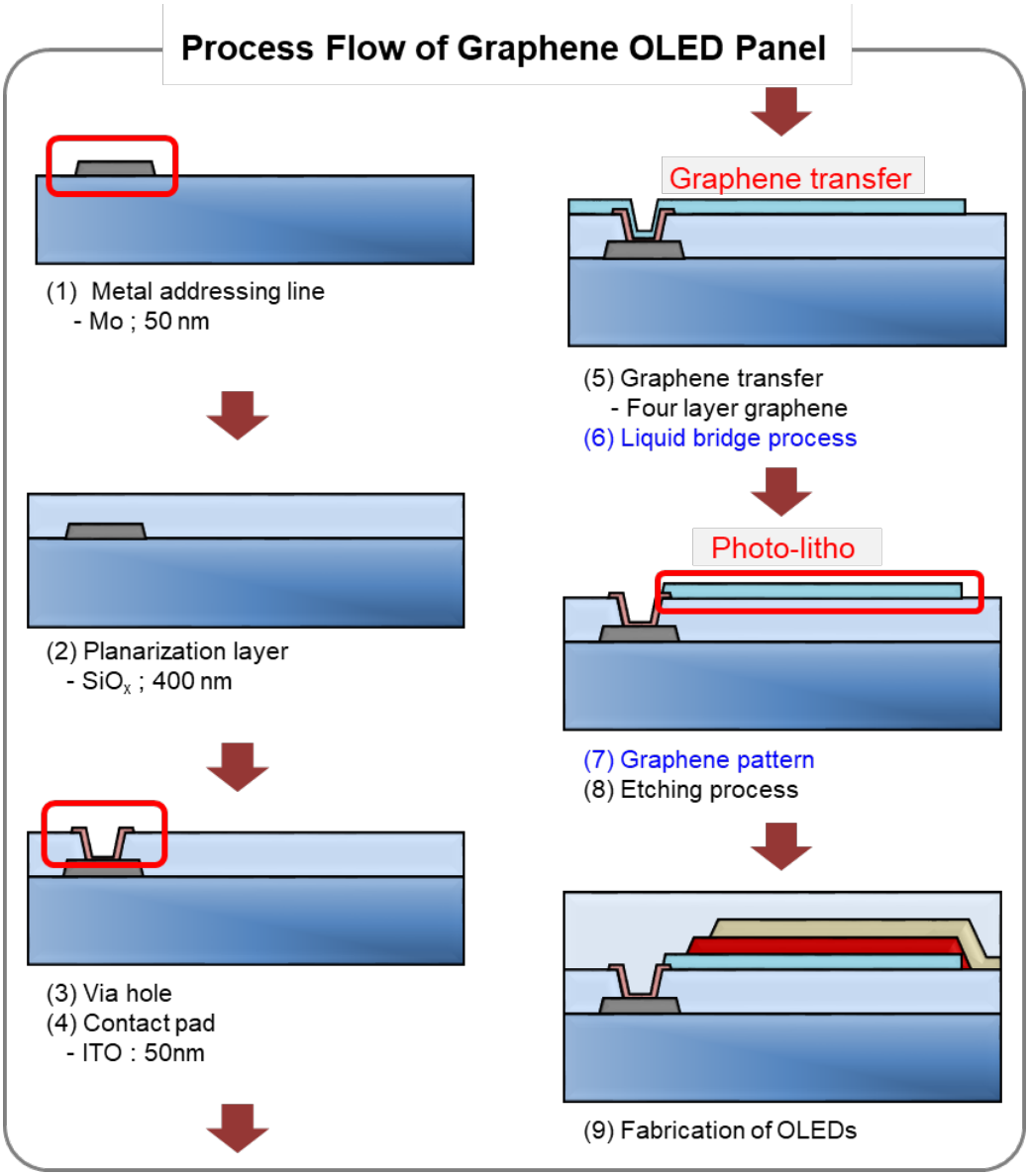

Figure 5.2. Process flow of graphene-pixel electrode OLED; backplane process (steps 1-4), graphene pattern process (steps 5-8), and OLED fabrication process (step 9).

5.3 Results and Discussion

5.3.1 Characteristics of graphene-OLED pixel

Figure 5.3 shows the actual implementation of our patterning and the surface treatment processes on a glass substrate of 100 × 100 mm^2 in size. We integrated a graphene pixel array with an active area of 80 × 60 mm^2 (Fig. 5(a)). The basic architecture of individual unit is identical to that of Fig 5.1(b). The array is composed of 33,000 graphene electrode pixels, connected by each column and weaved into odd-even pairs. This array corresponds to a resolution of 151.8 pixel/inch. The area of one pixel is 170 × 300 μm^2. The graphene electrode has an area of 100 × 250 μm^2, representing an aperture ratio of 49 %. Electrical contacts between the Mo addressing lines and the graphene pixels were established using via-holes and ITO contact pads. The ITO contact pads occupy only 6.8 % of the area, resulting in marginal influence on the overall display. Fig 5.3(b) shows a SEM image of graphene film pixel. It can be readily observed that our patterning process and surface treatment yields accurate graphene dimensions in the integration scheme.

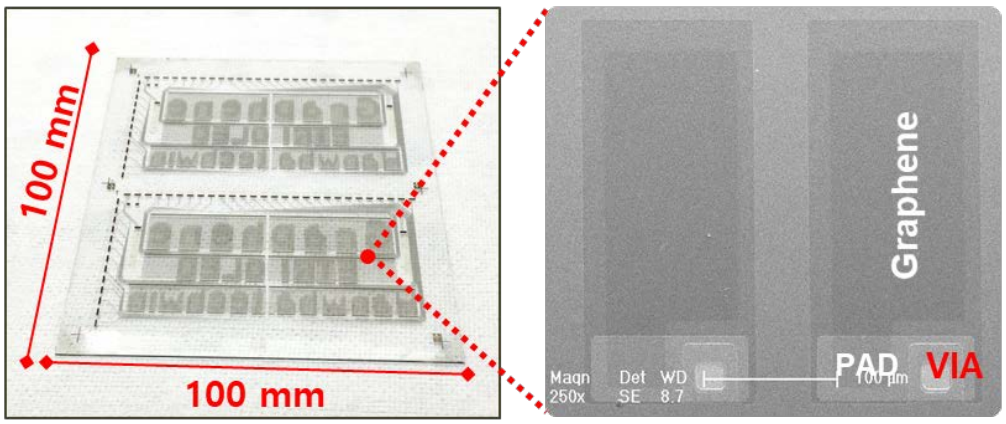

(a) (b)

Figure 5.3. (a) Actual image of a fabricated backplane with graphene film pixels. (b) A SEM image of graphene film pixel including the electrical pad, via hole and addressing metal line.

To evaluate the influence of graphene-pixel on the OLED device level, we fabricated a test device including 84 unit pixels in a 2 mm × 2 mm area. Figure 5.4(a) presents the *J*-*V*-luminance characteristics and the EL spectra of the OLED with graphene-pixel array. The device exhibits the stable *J*-*V*-luminance characteristic with low leakage current level and on/off ratios higher than 10^7. Compared to graphene-OLEDs without pixel array (fig. 4.10), there is a substantial difference in the EL spectra of graphene-pixel OLED. Furthermore, the device has the emission image similar to the graphene-pixel array (Fig. 5. 4(b) and (c)). These results imply that the graphene-pixel manufactured using our patterning process is well positioned as a component in the OLED pixel.

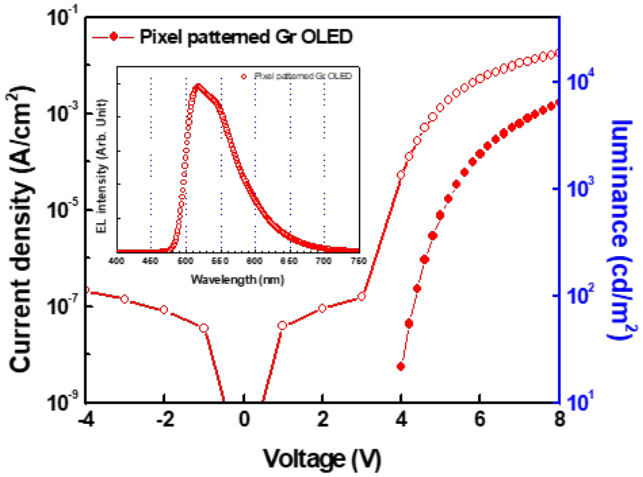

(a)

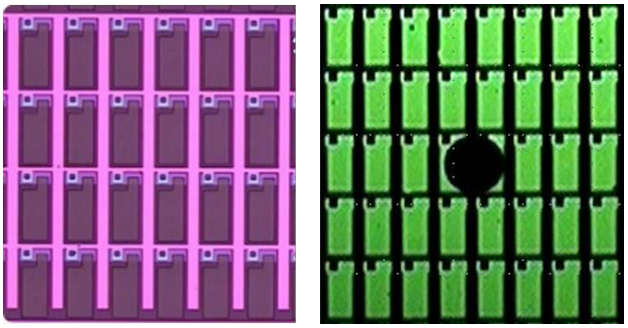

(b) (c)

Figure 5.4. (a) The *J*-*V*-luminance and EL spectra characteristic of graphene-pixel electrode OLED, (b) Actual image of graphene pixel array and (c) emission image of OLED with graphene pixel array.

5.3.2 Graphene OLED display panel

Figure 5.5 shows a fabricated two-color OLED module. The OLED was formed by a thermal evaporation method. We used phosphorescent red (λ=620 nm) and phosphorescent yellow-green (λ= 560 nm) as our emissive layer materials. The fabricated OLED panels were glass encapsulated and connected to a driving board. Our OLED was fully operational without any noticeable defect. To date there have been difficulties in overcoming the hurdles imposed by various processing difficulties with graphene. Many graphene applications have been successful beyond the "proof of concept" stage. The fine operation shown in Fig. 5.5 is an actual demonstration of graphene application on practically meaningful level. Because all the implemented processes are compatible with existing display fabrication methods, our approach can be readily applied at the commercial level. As graphene films have mechanical compliance, they can be very useful alternatives to brittle ITO.

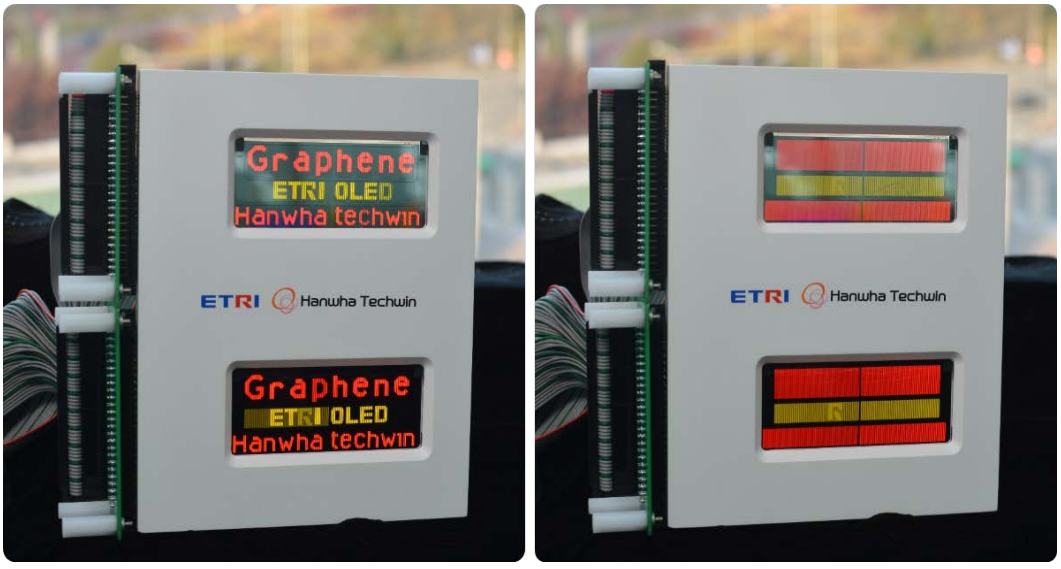

Figure 5.5. Two-color OLED with pixelated graphene films as transparent electrodes.

5.3.3 Flexible graphene OLED display panel

Finally, we demonstrated a prototype flexible OLED panel including graphene pixel electrode. Figure 5.6 presents the process flow of methods schematically. Polyimide (PI) varnish was coated and cured on a glass substrate to form a PI film. To prevent the degradation of OLED components, the oxide-based barrier was formed on the PI film [6-8]. The addressing metal line with via hole and contact pad, graphene electrode, and OLED stack was formed in sequence. We defined the pixel area of graphene by using our patterning process and encapsulated the OLED using an ALD Al_2O_3 layer and a commercially available encapsulation film [9-11]. Finally, the flexible OLED panel was detached from the glass using a laser lift-off (LLO) method [12-14]. Figure 5.7 shows the actual image of the flexible graphene OLED panel. Our flexible panel was successfully operated under bending condition. In the near future, we believe the emergence of graphene in flexible OLED display on a commercial large area scale.

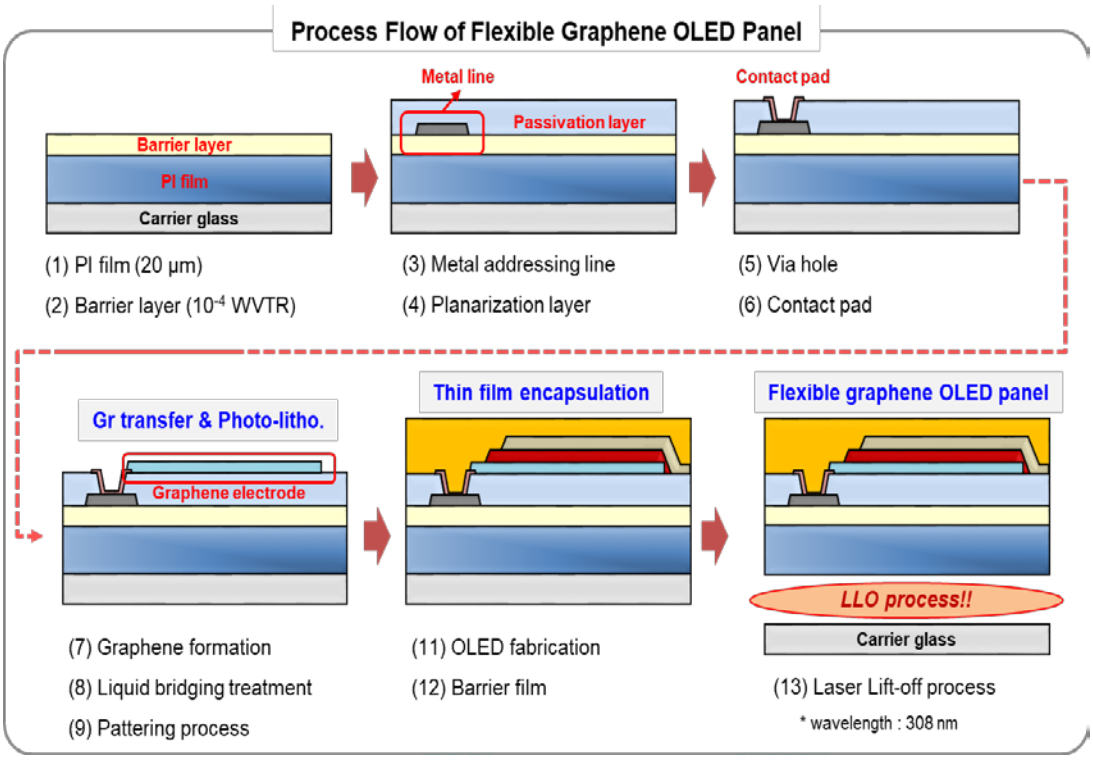

Figure 5.6. Process flow of flexible graphene-pixel electrode OLED.

Figure 5.7. Flexible OLED with pixelated graphene films as transparent electrodes.

5.4 Conclusion

With the aim of utilizing graphene films as transparent electrodes for OLED display applications, we patterned a graphene film into 170 × 250 μm^2 pixels over a large area. Graphene pixel was defined by our patterning process combined with liquid bridging and modified photolithography process. Our patterning process provided dimensionally correct graphene pixels without surface contamination. Also, graphene-pixel electrode was evaluated on the OLED device level. This graphene pixel electrode OLED exhibited the stable performance without the damage. We applied our graphene patterning process to fabricate an entirely operational two-color OLED and flexible OLED and successfully demonstrated panel operation. Our results signify the technical possibility of using graphene films as actual components in commercial OLED products.

Our results are expected to find direct applications not only in conventional displays but also in flexible and/or stretchable display in which a thin thickness and high flexibility are both required.

Reference

[1] B. Geffroy, P. L. Roy, and C. Prat, polym. Int. **55**, 572 (2006)

[2] A. Yoshida, S. Fujimura, T. Miyake, T. Yoshizawa, H. Ochi, A. Sugi-moto, H. Kubota, T. Miyadera, S. Ishizuka, M. Tsuchida, and H. Nakada, SID Symposium Digest Tech. Papers **34**, 856 (2003).

[3] M. Mizukami, N. Hirohata, T. Tseki, K. Ohtawara, T. Tada, S. Yagyu, T. Abe, T. Suzuki, Y. Fujisaki, Y. Inoue, S. Tokito, and T. Kunita, IEEE Electron Dev. Lett. **27**, 249 (2006)

[4] S.-H. K. Park, C.-S. Hwang, M. Ryu, S. Yang, C. Byun, J.-I. Lee, K. Lee, M. S. Oh, and S. lm, adv. Mater. **21**, 678, 2009.

[5] M. Stewart, R. S. Howell, L. Pires, and M. K. Hatalis, IEEE Trans. Electron Devices **48**, 845 (2001).

[6] C. Charton, N. Schiller, M. Fahland, A. Hollander, A. Wedel, K. Noller, Thin Solid Films **502**, 99 (2006).

[7] A. A. Dameron, S. D. Davidson, B. B. Burton, P. F. Carcia, R. S. McLean and S. M. George, J. Phys. Chem. C, **112**, 4573 (2008).

[8] M. D. Groner, S. M. George, R. S. McLean and P. F. Carcia, Appl. Phys. Lett., **88**, 051907 (2006).

[9] Y. C. Han, E. G. Jeong, H. Kim, S. Kwon, H.-G. Im, B.-S. Bae, and K. C. Choi, RSC Adv. **6**, 40835 (2016).

[10] J.-S. Park, H. Chae, H. K. Chung, and S. I. Lee, Semicond. Sci. Technol. **26**, 034001 (2011).

[11] Y. G. Lee, Y.-H. Choi, I. S. Kee, H. S. Shim, Y. Jin, S. Lee, K. H. Koh and S. Lee, Org. Electron. **10**, 1352 (2009).

[12] K. Kim, S. Y. Kim, and J.-L. Lee, J. Mater. Chem. C **2**, 22144 (2014).

[13] R. Paetzel, J. Soc. Inf. Disp. **25**, 20 (2009).

[14] M. F. Al-Kuhaili, S. M. A. Durrani and E. E. Khawaja, Appl. Phys. Lett. **83**, 4533 (2003).

6

Conclusion

Graphene has attracted attention as one of the next generation transparent electrode candidate for flexible OLED applications due to its excellent electrical, optical, and mechanical properties which include the extremely high electrical conductivity, transparency, surface flatness, and flexibility. Its chemical stability as well as its process compatibility to existing OLED process are also beneficial. This dissertation, proposed to the development on graphene as a transparent electrode for flexible OLED applications, has been focused on improving the optical efficiency of graphene-OLED and on developing a new method for the required accurate patterning. The following is the summary of each chapter.

Chapter 2. Electrical and optical characterization of classical graphene- OLEDs

Although the graphene-OLED has exhibited stable electrical and optical properties, the overall performance is lower than that of ITO-OLEDs; The external quantum efficiency (EQE) of the graphene-OLED is approximately 80% of the ITO-OLED. This is due to the lower electrical conductivity and the weaker microcavity effect in the graphene-OLED. In particular, the very weak microcavity effect in graphene-OLED limits its out-coupling efficiency. It has a benefit, however, that it provides optical stability over a wide angle range. Although graphene is an attractive transparent electrode material for OLED applications, it is necessary develop several technologies to improve the

optical efficiency of graphene-OLED up to comparable values of existing devices, which forms the target of this study.

Chapter 3. Improvement of light extraction efficiency of graphene electrode OLEDs

As an effort to improve the optical efficiencies of graphene-OLEDs, we evaluated the optical absorption of graphene and explored the use of the scattering layer. A comparison between simulations and device characterizations have shown that the optical absorption and the substantial reduction of the microcavity effect limit the efficiencies of the graphene-OLED. Introduction of a scattering layer between the substrate and the graphene anode was found to enhance EQE and LE by more than 50%. As a result, we succeeded in the fabrication of graphene-OLEDs having efficiencies comparable to those of conventional OLEDs with oxide anodes. Furthermore, the angular EL spectrum variations were stabilized, which is difficult to achieve using conventional OLEDs accompanied with substantial microcavity effects.

Chapter 4. Formation of accurate graphene patterns using liquid bridging treatment

The weak adhesion of graphene against the supporting layers are found to impede the formation of accurate graphene pattern by causing damages to graphene during the photolithographic patterning process. In order to position graphene electrodes as the critical component in the OLED display, the accurate patterning of graphene has to be achieved. To overcome the weak adhesion of graphene and to enable the desired patterning process, we developed the liquid bridge treatment to improve the effective adhesion energy of the graphene film. Our patterning method provided accurate dimensions of graphene pattern and preserved its quality without surface contamination. Also, the OLED using the patterned graphene electrode exhibited a stable electrical and optical performance.

Chapter 5. Integration of graphene electrode and fabrication of OLED panel

With the aim of utilizing graphene films as transparent electrodes for OLED display applications, we patterned a graphene film into 170×250 μm^2 pixels over a large area. Graphene pixel was defined by our patterning process combined with liquid bridging and modified photolithography process. Our patterning process provided dimensionally correct graphene pixels without surface contamination. Also, the graphene-pixel electrode was evaluated on the OLED device level. This graphene-pixel electrode OLED exhibited the stable performance without the damage. We applied our graphene patterning process to fabricate an entirely operational two-color OLED and flexible OLED and successfully demonstrated panel operation.

We believe that our result is an important precursor toward graphene OLED applications. Our results are expected to find direct applications not only in conventional displays but also in flexible and/or stretchable display in which a thin thickness and high flexibility are both required.

Publications and Conference Proceedings

List of Publications

1. **Jin-Wook Shin,** Jun-Han Han, Hyunsoo Cho, Jaehyun Moon, Byoung-Hwa Kwon, Sengmin Cho, Taeshik Yoon, Taek-Soo Kim, Maki Suemitsu, Jeong-Ik Lee and Nam Sung Cho, "Display process compatible accurate graphene patterning for OLED application", 2D materials 5, 014003 (2017).

2. **Jin-Wook Shin,** Hyunsu Cho, Jonghee Lee, Jaehyun Moon, Jun-Han Han, Kisoo Kim, Seungmin Cho, Jeong-Ik Lee, Byoung-Hwa Kwon, Doo-Hee Cho, Kang Me Lee, Maki Suemitsu, and Nam Sung Cho, "Overcoming the Efficiency Limit of Organic Light-Emitting Diodes using Ultra-Thin and Transparent Graphene Electrodes", Opt. Express, 26, 617 (2018).

3. Chul Woong Joo, Keunsoo Lee, Jonghee Lee, Hyunsu Cho, **Jin-Wook Shin,** Nam Sung Cho, Jaehyun Moon, "Optical and structural approaches for improved luminance distribution and enhanced efficiency of organic light emitting diodes", J. Lumin. 187, 433 (2017).

4. Keunsoo Lee, **Jin-Wook Shin,** Jun-Hwan Park, Jonghee Lee, Chul Woong Joo, Jeong-Ik Lee, Doo-Hee Cho, Jong Tae Lim, Min-Cheol Oh, Byeong-Kwon Ju, and Jaehyun Moon, "A Light Scattering Layer for Internal Light Extraction of Organic Light-Emitting Diodes Based on Silver Nanowires", ACS appl. Mater. Interfaces 8, 17409 (2016).

5. Hyunsu Cho, Hyunkoo Lee, Jonghee Lee, Woo Jin Sung, Byoung-Hwa Kwon, Chul-Woong Joo, **Jin-Wook Shin,** Jun-Han Han, Jaehyun Moon, Jeong-Ik Lee, Seungmin Cho, and Nam Sung Cho, "Stable angular emission spectra in white organic light-emitting diodes using graphene/PEDOT:PSS composite electrode", Opt. Express 25, 9734 (2017).

6. 6. Jin Sik Choi, Hongkyw Choi, Ki-Chul Kim, Hu Young Jeong, Young-Jun Yu, Jin Tae Kim, Jin-Soo Kim, **Jin-Wook Shin,** Hyunsu Cho, and Choon-Gi Choi, "Facile fabrication of

properties controllable graphene sheet", Sci. Rep. 6, 24525 (2016).

7. 7. Chul Woong Joo, **Jin-Wook Shin,** Jaehyun Moon, Jin Woo Huh, Doo-Hee Cho, Jonghee Lee, Seung Koo Park, Nam Sung Cho, Jun-Han Han, Hye Yong Chu, Jeong-Ik Lee, "Highly efficient white transparent organic light emitting diodes with nano-structured substrate", Org. Electron. 29, 72 (2016).

8. 8. Byoung-Kuk Kang, Hyunsu Cho, Jun-Han Han, **Jin-Wook Shin,** Jinouk Song, Seung Koo Park, Jonghee Lee, Chul Woong Joo, Eunhye Kim, Seunghyup Yoo, Jeong-Ik Lee, Byeong-Kwon Ju, and Jaehyun Moon, "Area-selective external light extraction for metal bus equipped large area transparent organic light-emitting diodes", Opt. Express 24, 5356 (2016).

9. **Jin-Wook Shin,** Jaehyun Moon, Doo-Hee Cho, Chul Woong Joo, Seung Koo Park, Jonghee Lee, Jun-Han Han, Nam Sung Cho, Hyunsu Cho, and Jeong-Ik Lee, "White Organic Light Emitting Diodes with a Random Scattering Layer for an Internal Light Extraction", ECS J. Solid State Sci. Technol. 5, R3126, (2016).

10. Hyunsu Cho, **Jin-Wook Shin,** Nam Sung Cho, Jaehyun Moon, Jun-Han Han, Young-Duck Kwon, Seungmin Cho, and Jeong-Ik Lee, "Optical Effects of Graphene Electrodes on Organic Light-Emitting Diodes", IEEE J. Sel. Topics quantum electron. 22, 2000306 (2016).

11. Chul Woong Joo, Jaehyun Moon, Jun-Han Han, Jin Woo Huh, **Jin-Wook Shin,** Doo-Hee Cho, Jonghee Lee, Nam Sung Cho and Jeong-Ik Lee, "White transparent organic light-emitting diodes with high top and bottom color rendering indices", J. Info. Display 16, 161 (2015).

12. Jaehyun Moon, **Jin-Wook Shin,** Hyunsu Cho, Jun-Han Han, Nam Sung Cho, Jong Tae Lim, Seung Koo Park, Hong Kyw Choi, Sung-Yool Choi, Ji-Hoon Kim, Min-Jae Maeng, Jaewon Seo, Yongsup Park, and Jeong-Ik Lee , "Technical issues in graphene anode organic light emitting diodes", Diam. Relat. Mater. 57, 68 (2015).

13. Seung Koo Park, Chul Woong Joo, Joo Yeon Kim, Byoung-Hwa Kwon, **Jin-Wook Shin,** Doo-

Hee Cho, Jaehyun Moon, and Jeong-Ik Lee, “Highly smooth and refractive films fabricated from titanium oxide hydrate solution”, Mater. Lett. 157, 248 (2015).

14. Jaehyun Moon, Eunhye Kim, Seung Koo Park, Keunsoo Lee, **Jin-Wook Shin,** Doo-Hee Cho, Jonghee Lee, Chul Woong Joo, Nam Sung Cho, Jun-Han Han, Byoung-Gon Yu, Seunghyup Yoo, Jeong-Ik Lee, “Organic wrinkles for energy efficient organic light emitting diodes”, Org. Electron. 26, 273 (2015).

15. Jin Woo Huh, **Jin-Wook Shin,** Doo-Hee Cho, Jaehyun Moon, Chul Woong Joo, Seung Koo Park, Joohyun Hwang, Nam Sung Cho, Jonghee Lee, Jun-Han Han, Hye Yong Chu and Jeong-Ik Lee, “A randomly nano-structured scattering layer for transparent organic light emitting diodes”, Nanoscale 6, 10727 (2014).

16. Doo-Hee Cho, **Jin-Wook Shin,** Jaehyun Moon, Seung Koo Park, Chul Woong Joo, Nam Sung Cho, Jin Woo Huh, Jun-Han Han, Jonghee Lee, Hye Yong Chu, and Jeong-Ik Lee, “Surface Control of Planarization Layer on Embossed Glass for Light Extraction in OLEDs”, ETRI J. 36, 847 (2014).

17. Doo-Hee Cho, **Jin-Wook Shin,** Chul Woong Joo, Jonghee Lee, Seung Koo Park, Jaehyun Moon, Nam Sung Cho, Hye Yong Chu, and Jeong-Ik Lee, “Light diffusing effects of nano and microstructures on OLED with microcavity”, Opt. Express 22, A1507 (2014)

18. **Jin-Wook Shin,** Doo-Hee Cho, Jaehyun Moon, Chul Woong Joo, Jonghee Lee, Jin Woo Huh, Seung Koo Park, Jun-Han Han, Nam Sung Cho, Joohyun Hwang, Hye Yong Chu, and Jeong-Ik Lee, “Random nanostructure scattering layer for suppression of microcavity effect and light extraction in OLEDs”, Opt. Lett. 39, 3527 (2014).

19. Seung Koo Park, Byoung-Kuk Kang, **Jin-Wook Shin,** Chul Woong Joo, Jaehyun Moon, Doo-Hee Cho, Byounggon Yu, Hye Yong Chu and Jeong-Ik Lee, “Triethylene glycol–titanium oxide hydrate hybrid films with high refractive index and surface evenness”, J. Mater. Chem. C 2, 4468 (2014).

20. Hongkyw Choi, Jin Sik Choi, Jin-Soo Kim, Jong-Ho Choe, Kwang Hyo Chung, **Jin-Wook Shin,** Jin Tae Kim, Doo-Hyeb Youn , Ki-Chul Kim, Jeong-Ik Lee, Sung-Yool Choi, Philip Kim, Choon-Gi Choi, and Young-Jun Yu, "Flexible and Transparent Gas Molecule Sensor Integrated with Sensing and Heating Graphene Layers", Small 10, 3685 (2014).

21. **Jin-Wook Shin,** Doo-Hee Cho, Jaehyun Moon, Chul Woong Joo, Seung Koo Park, Jonghee Lee, Jun-Han Han, Nam Sung Cho, Joohyun Hwang, Jin Woo Huh, Hye Yong Chu, Jeong-Ik Lee, "Random nano-structures as light extraction functionals for organic light-emitting diode applications", Org. Electron. 15, 196 (2014).

22. Jun-Han Han, Jaehyun Moon, Doo-Hee Cho, **Jin-Wook Shin,** Chul Woong Joo, Joohyun Hwang, Jin Woo Huh, Hye Yong Chu, and Jeong-Ik Lee, "Transparent OLED Lighting Panel Design Using Two-Dimensional OLED Circuit Modeling", ETRI J. 35, 559 (2013).

23. Jin Woo Huh, Jaehyun Moon, Joo Won Lee, Jonghee Lee, Doo-Hee Cho, **Jin-Wook Shin,** Jun-Han Han, Joohyun Hwang, Chul Woong Joo, Jeong-Ik Lee, Hye Yong Chu, "Organic/metal hybrid cathode for transparent organic light-emitting diodes", Org. Electron. 14, 2039, (2013).

24. Joohyun Hwang, Hong Kyw Choi, Jaehyun Moon, **Jin-Wook Shin,** Chul Woong Joo, Jun-Han Han, Doo-Hee Cho, Jin Woo Huh, Sung-Yool Choi, Jeong-Ik Lee, Hye Yong Chu, "Blue fluorescent organic light emitting diodes with multilayered graphene anode", Mater. Res. Bull. 47, 2796 (2012).

25. Jeong-Ik Lee, Jonghee Lee, Joo-Won Lee, Doo-Hee Cho, **Jin-Wook Shin,** Jun-Han Han, and Hye Yong Chu, "Dependence of Light-Emitting Characteristics of Blue Phosphorescent Organic Light-Emitting Diodes on Electron Injection and Transport Materials", ETRI J. 34, 690 (2012).

26. Chul Woong Joo, Jaehyun Moon, Joohyun Hwang, Jun-Han Han, **Jin-Wook Shin,** Doo-Hee Cho, Jin Woo Huh, Hye Yong Chu, and Jeong-Ik Lee, "Improved Device Performances in Phosphorescent Organic Light-Emitting Diodes by Microcavity Effects", Jpn. J. Appl. Phys. 51,

09MH01 (2012)

27. Joohyun Hwang, Hong Kyw Choi, Jaehyun Moon, Taek Yong Kim, **Jin-Wook Shin,** Chul Woong Joo, Jun-Han Han, Doo-Hee Cho, Jin Woo Huh, Sung-Yool Choi, Jeong-Ik Lee, and Hye Yong Chu, "Multilayered graphene anode for blue phosphorescent organic light emitting diodes", Appl. Phys. Lett. 100, 133304 (2012).

28. Jin Woo Huh, Jaehyun Moon, Joo Won Lee, Doo-Hee Cho, **Jin-Wook Shin,** Jun-Han Han, Joohyun Hwang, Chul Woong Joo, Jeong-Ik Lee, and Hye Yong Chu, "The Optical Effects of Capping Layers on the Performance of Transparent Organic Light-Emitting Diodes", IEEE Photonics J. 4, 39, (2012).

29. Jaehyun Moon, Joohyun Hwang, Jin Woo Huh, **Jin-Wook Shin,** Doo-Hee Cho, Seung Koo Park, Jun-Han Han, Chul Woong Joo, Jeong-Ik Lee, Hye Yong Chu, "A perturbation analysis on solid polymer surfaces", Mater. Res. Bull. 47, 2788(2012).

30. Doo-Hee Cho, **Jin-Wook Shin,** Jeong-Ik Lee, Jonghee Lee, Jun-Han Han, and Hye Yong Chu, "Light Extraction from Organic Light Emitting Diodes Using Chemically Etched Glass Substrates", J. Nanosci. Nanotechnol. 4, 3447 (2012).

31. **Jin-Wook Shin,** Doo-Hee Cho, Jeong-Ik Lee, Jonghee Lee, Joo-Han Lee, Jun-Han Han, and Hye Yong Chu, "The Fabrication and Characterization of Organic Light-Emitting Diodes by Using Laser Patterned Anode", JNO 5, 161 (2010).

32. **Jin-Wook Shin,** Won-Ju Cho, Chel-Jong Choi, and Moongyu Jang, "Characteristics of polycrystalline silicon Schottky barrier thin film transistors fabricated using metallic junction source/drain with erbium silicide and platinum silicide", Appl. Phys. Lett. 94, 053502 (2009).

33. **Jin-Wook Shin,** Chel-Jong Choi, Moongyu Jang, and Won-Ju Cho, "Schottky Barrier N-Type Thin Film Transistors With Polycrystalline Silicon Channel and Er-Silicided Metallic Junctions", IEEE Electron Device Lett 29, 1336 (2008).

34. **Jin-Wook Shin,** Chel-Jong Choi, Moongyu Jang, and Won-Ju Cho, "Fabrication of n- and p-Channel Schottky Barrier Thin-Film Transistors Crystallized by Excimer Laser Annealing and Solid Phase Crystallization Methods", Jpn. J. Appl. Phys. 48, 04C151 (2009).

35. Dae Hyun Ka, **Jin-Wook Shin,** Won-Ju Cho, Jong Tae Park, "Substrate bias and operating temperature effects on the performance of Schottky-barrier SOI nMOSFETs", Solid State Electron. 52, 1910 (2008).

36. Eun Kyu Kim, Dong Uk Lee, Seon Pil Kim, Tae Hee Lee, Hyun-Mo Koo, **Jin-Wook Shin,** Won-Ju Cho, and Young-Ho Kim, "Nano-Floating Gate Memory Devices with Metal-Oxide Nanoparticles in Polyimide Dielectrics", J. Semicond. Tech. SCI., 8, 21 (2008).

International conference

1. **Jin-Wook Shin,** Hyunsu Cho, Jonghee Lee, Jaehyun Moon, Jun-Han Han, Doo-Hee Cho, Byoung-Hwa Kwon, Jeong-Ik Lee, Kisoo Kim, Seungmin Cho, Maki Suemitsu, and Nam Sung Cho, Improvement of light extraction efficiency in graphene electrode OLEDs with the light extraction layer", International Meeting on information display (IMID), 2017.

2. **Jin-Wook Shin,** Jun-Han Han, Hyunsoo Cho, Jaehyun Moon, Byoung-Hwa Kwon, Seungmin Cho, Maki Suemitsu, Nam Sung Cho and Jeong-Ik Lee, "Integration of pixelated graphene as a bottom electrode into organic light-emitting diode panel technologies", International Workshop on Flexible & Printable Electronics (IWPFE), 2017.

3. **Jin-Wook Shin,** Hyunsu Cho, Jonghee Lee, Jaehyun Moon, Jun-Han Han, Doo-Hee Cho, Byoung-Hwa Kwon, Jeong-Ik Lee, Kisoo Kim, Seungmin Cho, Maki Suemitsu, and Nam Sung Cho, "Graphene electrode OLEDs with the scattering layer for an improvement in the light extraction efficiency", International Conference on Advanced Electromaterials (ICAE), 2017.

4. Jaehyun Moon, Jun-Han Han, **Jin-Wook Shin,** Hyunsu Cho, Byoung-Hwa Kwon, Jeong-Ik Lee, Nam Sung Cho, and Seungmin Cho, "Gen 2 (370 mm × 470 mm) Sized Graphene Anode OLED", International Meeting on information display (IMID), 2017.

5. Jeong-Ik Lee Jun-Han Han, **Jin-Wook Shin,** Hyunsu Cho, Jaehyun Moon, Byong-Hwa Kwon, Nam Sung Cho, and Seungmin Cho, "Pixelated Graphene Electrodes for OLED Display", Graphene 2017.

6. Jun-Han Han, **Jin-Wook Shin,** Nam Sung Cho, Hyunsu Cho, Jaehyun Moon, Byoung-Hwa Kwon, Kisoo Kim, Suengmin Cho, and Jeong-Ik Lee, "Organic Light-Emitting Diode Display Panel Integration Using Graphene Pixel Electrodes", Graphene 2016.

7. Jaehyun Moon, **Jin-Wook Shin,** Jun-Han Han, Nam Sung Cho, Hyunsu Cho, Byoung-Hwa Kwon, Kisoo Kim, Seungmin Cho, and Jeong-Ik Lee, "Integration of graphene pixel electrode and OLED panel for AM-OLED display applications", Graphene 2016.

8. Jun-Han Han, **Jin-Wook Shin,** Hyunsu Cho, Nam Sung Cho, Jaehyun Moon, Byoung-Hwa Kwon, Kisoo Kim, Seungmin Cho, and Jeong-Ik Lee, "Graphene as a transparent pixel electrode to fabricate organic light-emitting diode display panel", Nano Korea 2016

9. JongChan Jeong, **Jin-Wook Shin,** Jonghee Lee, ChulWoong Joo, HyunSu Cho, Jun Han Han, Byoung-Hwa Kwon, Eungjun Kim, Seunghyup Yoo, Jeong-Ik Lee, Nam Sung Cho, SungYun Yang, and Jaehyun Moon, "Improved outcoupling efficiency of organic light-emitting diodes by spontaneously formed internal wrinkles structures. – A radiation out coupling case", International Conference on Advanced Electromaterials (ICAE), 2017. (Scheduled to be 11/23/2017)

Awards

1. Best Poster Paper Award, International Workshop on Flexible & Printable Electronics (IWPFE) 2017.

Acknowledgement

First and above all, I would like to thank God for giving me wisdom and courage to complete my doctoral degree. I feel so grateful for you to give me the chance to meet people I got lots of help from.

I take this opportunity to express my gratitude to all those who supported me throughout the peaks and valleys of my journey in the graduate school at Tohoku University, Japan. First and foremost, I would like to express my deepest thanks to Professor Maki Suemitsu, my research supervisor at Research Institute of Electrical Engineering (RIEC), Tohoku University, Japan for his continual encouragement, strong support/guiding, and valuable advices throughout this work. His enthusiasm, guidance and wealth of technical knowledge provided excellent inspiration and insight to my research. I am also very grateful for his valuable suggestions and help regarding many other aspects of my life.

I would like to thank the rest of my thesis committee for their support. Prof. Shigeo Sato and Toshiro Kaneko, who all provided me with invaluable advice and comments on both my research and my future research career plans.

I've been very lucky throughout most of my life in graduate school, in that I've been able to concentrate mostly on my research. In particular, this work would not have been possible without the support of Suemitsu laboratory members. I would like to thank Ph.D. Goon-Ho Park and Kwan-Su Kim for providing me a relaxed environment during the doctoral course.

I would also like to acknowledge my research advisor, Ph.D. Jaehyun Moon at ETRI in Korea, and Prof. Won-Ju Cho at Kwangwoon University in Korea. They have been my mentor, my confidant, my colleague, and a never-ending fount of moral support. They have given me so much of himself to help me succeed.

Further, I thank Hong Kyw Choi, Seoheun Hong, Jeong-Ik Lee, Nam Sung Cho, Jonghee Lee, Jong-Heon Yang, Chul Woong Joo, Hyunsu Cho, Byoung-Hwa Kwon, Kang Me Lee, Jun-Han Ha n, and Seung Koo Park for providing me with useful comment, help and encouragement. I also extend my gratitude to all members of SEMATEC laboratory at Kwangwoon University.

Finally, I want to give my great appreciation to my family, especially my parents, Jae Won Shin and Myung Hee Kim, my sisters, Sung Hee Shin, Hye Young Shin, and Ja Young Shin, parents-in-law, Seung Hee Choi and Sung Ho Yun, and sister-in-law, Seo Ah Yun. Without their unending support and love childhood to now, I never would have made it through this process or any of the tough time in my life.

My lovely wife, Seoyoon Yun. *"This would not have been done without your support and love."*